GEODETIC POSITIONING SYSTEMS USING REPEATER SATELLITES

by

LAUREANO ALBERTO CANGAHUALA

B.S., Aeronautics and Astronautics,
Earth, Atmospheric, and Planetary Sciences, M.I.T., 1987

M.S., Aeronautics and Astronautics, M.I.T., 1989

SUBMITTED TO THE DEPARTMENT OF AERONAUTICS AND ASTRONAUTICS IN PARTIAL FULFILLMENT OF THE REQUIREMENTS FOR THE DEGREE OF

DOCTOR OF PHILOSOPHY

at the

MASSACHUSETTS INSTITUTE OF TECHNOLOGY
April 1992

Signature of Author _____
Department of Aeronautics and Astronautics
April 29, 1992

Certified by _____
Professor Charles C. Counselman III
Department of Earth, Atmospheric, and Planetary Science
Thesis Committee (Chairman)

Certified by _____
Professor R. John Hansman
Department of Aeronautics and Astronautics
Thesis Committee

Certified by _____
Professor Thomas A. Herring
Department of Earth, Atmospheric, and Planetary Science
Thesis Committee

Certified by _____
Professor Walter M. Hollister
Department of Aeronautics and Astronautics
Thesis Committee

Certified by _____
Dr. Robert W. King
Department of Earth, Atmospheric, and Planetary Science
Thesis Committee

Accepted by _____
Professor Harold Y. Wachman
Chairman, Departmental Graduate Committee

GEODETIC POSITIONING SYSTEMS USING REPEATER SATELLITES

by

Laureano Alberto Cangahuala

Submitted to the Department of Aeronautics and Astronautics on April 27, 1992
in partial fulfillment of the requirements for the degree of Doctor of Philosophy

Abstract: A proposed satellite system (named "GeoBeacons") can detect and locate small transmitters on the Earth's surface. Transmitted code-modulated signals will be relayed to a central processing site by a constellation of repeater satellites. This system could provide an inexpensive way to monitor geodetic networks with more sites than can be monitored with NAVSTAR GPS (Global Positioning System) receivers. GeoBeacons will use doubly differenced observations, as are used in current geodetic GPS research.

Two particularly simple constellations of GeoBeacon satellites are considered: (i) a coplanar pair of polar orbiting satellites, with differing mean motions such that one overtakes the other fortnightly, and (ii) 16 satellites in the same sun-synchronous orbit. Observations from consecutive passes are used to obtain three-dimensional position estimates. In both cases, the satellites could be small and lightweight, similar to the Microsat spacecraft (28 cm cubes with masses of ~10 kg) currently used by the amateur radio community. A gravity gradient system is considered as an alternative to the passive magnetic stabilization system used by Microsats. Either of these constellations could be established with just one launch of a small-payload launch vehicle, such as the Pegasus. The ground transmitter and satellite repeater power requirements are estimated to be on the order of 100 mw and 500 mw, respectively. Lack of knowledge of the radio noise environment as seen from orbit is the chief cause of uncertainty of these estimates.

Position-estimation error-covariance matrices for both GeoBeacon configurations are comparable to that for GPS, especially for networks at higher latitudes. However, a satellite visibility limitation, due to the lower orbits, restricts the GeoBeacon configuration network dimensions to 1500 - 2000 km, versus 4000 - 8000 km for GPS networks. In addition, GPS observation opportunities exist continuously, and only a brief observation is needed for a non-degenerate three-dimensional position estimate. The GeoBeacon 16-satellite configuration, on the other hand, would require about one day to obtain similar results.

A satellite-based system is recommended as a cost-effective means of retrieving data from GPS receivers. If GeoBeacon users must finance the entire project, a network on the order of 10,000 sites would be required to be more cost-effective than a GPS-based system. If users did not have to pay for GeoBeacon satellite construction and launch costs, (as is the case with GPS), the break-even point would drop to about 1,000 sites.

A demonstration of the GeoBeacons concept was designed. Covariance analysis results for a small (~1 km maximum baseline length) transmitter network, using GOES (Geostationary Operational Environmental Satellites), show that it should be possible to solve for the three coordinates of a transmitter and all three GOES orbits, and to resolve the integer-cycle

ambiguities of the doubly differenced phase observations, with a five-station fiducial network. Orbit estimation variances are smaller for well-spaced satellites in high inclination orbits, for transmitters spaced apart as far as possible in both latitude and longitude, centered beneath the satellites at low latitudes.

Due to recent advances in proposed satellite-based data retrieval schemes, GeoBeacons at present cannot offer a significant improvement in cost-effectiveness over GPS. Since a large network is required to show sponsors any savings in cost per site, GeoBeacons is not likely to be implemented in its present form. However, the geodetic community recognizes the need for measurements from independent sources; if a compatible constellation of orbiting transponders became available, they could be the basis for a GeoBeacon system. Another possible scenario for a geodetic network to be implemented with repeater satellites is on another body in the solar system, using low-power transmitters on or near the body of interest.

Thesis Supervisor: Charles C. Counselman III
Title: Professor of Planetary Sciences

Thesis Supervisor: R. John Hansman
Title: Associate Professor of Aeronautics and Astronautics

Thesis Supervisor: Thomas A. Herring
Title: Kerr-McGee Jr. Development Associate Professor of Geophysics

Thesis Supervisor: Walter M. Hollister
Title: Professor of Aeronautics and Astronautics

Thesis Supervisor: Robert W. King, Ph.D.
Title: Principal Research Scientist, Department of Earth, Atmospheric, and Planetary Sciences

Acknowledgements

I am grateful for the support provided by the National Science Foundation (through a Minority Fellowship, with tenureship covering the 1987 - 90 academic years) and the Phillips Laboratory at Hanscom AFB, Lexington, Massachusetts (through a National Defense Science and Engineering Fellowship, with tenureship covering the 1990 - 92 academic years). Work done with the MIT Center for Space Research / Space Geodesy Group was made possible by Air Force Contract F19628-86-K-0009 with the Air Force Geophysics Laboratory.

There are many people I wish to thank for their support and constructive help. First, I would like to thank Professor Charles Counselman for providing the opportunity to perform research in space geodesy. Through his patience, guidance, and encouragement he has set an example which I hope to pass on to others. Working with you has been a rewarding experience, and a pleasure.

I would also like to thank Professors John Hansman, Tom Herring, Walter Hollister, and Dr. Robert King for their contributions as members of my thesis committee. I appreciate their useful comments and the discussions that we have had. With their constructive criticisms I was able to produce a more robust dissertation.

In addition, I owe a great debt of thanks to the AMSAT community: Dr. Thomas Clark, Dr. Robert McGwier, and Jan King. Through them I became aware of the opportunities available through very small satellites, and was introduced to the fascinating amateur radio satellite community.

Over the years, I also received much assistance and advice from Drs. Rick Abbot and Sergei Gourevitch in the MIT Center for Space Research, and Kurt Feigl and Danan Dong from the MIT Department of Earth, Atmospheric, and Planetary Science. These four

men enthusiastically helped me out of the morass of software problems which I frequently encountered.

In addition, I have received much support from my friends, as well as help in the proofreading of this document. Therefore, I would like to thank Deanna Hiltner, Bill Irving, Anthony Joseph, and Jayant Sharma.

Finally, I wish to acknowledge the efforts and sacrifices made by my family, especially my parents Armando and Yolanda. *¡Hoy triunfamos!*

Biographical Note

Laureano Alberto Cangahuala was born in Pittsburgh, Pennsylvania on 18 September 1965. He graduated from Baldwin Township High School, Pittsburgh, Pennsylvania in 1983, and has attended the Massachusetts Institute of Technology since that year. He received B. S. degrees in Aeronautics and Astronautics, and in Earth, Atmospheric, and Planetary Sciences, in 1987, followed by the M. S. degree in Aeronautics and Astronautics in 1989. His graduate study has been supported by a National Science Foundation Minority Fellowship (1987 - 1990), and a National Defense Science and Engineering Fellowship (1990 - 1992), administered through the Phillips Laboratory at Hanscom AFB, Lexington, Massachusetts.

Table of Contents

Abstract 2

Acknowledgements 4

Biographical Note 6

Table of Contents 7

List of Figures 10

List of Tables 12

1. Introduction 14
   1.1 Modern Satellite Geodesy 15
      1.1.1 Positioning by Radio Interferometry 16
      1.1.2 Double-Differencing 18
      1.1.3 Mathematical Model 19
      1.1.4 Solution Algorithm 22
      1.1.5 Nautilus Network 25
   1.2 Description of GeoBeacons 26
   1.3 GeoBeacon Project History 28

2. Proposed Systems 30
   2.1 Introduction 30
   2.2 Design Assumptions 30
   2.3 Design Features 32
      2.3.1 GeoBeacon Frequency Allocations 32
      2.3.2 Uplink Antenna 36
      2.3.3 Propagation Losses 36
      2.3.4 Orbit Altitude 37
      2.3.5 Constellation Selection 38
         2.3.5.1 Use of Relative Mean Motion 38
         2.3.5.2 Polar Orbits 41
         2.3.5.3 Probability of Favorable Conditions with Coplanar Multiple Satellites 42
         2.3.5.4 Another 2-Satellite Constellation Possibility 47
      2.3.6 GeoBeacon Satellite Requirements and Microsat Spacecraft 48
         2.3.6.1 Antennas 49

2.3.6.2 Pointing Requirements 53
2.3.7 Carrier-to-Noise Ratio 56
2.3.7.1 Natural Noise Sources 57
2.3.7.2 Man-Made Noise Sources 57
2.3.7.3 Crosstalk Among Transmitters 60
2.3.8 Required Carrier-to-Noise Density Ratios 61
2.3.9 Required Transmitter Power 63

3. Comparison of GeoBeacons and GPS Positioning Capabilities 67
3.1 PDOP Comparison for Small Networks 68
3.2 PDOP Comparison for a California Network 72
3.3 Maximum Length Baseline in a Network 76
3.4 Maximum Measurement Density 78
3.4.1 Spatial Density 78
3.4.2 Temporal Density 79

4. Comparison of GeoBeacons and GPS Costs 80
4.1 Initial Cost Assumptions 80
4.2 Total Network Cost Comparison 83
4.3 User Cost Comparison 85

5. Demonstration Experiment 87
5.1 Experiment History 87
5.2 Experiment Configuration 88
5.2.1 Network Geometry 89
5.2.2 Bias-Resolution Strategy 91
5.3 Link Calculations 92
5.4 Transmitter Code 95
5.5 Covariance Analysis 101
5.5.1 Partial Derivatives With Respect to Non-Bias Parameters 101
5.5.2 Covariance Analysis Results 103
5.5.3 Consequences of Satellite and Network Selection 109

6. Recommendations for Further Research 113
6.1 Demonstrating the GeoBeacon System with Other Satellite Repeaters 113
6.2 Orbit Determination of Proposed GeoBeacon Satellites 115
6.3 Extending the GeoBeacon Concept to Other Bodies in the Solar System 117

7. Conclusions 119

Appendices 124
A. Uplink and Downlink Power Budgets 124
A.1 Uplink Budgets 127
A.2 Downlink Budgets 129

B. Analytic Expressions for Satellite Partial Derivatives 131

References 138

List of Figures

Figure 1.1	The Three Components of the GeoBeacons System	27
Figure 1.2	Schematic of a Proposed GeoBeacons Transmitter	28
Figure 2.1	Pegasus Payload Capabilities to Circular Polar Orbit	38
Figure 2.2	Footprints from Two GeoBeacon Satellites	39
Figure 2.3	Sky Plots Illustrating a Two-Satellite Pass, Set, and Session	40
Figure 2.4	Number of Passes & Sets of Passes Versus Satellite Overlap Time	41
Figure 2.5	Ground Track of Overlapping Satellite Footprints	43
Figure 2.6	GeoBeacon PDOP Versus Satellite Geocentric Angle of Separation	45
Figure 2.7	Two-Satellite Pass Duration Versus Geocentric Angle of Separation	46
Figure 2.8	Standard Microsat Exploded View	50
Figure 2.9	Satellite Footprint and Ground Transmitter Diagram	51
Figure 2.10	MITES Ant. Gain Pattern Versus Required Path Loss Compensation	52
Figure 2.11	Spacecraft Diagram	54
Figure 2.12	Torque Magnitudes Versus Satellite Boom Length	56
Figure 2.13	Estimated Ambient Noise Temperature as Seen from 1000 km Altitude	59
Figure 2.14	Crosstalk Interference Diagram	61
Figure 2.15	Mean Acquisition Time and Its Standard Deviation Versus $(C/N_0)_{req}$	63
Figure 2.16	Satellite Transmitter Power Versus Ground Transmitter Power and Receiving Dish Diameter	65 - 66
Figure 3.1	DOP Versus Network Latitude	70
Figure 3.2	Sky Plots of Two Simultaneously Visible GeoBeacon Satellites	71
Figure 3.3	Sites Considered for 'California' Network	73
Figure 3.4	PDOP Versus Observation Duration	75
Figure 3.5	Maximum Baseline Length Versus Network Latitude	77

Figure 4.1 Comparison of GPS and GeoBeacon Total System Costs 85
Figure 4.2 Comparison of GPS and GeoBeacon User Costs 86

Figure 5.1 Sky Plots for GOES-2, 5, 6, and 7 as Seen from the GORF Range 89
Figure 5.2 Layout of Ground Transmitters for Demonstration Experiment 91
Figure 5.3 Downlink Dish Diameter Versus Uplink Transmitter Power Tradeoff 94
Figure 5.4 Maximal Length Linear Feedback Shift Register 97
Figure 5.5 Partial Crosscorrelations of Candidate Sequences ..... 99 - 100
Figure 5.6 Bias Fixing through Multiple Iterations 105
Figure 5.7 Transmitter Position Formal Error Eigenvectors (GOES-2, 5, and 6) 106
Figure 5.8 Transmitter Position Formal Error Eigenvectors (GOES-2, 5, 6, and 7) 107
Figure 5.9 Satellite Position and Velocity Formal Errors ..... 108 - 109
Figure 5.10 Nominal Keplerian Orbital Elements and Sky Plots for Geosynchronous Satellite Covariance Investigation 110

List of Tables

Table 1.1	Types of Motions at the Earth's Surface	16
Table 1.2	Examples of Non-Bias Parameters	20
Table 1.3	GeoBeacons Demonstration Experiment Team	29
Table 2.1	Satellite-Based Positioning Systems and Signal Bandwidths	34
Table 2.2	GeoBeacon Candidate Frequency Allocations and Current Status	35
Table 2.3	Number of Satellites Required Versus Maximum Allowable PDOP and Probability That Adequate Satellite Spacing Is Not Encountered	47
Table 2.4	AMSAT Microsat Spacecraft Characteristics	49
Table 2.5	MITES Ant. Gain Pattern Versus Required Path Loss Compensation	52
Table 2.6	Required Ground and Satellite Transmitter Powers	64
Table 3.1	GPS Constellation ('18 + 3 Spare' Arrangement)	68
Table 4.1	Examples of Services To Be Provided by ORBCOMM	83
Table 5.1	Orbital Elements for GOES-2, 5, 6, and 7	88
Table 5.2	Uplink and Downlink Power Budgets for Demonstration Experiment	93
Table 5.3	Candidate Pseudorandom Sequences for Demonstration Experiment	96
Table 5.4	Effects of Satellite and Network Variations Upon Orbit and Station Estimation Errors	112
Table 6.1	Technical Requirements for Satellites used in the GeoBeacons System	115
Table 6.2	Proposed Low-Earth Orbit Mobile-Satellite Communication Systems	116
Table 6.3	Proposed Mars 'Double Coverage' Constellation	118

Table 7.1 Overall Comparison of GPS and GeoBeacon Systems 121

Table A.1 Uplink Power Budgets ..... 127 - 128

Table A.2 Downlink Power Budgets ..... 129 - 130

1. Introduction

Throughout the 1980's and into the 1990's, satellites of the Global Positioning System (GPS) have been launched into orbit by the United States. This constellation of satellites, through the signals it broadcasts towards the Earth, has provided many different opportunities to perform positioning and navigation on the Earth. One of these terrestrial applications is that of high accuracy relative positioning between points on the Earth's surface (hereafter referred to as geodetic positioning).

Despite the successes in geodetic positioning achieved with GPS, there is currently a logistical limit to the number of sites that can be monitored simultaneously with this system. There is a need to retrieve data from every receiver in the network, requiring periodic visits to each site, or the addition of an entire data retrieval system (land lines, radio links, or data relay satellites). At present, there is no inexpensive (relative to the cost of the GPS receiver) method to gather phase measurements in a GPS-based network.

Instead of using signals transmitted from GPS satellites, one could transmit signals from ground sites, through repeater satellites, to one site (hereafter referred to as the central site) located amidst the transmitters. At the central site the signal processing and calculations would be performed. All you would need at each site whose position was to be measured would be an inexpensive transmitter, and there would be no need to revisit any site after the initial transmitter deployment. The reduction in cost and visits per site would make monitoring larger networks easier, and is the motivation for this new system.

The object of this study is to design and to evaluate a space-based geodetic positioning system using repeater satellites (hereafter referred to as "GeoBeacons"), and to ascertain the conditions under which it could facilitate the study of crustal deformation. This study begins with an introduction to modern satellite geodesy and some of the

measurement techniques used by geodesists. After the presentation of this background material, a brief history of the project follows. Two low-cost prototype GeoBeacon designs are presented as baselines for systems evaluation. The positioning capabilities and costs of these two designs are then compared to a system which is already being deployed. Finally, after demonstrating the feasibility of a proposed 'proof of concept' experiment, a judgement is made of whether a GeoBeacons-type project should be initiated.

Prior to the design of any large measurement system, it is important to understand the background of the research to be performed and the impetus for creation of the new instrument. In this chapter we present an overview of the present 'state of the art' of geodetic positioning for crustal deformation monitoring, including relevant mathematical models. A least-squares-estimation algorithm used for high accuracy positioning is also presented. Following this overview, it is shown how satellite orbits as well as site positions can be estimated, without additional measurement sources. Finally, the rationale for the GeoBeacon system is shown, as well as a summary of work performed on the proof-of-concept experiment.

1.1 Modern Satellite Geodesy

The Earth is a dynamic body, and deforms in response to forces both terrestrial and extra-terrestrial in origin. These forces manifest themselves in motions that vary over several orders of magnitude, both spatially and temporally. Many of these forces cause both temporary and lasting deformations of the Earth's crust (see Table 1.1). Geodesy is the branch of science and mathematics which seeks an understanding of such phenomena by measuring changes in positions of points on the Earth's surface.

MOTION	SECULAR	TRANSIENT
HORIZONTAL	Plate Motion Boundary-zone tectonics Post-glacial Rebound Intraplate Deformation	(Pre, co, post)-seismic Fault Creep Stress Redistribution
VERTICAL	Tectonic Motions Thermal Subsidence Crustal Loading Post-glacial Rebound Water Withdrawal	(Pre, co, post)-seismic Magma Inflation Tidal Loading

Table 1.1 Types of Motions at the Earth's Surface[1]

1.1.1 Positioning by Radio Interferometry

The main geodetic tool which has enabled present-day crustal motion to be observed is Very Long Baseline Interferometry (VLBI). A relative position vector between two sites, known as an interferometer baseline, is determined by making simultaneous observations at each site of radio signals emitted by quasars.

A radio telescope is needed at the end of each baseline, as well as a hydrogen maser frequency source to time-tag the received signals, so it is expensive to observe many baselines. A major advance in interferometry came in using artificial earth satellites as sources of radio signals instead of quasars[2]. Since the launch of Sputnik, radio

[1]Mueller, I. I. and Zerbini, S., eds., *The Interdisciplinary Role of Space Geodesy*, Lecture Notes in Earth Sciences, Springer-Verlag Publishers, 1989, Chapter 3.

[2]The first use of signals from GPS satellites for geodetic positioning was reported in Counselman III, C. C. and Gourevitch, S. A., "Miniature Interferometer Terminals for Earth Surveying: Ambiguity and

transmissions from satellites had been used to determine the Earth's gravitational potential, as well as other parameters which affect satellite orbits[3]. At the Earth's surface, one can obtain a higher signal-to-noise ratio with signals from satellites than those from quasars, using a much smaller (and less expensive) radio antenna.

The satellites whose signals are most used for geodetic measurements are those of the Global Positioning System (hereafter referred to as GPS). When fully deployed, the GPS constellation will be made up of 21 satellites (plus 3 spares). GPS satellites broadcast signals in two bands of frequencies. A user on the ground, upon acquiring the signals from at least four GPS satellites, is able to determine his position within seconds with an accuracy of the order of tens of meters. From these signals, measurements (known as pseudoranges) are made of the ranges from the user to the observed satellites (these estimates include an unknown time offset in the ground receiver that must also be estimated with the position). The accuracy of such a nearly instantaneous position determination is limited by the resolution with which the time delay of the coded modulation of the GPS radio signals can be estimated.

For the most precise geodetic position determination, observations of the phase of the carrier (actually the reconstructed carrier from the modulated GPS signal) are used. By using these phase measurements in linear combinations which cancel common mode errors, in a technique known as double differencing[4], it is possible to determine relative baseline vectors between GPS receivers to within one part in 10^8.

Multipath with Global Positioning System," in *IEEE Transactions on Geoscience and Remote Sensing*, Vol. GE-19, No. 4, October 1981.

[3]First reported in Brown, R. R., *et al.*, "Radio Observations of the Russian Earth Satellite," *Proc. IRE*, 45, 1552-1553, 1957, and Peterson, A. M., "Radio and Radar Tracking of the Russian Earth Satellite," *Proc. IRE*, 45, 1553-1555, 1957.

[4]The earliest known reference to the use of doubly differenced carrier phase is Counselman III, C. C., *et al.*, "Astronomical Applications of Differential Interferometry," *Science*, Vol. 178, pp. 607-608, November 10, 1972.

1.1.2 Double-Differencing

The phase of a signal measured from a satellite i at a ground site j has contributions from many sources[5], including a random transmitter and receiver phase component:[6]

$$\phi^{i}_{jk}(t_j) = - f_k(t_j)\,\tau^{i}_{j}(t_j) + \phi^{i}_{j\ neu}(t_j) + \phi^{i}_{j\ clock}(t_j) + \frac{\kappa^{i}_{j}}{f_k(t_j)} + b^{i}_{jk} + \nu^{i}_{jk}(t_j) \tag{1.1}$$

$$\tau^{i}_{j}(t_j) = \frac{\left| s^{i}(t_j) - r_j\left[t_j - \tau^{i}_{j}(t_j)\right]\right|}{c} \tag{1.2}$$

where

ϕ^{i}_{jk} Carrier one way phase observable

k Signal frequency index (1 to # of frequencies)

t_j Signal reception time

$f_k(t_j)$ Signal frequency

τ^{i}_{j} Signal travel time (in vacuum) between satellite i and receiver j

r_j Ground station j position vector

s^i Satellite i position vector

$\phi^{i}_{j\ clock}$ Random transmitter and receiver phase offsets (due to oscillator instabilities)

$\phi^{i}_{j\ neu}$ Phase delay due to neutral atmosphere along signal propagation path

κ^{i}_{j} Ionospheric phase contribution

---

[5]In this overview, the 'i' superscripts refer to satellites, and the 'j' subscripts will refer to ground stations, unless otherwise indicated.

[6]King, R. W., *et al.*, *Surveying With GPS*, Monograph 9, School of Surveying, The University of New South Wales, Kensington, N.S.W. Australia, 1985.

b_j^i Integer cycle component

ν_j^i Measurement error and phase contributions from unmodeled effects

Differencing the phases of the signals received simultaneously at one station from two satellites results in an observable whose random receiver phase contribution is canceled. Likewise, differencing phases of signals sent by a satellite to two stations cancels the satellite phase contribution. Simultaneously differencing both satellites and transmitters cancels both transmitter and receiver phase errors. This technique is known as double differencing, and the observable created is known as the double difference observable. For signal propagation paths which pass through essentially the same portion of the troposphere and ionosphere, i.e., for line-of sight vectors from satellites to receivers located within less than ~1 km on the Earth's surface, the ionospheric and tropospheric phase contributions to different phase observations nearly cancel when differenced between stations[7]. Equation (1.3) presents the one-way phase observable with the contributions which remain after double differencing. Only the integer portion of b_j^i remains; it is renamed the 'bias' (n_j^i) (for the i^{th} satellite pair and the j^{th} station pair).

$$\phi_{jk}^{i}(t_j) = -f_k \tau_j^{i}(t_j) + n_{jk}^{i} + \nu_{jk}^{i}(t_j) \qquad (1.3)$$

An integer bias is present because there is no way, *a priori*, for the receivers at both sites to identify the same carrier cycle.

1.1.3 Mathematical Model

As expressed in Equation 1.1, the phase observation is a non-linear function of many parameters (*e.g.* satellite and ground station positions). However, if sufficiently

---

[7] κ_j^i is inversely proportional to frequency, so signals from at least two well spaced frequencies are needed to distinguish the ionospheric contribution from other contributions. The details of ionospheric phase estimation will not be included in this overview.

accurate *a priori* values of these unknown parameters are available, a linear relation between observation deviation and parameter deviation from these values can be established. Once this relationship is obtained, a linear-estimation solution can be calculated which minimizes the sum of the squares of the calculated observation residuals. Let **y** be the observation deviation vector (observed minus calculated (using *a priori* parameter values) one way phases), and let **x** be the parameter deviation vector. If we substitute these vectors into Equation 1.1, expand it in a Taylor series, and discard all terms higher than first order, we are left with the linear theoretical relation

$$\mathbf{y} = \tilde{\mathbf{A}}\,\mathbf{x} + \mathbf{v} \tag{1.4}$$

where

$\tilde{\mathbf{A}} = \dfrac{\delta \mathbf{y}}{\delta \mathbf{x}}$ Matrix of partial derivatives of observable phases with respect to parameters of interest (to be discussed in further detail)

$\mathbf{v}$ Vector of observation errors

The parameters to be estimated are divided into two groups, the integer bias ambiguities **n** and the non-bias parameters $\mathbf{x}_{nb}$ (see Table 1.2).

NON-BIAS PARAMETERS	EXAMPLE
Ground Station Coordinates	Geocentric Latitude, Longitude, and Radius
Satellite Position and Velocity (at Epoch t_0)	$\left(x^i\ y^i\ z^i\ \dot{x}^i\ \dot{y}^i\ \dot{z}^i\right)_{t=t_0}$ (in Earth-Centered Inertially Nonrotating Frame)
Tropospheric Phase Delay	Zenith Delay (used by a model to predict delays at lower elevation angles)

Table 1.2 Examples of Non-Bias Parameters

Using the doubly differenced phase as the new observable, the linearized observation equation is now

$$\mathbf{D}\,\mathbf{y} = \mathbf{D}\,\tilde{\mathbf{A}}\,\mathbf{x} + \mathbf{D}\,\mathbf{v} = \mathbf{D}\left[\mathbf{A}\ \mathbf{I}\right]\begin{bmatrix}\mathbf{x}_{nb}\\ \mathbf{n}\end{bmatrix} + \mathbf{D}\,\mathbf{v} \tag{1.5}$$

where

r = Number of stations

s = Number of satellites

r s = Number of one-way carrier phase observations

(r-1) (s-1) = Number of linearly independent double-difference observables

and **D** is the double-difference operator, with dimensions [(r-1) (s-1) × rs]. **Dy** has dimensions [(r-1) (s-1) × 1], and $\mathbf{D}\tilde{\mathbf{A}}$ has dimensions [(r-1) (s-1) × (# of non-bias parameters + (r-1) (s-1))].

The details of **D** will be elaborated upon in section 1.1.4. With equally weighted one-way phase measurements with measurement rms error σ and covariance matrix

$$\Sigma_v = \sigma^2\mathbf{I}, \tag{1.6}$$

the double-difference observation error covariance matrix is no longer diagonal.

$$\Sigma_{Dv} = \sigma^2\mathbf{D}\mathbf{D}^T \tag{1.7}$$

Assuming that the set of integer biases to be solved for is the complete set of biases formed by the double-difference operator **D**, the normal equations can be expressed as

$$\sum_{n=1}^{N}\left\{\begin{bmatrix} \mathbf{N}_{11} & \overline{\mathbf{N}}_{21}^{T} \\ \overline{\mathbf{N}}_{21} & \overline{\mathbf{N}}_{22} \end{bmatrix}\right\}\begin{bmatrix} \mathbf{x}_{nb} \\ \mathbf{Dn} \end{bmatrix} = \sum_{n=1}^{N}\left\{\begin{bmatrix} \mathbf{u}_1 \\ \mathbf{u}_2 \end{bmatrix}\right\} \tag{1.8}$$

where

N= Number of observation epochs

$$\mathbf{N}_{11} = \mathbf{A}^T \mathbf{D}^T \Sigma_{Dv} \mathbf{D}\ \mathbf{A} = \sigma^2 \mathbf{A}^T \mathbf{D}^T (\mathbf{D}\ \mathbf{D}^T)^{-1} \mathbf{D}\ \mathbf{A}$$

$$\overline{\mathbf{N}}_{21} = \mathbf{D}^T \Sigma_{Dv} \mathbf{D}\ \mathbf{A} = \sigma^2 \mathbf{D}^T (\mathbf{D}\ \mathbf{D}^T)^{-1} \mathbf{D}\ \mathbf{A}$$

$$\overline{\mathbf{N}}_{22} = \mathbf{D}^T \Sigma_{Dv} \mathbf{D} = \sigma^2 \mathbf{D}^T (\mathbf{D}\ \mathbf{D}^T)^{-1} \mathbf{D}$$

$$\mathbf{u}_1 = \sigma^2 \mathbf{A}^T \mathbf{D}^T (\mathbf{D}\ \mathbf{D}^T)^{-1} \mathbf{y}$$

$$\mathbf{u}_2 = \sigma^2 \mathbf{D}^T (\mathbf{D}\ \mathbf{D}^T)^{-1} \mathbf{y}$$

The least squares estimate $\hat{\mathbf{x}}$ and estimate covariance $\Sigma_{\hat{\mathbf{x}}}$ are

$$\hat{\mathbf{x}} = (\tilde{\mathbf{A}}^T \mathbf{D}^T (\mathbf{D}\ \mathbf{D}^T)^{-1} \mathbf{D}\ \tilde{\mathbf{A}})^{-1} \tilde{\mathbf{A}}^T \mathbf{D}^T (\mathbf{D}\ \mathbf{D}^T)^{-1} \mathbf{D}\ \mathbf{y} \tag{1.9}$$

$$\Sigma_{\hat{\mathbf{x}}} = \sigma^2 (\tilde{\mathbf{A}}^T \mathbf{D}^T (\mathbf{D}\ \mathbf{D}^T)^{-1} \mathbf{D}\ \tilde{\mathbf{A}})^{-1} . \tag{1.10}$$

1.1.4 Solution Algorithm

Historically, the first computer code to generate doubly differenced observables for geodetic positioning was developed at MIT, for determining positions of ALSEP (Apollo Lunar Surface Experiments Package) telemetry transmitters on the Lunar surface[8,9]. That software evolved into the GAMIT (GPS at MIT) software package[10], which is one of

---

[8]Counselman III, *et al.*, "Astronomical Applications of Differential Interferometry," *Science*, Vol. 178, pp. 607-608, November 10, 1972.

[9]Counselman III, *et al.*, "Precision Selenodesy via Differential Interferometry," *Science*, Vol. 181, pp. 772-774, August 11, 1973.

[10]The GAMIT software is maintained by the MIT Department of Earth, Atmospheric, and Planetary Sciences, and the Institute of Geophysics and Planetary Physics at the University of California, San Diego.

several packages currently available. The following example demonstrates how the GAMIT software creates least-squares estimates of position from one-way phase observations.

Consider four stations observing three satellites at one epoch. The resulting one-way observation vector is

$$\mathbf{y}^T = \left[\phi_1^1 \; \phi_1^2 \; \phi_1^3 \; \phi_2^1 \; \phi_2^2 \; \phi_2^3 \; \phi_3^1 \; \phi_3^2 \; \phi_3^3 \; \phi_4^1 \; \phi_4^2 \; \phi_4^3 \right] \tag{1.11}$$

As before, subscripts denote station number and superscripts denote satellite number.

In the GAMIT software, double-differences are formed from one way observations from one satellite pair and one station pair. A single difference for each satellite is created by subtracting the one way phase measurements of each station. These two single differences are themselves differenced to create the double difference observable. With (r-1) station pairs and (s-1) satellite pairs, (r-1)(s-1) double differences are formed. Stations in this case are ordered such that the baseline between stations 1 and 2 is the shortest in the network, the baseline between stations 2 and 3 is the shortest baseline in the network with station 1 removed, etc. As a result of this ordering, when double differences are formed, the station pairs that are used are stations 1 & 2, 2 & 3, ... , (r-1) & r, with each succeeding station pair having a greater baseline length. This ordering makes bias parameter determination more convenient, as will be shown in the following section.

For illustrative purposes, the vector **y** may be arranged in a matrix such that stations correspond to rows and satellites correspond to columns, so it will be easier to show how

---

For more details on GAMIT estimation algorithms, the reader is referred to Bock, Y., *et al.*, "Interferometric Analysis of GPS Phase Observations," *Manuscripta Geodaetica*, Vol. 11, pp. 282 - 288, 1986, and Schaffrin, B., and Bock, Y., "A Unified Scheme for Processing Phase Observations," *Bulletin Geodesique*, Vol. 62, pp. 142 - 160, 1988.

the one-ways are incorporated into the double-differences. So if we use the following arrangement

$$\begin{bmatrix} \phi_1^1 & \phi_2^1 & \phi_3^1 \\ \phi_1^2 & \phi_2^2 & \phi_3^2 \\ \phi_1^3 & \phi_2^3 & \phi_3^3 \\ \phi_1^4 & \phi_2^4 & \phi_3^4 \end{bmatrix}$$

the addition and subtraction of one way phases to form the double difference observable can be shown by corresponding 1's and -1's. A '1' denotes an added phase, a '-1' denotes a subtracted phase, and x's denote unused measurements. The phase coefficients of the six double differences are

$$\begin{bmatrix} -1 & 1 & x \\ 1 & -1 & x \\ x & x & x \\ x & x & x \end{bmatrix}$$ Stations 1,2 Satellites 1,2

$$\begin{bmatrix} x & x & x \\ -1 & 1 & x \\ 1 & -1 & x \\ x & x & x \end{bmatrix}$$ Stations 2,3 Satellites 1,2

$$\begin{bmatrix} x & x & x \\ x & x & x \\ -1 & 1 & x \\ 1 & -1 & x \end{bmatrix}$$ Stations 3,4 Satellites 1,2

$$\begin{bmatrix} -1 & x & 1 \\ 1 & x & -1 \\ x & x & x \\ x & x & x \end{bmatrix}$$ Stations 1,2 Satellites 1,3

$$\begin{bmatrix} x & x & x \\ -1 & x & 1 \\ 1 & x & -1 \\ x & x & x \end{bmatrix}$$ Stations 2,3 Satellites 1,3

$$\begin{bmatrix} x & x & x \\ x & x & x \\ -1 & x & 1 \\ 1 & x & -1 \end{bmatrix}$$ Stations 3,4 Satellites 1,3

and the **D** generated is

$$\mathbf{D}_{\text{GAMIT}} = \begin{bmatrix} -1 & 1 & 0 & 1 & -1 & 0 & 0 & 0 & 0 & 0 & 0 & 0 \\ 0 & 0 & 0 & -1 & 1 & 0 & 1 & -1 & 0 & 0 & 0 & 0 \\ 0 & 0 & 0 & 0 & 0 & 0 & -1 & 1 & 0 & 1 & -1 & 0 \\ -1 & 0 & 1 & 1 & 0 & -1 & 0 & 0 & 0 & 0 & 0 & 0 \\ 0 & 0 & 0 & -1 & 0 & 1 & 1 & 0 & -1 & 0 & 0 & 0 \\ 0 & 0 & 0 & 0 & 0 & 0 & -1 & 0 & 1 & 1 & 0 & 1 \end{bmatrix} \tag{1.12}$$

The double difference weighting matrix $\mathbf{D}^T(\mathbf{D}\,\mathbf{D}^T)^{-1}\mathbf{D}$ is used in the normal equations (see Equation 1.8):

$$\left(\mathbf{D}^{\mathrm{T}}\left(\mathbf{D}\mathbf{D}^{\mathrm{T}}\right)^{-1}\mathbf{D}\right)_{\mathrm{GAMIT}} = \frac{1}{12}\begin{bmatrix} 6 & -3 & -3 & -2 & 1 & 1 & -2 & 1 & 1 & -2 & 1 & 1 \\ -3 & 6 & -3 & 1 & -2 & 1 & 1 & -2 & 1 & 1 & -2 & 1 \\ -3 & -3 & 6 & 1 & 1 & -2 & 1 & 1 & -2 & 1 & 1 & -2 \\ -2 & 1 & 1 & 6 & -3 & -3 & -2 & 1 & 1 & -2 & 1 & 1 \\ 1 & -2 & 1 & -3 & 6 & -3 & 1 & -2 & 1 & 1 & -2 & 1 \\ 1 & 1 & -2 & -3 & -3 & 6 & 1 & 1 & -2 & 1 & 1 & -2 \\ -2 & 1 & 1 & -2 & 1 & 1 & 6 & -3 & -3 & -2 & 1 & 1 \\ 1 & -2 & 1 & 1 & -2 & 1 & -3 & 6 & -3 & 1 & -2 & 1 \\ 1 & 1 & -2 & 1 & 1 & -2 & -3 & -3 & 6 & 1 & 1 & -2 \\ -2 & 1 & 1 & -2 & 1 & 1 & -2 & 1 & 1 & 6 & -3 & -3 \\ 1 & -2 & 1 & 1 & -2 & 1 & 1 & -2 & 1 & -3 & 6 & -3 \\ 1 & 1 & -2 & 1 & 1 & -2 & 1 & 1 & -2 & -3 & -3 & 6 \end{bmatrix} \tag{1.13}$$

1.1.5 Nautilus Network

In order to obtain meaningful position estimates, it is necessary to have accurate orbit estimates. If the integer biases of the double differences created are determined, the orbital parameter estimate covariances decrease. Assigning fixed integer values to these parameters is known as 'fixing' the biases. In an experiment performed by Abbot *et al.*[11], a dozen receivers were arranged in a logarithmic 'Nautilus' spiral, with baseline lengths ranging from 10 to 320 km. A bootstrapping strategy was used to solve for the unknown bias parameters. First, biases for the more closely spaced stations were fixed. This reduced the uncertainty of the orbit determination sufficiently so that biases for more widely spaced stations could be fixed. This procedure was repeated until all the bias parameters were fixed. With this arrangement of stations, it was possible to determine the biases, the relative station positions, and GPS satellite orbits accurately using a few hours of observations, without orbit information from outside sources[12]. The station position determinations had precisions of 2 mm in horizontal coordinates.

---

[11]Abbot, R. I., *et al.*, "GPS Orbit Determination: Bootstrapping to Resolve Carrier Phase Ambiguity," in *Proc. Fifth Intl. Geodetic Symposium on Satellite Positioning*, Vol. I, pp. 224-233, March, 1989.
[12]Counselman III, C. C., "Ambiguity Bootstrapping to Determine GPS Orbits and Baselines," Report No. GL-TR-89-0278, Geophysics Laboratory, Air Force Systems Command, 11 pp., October 10, 1989.

This spiral arrangement of stations does not necessarily aid in obtaining geophysical information in a geodetic survey. However, in cases where the satellites have little apparent motion in the sky, satellite partial derivatives with respect to satellite orbit parameters are nearly constant. Bootstrapping across a wide range of baselines in the Nautilus network makes bias-fixing possible in such cases. This possibility will be elaborated upon in Chapter 5.

1.2 Description of GeoBeacons

The following is a description of a candidate space project to perform millimeter-level-accuracy positioning on the Earth's surface by means of repeater satellites. Figure 1.1 shows radio signals from transmitters located at remote ground sites being received by repeater satellites in low Earth orbit, then rebroadcast to the central site. Upon reception at the central site, the signals are processed and transmitter positions (baseline vectors of transmitter sites) are estimated. This strategy for performing geodetic measurements has been nicknamed 'GeoBeacons,' for the beacon-like character of the ground transmitters. The primary objective of the design process undertaken in this study and described in Chapter 2 has been to make the implementation of a 'demonstration' system as inexpensive as possible. This end is achieved by minimizing the complexity and cost of the ground transmitters, central site, and required satellites.

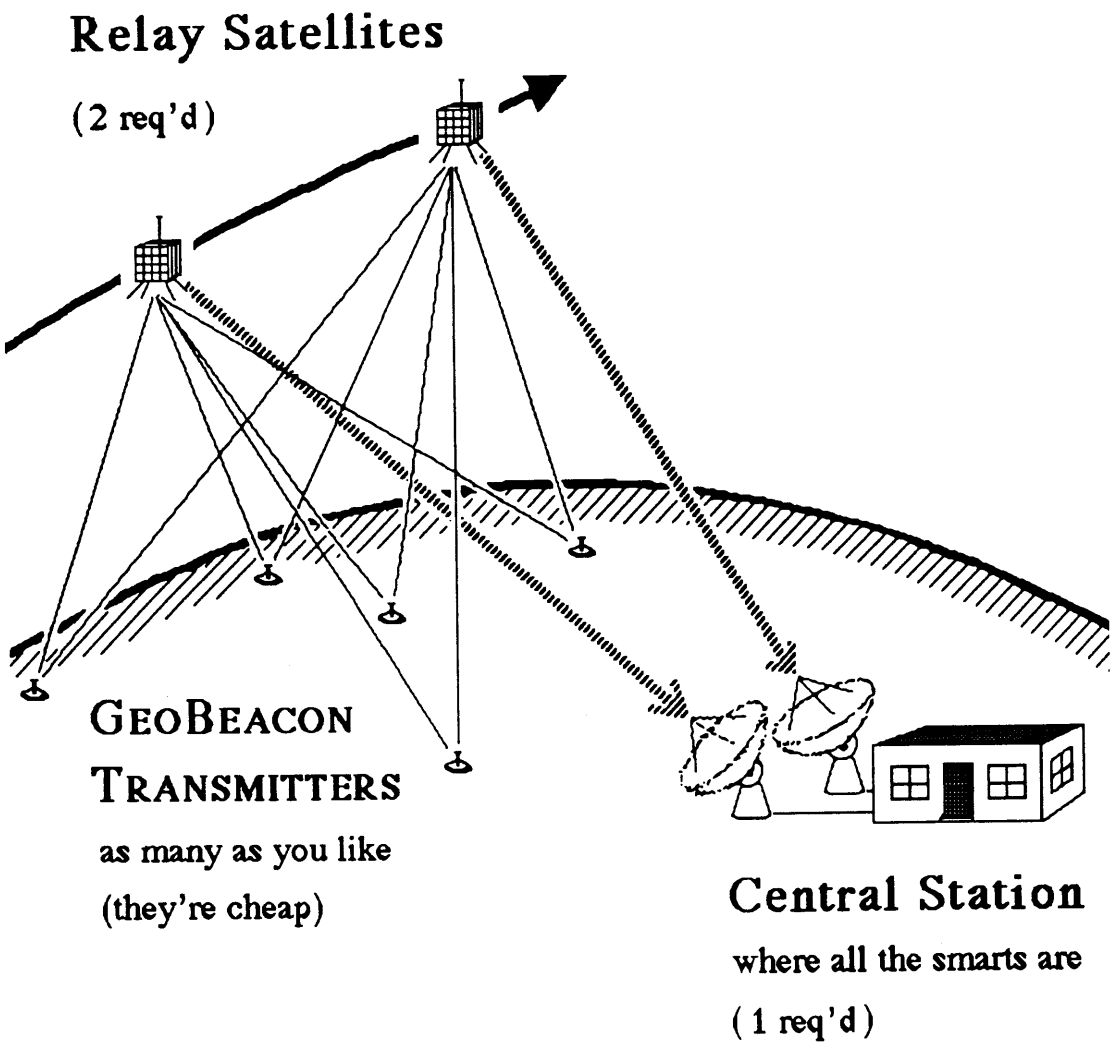

Figure 1.1 The Three Components of the GeoBeacons System

Figure 1.2 shows a prototype GeoBeacons transmitter. One crystal oscillator is used as the frequency source for signals at frequencies f_1 and f_2. Each transmitter will have a unique code so that the signal from each transmitter can be identified at the central site. The GeoBeacon transmitter is similar to the Emergency Locator Transmitter (ELT) used in the SARSAT (Search And Rescue Satellite-Aided Tracking) system. ELTs are commercially available at present for $100.

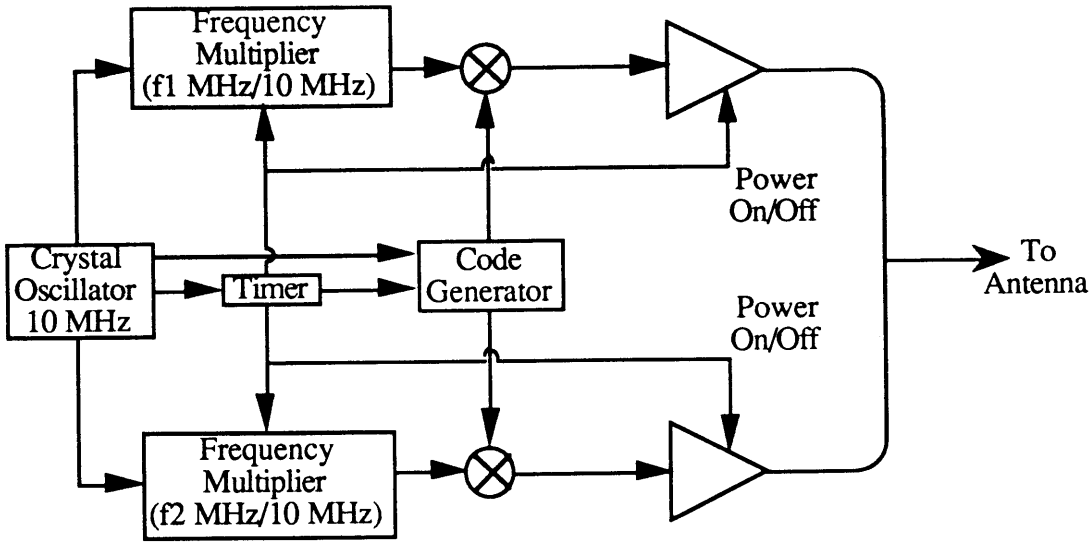

Figure 1.2 Schematic of a Proposed GeoBeacon Transmitter
(Broadcasting at 2 Frequencies)

The repeater satellites would receive signals from the transmitters in view, and rebroadcast them down to the Earth's surface. No processing or calculation would be performed on board the satellite. At the central station, there would be one receiving dish per satellite in view. Only at this site would signal processing be performed.

1.3 GeoBeacon Project History

Although not an operating system, the GeoBeacons project has received attention from the geodetic community over the past three years. In addition to the strawman design presented in this study, the groundwork was laid for a proof-of-concept experiment.

Through a series of meetings throughout 1990, interested people from MIT, the amateur radio satellite community (through AMSAT-NA, the Radio Amateur Satellite Corporation of North America), the Crustal Dynamics Project of NASA / Goddard, and Interferometrics, Inc. of Vienna, VA (see Table 1.3) planned and began work on an experiment to demonstrate the feasibility of the GeoBeacons concept. This experiment was to incorporate all three parts of the GeoBeacon plan: inexpensive transmitters, repeaters in orbit, and a central site where all of the processing would be performed. The role of the

GeoBeacon repeaters was to be played by GOES (Geostationary Operational Environmental Satellite) transponders. Through these meetings, many details of the experiment (which will be presented in Chapter 5) were researched.

AMSAT-NA	Dr. Roger Allshouse Jan King Dr. Bob McGwier
Interferometrics, Inc.	Dr. Dino Lorenzini Dr. Nancy Vandenberg
MIT	Al Cangahuala Prof. Charles Counselman Prof. Tom Herring
NASA / Goddard	Dr. Tom Clark

Table 1.3 GeoBeacons Demonstration Experiment Team

2. Proposed Systems

Two strawman designs of a GeoBeacons system are presented here as low-cost systems worthy of consideration for systems evaluation. In each case, all satellites are installed in orbit by a single launch vehicle. One of these designs (hereafter referred to as the '2-sat' configuration) uses only two satellites, the absolute minimum number required to perform geodetically valuable measurements. The other design (referred to as the 'Multi-sat' configuration) incorporates more satellites, in order to provide more frequent measurement opportunities.

2.1 Introduction

In the remainder of this chapter, initial design assumptions for prototype GeoBeacon systems are presented and justified. The design features are then described. These include candidate frequency allocations, altitude, inclination, spacing and design of satellites in the GeoBeacon constellation, the expected radio noise environment, and the estimated ground and satellite transmitter power requirements. The power link budgets, which reflect the design decisions made in this chapter, are presented in Appendix A.

2.2 Design Assumptions

It is important to define and state clearly the set of initial assumptions in an iterative design process, such as for the GeoBeacon system. With too few assumptions, it becomes difficult to identify important design tradeoffs, and the design fails to converge. With too many assumptions, the design becomes too restricted, and the designer may (incorrectly) conclude that a particular set of mission goals is not possible. Also, it is important to understand which assumptions are critical, i.e. controlling the design and/or limiting system performance.

There are four primary assumptions in this study. The first assumption is a fixed technical requirement that involves the minimum number of satellites needed to perform useful geodetic measurements. As shown in the introductory chapter, in order to cancel GeoBeacon transmitter-related random phase shifts, it is necessary to observe a transmitter simultaneously through two satellites, differencing the observed phases. Therefore, the proposed GeoBeacon satellite constellation must consist of at least two satellites which must be simultaneously visible at both transmitters as well as at the central site.

The second assumption is another technical requirement. In order to separate the ionospheric phase contribution from the geometric contribution to the phase measurements, it is necessary to receive signals simultaneously at two different frequencies. It is preferred that these frequencies be well separated in order to better separate the geometric and ionospheric components of the received signal phases.

The third assumption is a desire to minimize the total cost of the system to the user. There are actually two classes of users that are considered in this study: (i) organizations that finance the total project (satellites and their launch, central and remote site hardware and operating costs), and (ii) groups that take advantage of the positioning service (and pay for only operating costs). In order to minimize launch costs, I assume that all the satellites needed will be delivered into orbit with one small launch vehicle. While no specific launch vehicle has been selected for the '2-sat' design, it has been shown that up to 16 small (~ 10 kg) spacecraft can be launched aboard a Pegasus launch vehicle.[1] The Pegasus has also been chosen as the launch vehicle for NASA's Explorer program[2], through which the GeoBeacon concept may be tested. For the system users, we seek to minimize transmitter cost through the elimination of pointing and timing requirements, and the minimization of

---

[1]Cangahuala, L. A., *et al.*, "GeoBeacon Satellite Orbit and Launch Possibilities," *Eos*, Vol. 71, p. 1277, 1990.
[2]Baker, D. N., *et al.*, "NASA's Small Explorer Program," *Physics Today*, Vol. 44, No. 12, pp. 44-51, December 1991.

required transmitter power.

Since the GeoBeacon system will be using phase measurements as is done in GPS-based geodesy, the final assumption is that the rms phase errors obtained through GeoBeacons will be the same as or smaller than those obtained with GPS for the same network. No new significant error sources will be introduced.

2.3 Design Features

The details of the two GeoBeacon configurations are presented in this section. Factors relevant to the calculation of the power link budgets are also shown. The aim of this section is to show that the required ground transmitter and satellite transmitter power are reasonable for a low-cost system.

2.3.1 GeoBeacon Frequency Allocations

In an earlier attempt to calculate GeoBeacon uplink-power budgets, frequencies from 100 MHz to 100 GHz were considered[3]. In that study, it was assumed that signals at more than one frequency allocation would be used. Lower frequency signals, easier to acquire initially, would aid the acquisition of higher frequency signals. For signals being received at the same signal-to-noise ratio, the higher frequency signal yields smaller rms phase errors (in units of distance).

An issue that was not explicitly considered in that study was the constraint placed upon frequency allocations by international regulations. In 1992, the international radio community at the World Administrative Radio Conference (WARC-92) reassigned many bandwidth slots, especially in the 500 - 3000 MHz range, to accommodate mobile and satellite-based communication services. It is not yet clear what the size and number of

---

[3]Cangahuala, L. A., "Feasibility of Millimeter-Accuracy Geodetic Positioning and Vehicle Tracking with Repeater Satellites," AFGL Report GL-TR-89-0231, 27 July 1989.

'Earth-to Space' and 'Space-to-Earth' allocations will be. Assuming that allocations currently used by existing space-based positioning systems will be preserved, frequency allocations (available to civilian users) for these systems may be considered as possibilities (see Table 2.1).

System	Sponsoring Agencies	Uplink Frequencies (Bandwidth)	Downlink Frequencies (Bandwidth)	Comments
Argos	CNES (France) NASA, NOAA	401.65 MHz (??)	N. A.	Operational Since 1978
CICADA[4]	USSR	None	150, 400 MHz (52 kHz, unmodulated)	Similar to TRANSIT
COSPAS / SARSAT[5]	Multi-national	121.5, 243 MHz (25, 50 kHz)	None	Operational since 1982
DORIS[6]	CNES (France)	401.25, 2036.25 MHz	None	Operational since 1990
GeoStar[7]	Geostar Corp. (USA)	1618 MHz (16 MHz)	2492 MHz (16 MHz)	Proposed
GLONASS	USSR	None	1246 + 7k/16, 1602 + 9k/16 MHz (10.22, 10.22 MHz) k: satellite index (1 - 24)	13 of 24 in operation as of April 1991[8]
GPS	US DoD	None	1227.6, 1575.42 MHz (20.46, 20.46 MHz)	16 of 24 in operation as of April 1992
NAVSAT[9]	ESA	None	1596 MHz (20 MHz)	Proposed
PRARE[10]	Germany	7.2 GHz (10 MHz)	2.2, 8.5 GHz (1, 10 MHz)	Failed
Transit	US Navy	None	150, 400 MHz	Civil use since 1964

Table 2.1. Satellite-Based Positioning Systems and Signal Bandwidths

---

[4]Wood, C. D., and Perry, G. E., "The Russian Satellite Navigation System," *Phil. Trans. R. Soc. Lond.* A Vol. 294, pp. 307-315, 1980.

[5]There is a series of papers on the SARSAT system by C. R. Carter, *et al.*, in *IEEE Transactions on Aerospace and Electronic Systems*, from 1985 to the present.

[6]Dorrer, M, *et al.*, "DORIS: System Assessment Results with DORIS on SPOT 2", IAF 90-336, 1990.

[7]Richards, R. T., and Snively, L. O., "Geostar Positioning Analysis," *Proceedings of IEEE PLANS '86*, pp. 13-19, 1986.

[8]GLONASS Update, *The ION Newsletter*, The Institute of Navigation, Spring 1991.

[9]Rosetti, C., "Annex: Satellite Land Navigation - Dreams and Reality," *Proceedings of Nav-85 Conference, Land Navigation and Location for Mobile Applications*, Royal Institute of Navigation, 1985.

[10]Mueller, I. I., and Zerbini, S. (eds.), *The Interdisciplinary Role of Space Geodesy*, Vol. 22, Lecture Notes in Earth Sciences, pp. 161-162, 1989.

Since we seek especially to minimize the required uplink transmitter power for the user, positioning accuracy may become uplink limited. Because of this constraint, the choice of uplink allocations is more important than that of downlink allocations. An existing system whose frequency allocations could prove useful for GeoBeacons is DORIS (Doppler Orbitography and Radiopositioning Integrated from Space). The roughly 5:1 ratio of the two DORIS ground beacon uplink frequencies will aid in ionosphere correction. Dr. Tom Clark of NASA/Goddard and former president of AMSAT, Inc., suggested using these allocations during the 1990 Fall AGU meeting[11].

Two candidate downlink frequencies were also chosen, based upon their previous use in other space-based positioning applications and their current designations by the International Telecommunications Union[12]. Table 2.2 lists the uplink and downlink frequency choices, the bandwidth of the proposed signals, and notes relevant to the use of these allocations. The proposed bandwidths for the coded uplink signals are intended to use a fraction of the allotted bandwidth commensurate with that used by existing systems in Table 2.1.

	Proposed Frequency (MHz)	Proposed Bandwidth (MHz)	Allotted Bandwidth (MHz)	International Designation and Comments
Uplink	401	0.1	401-403	"Earth Exploration Satellite (Earth-to-space)." Allocation applies to all regions of the world.
	2036	1.0	2025-2110	"Earth Exploration Satellite Service (uplink & downlink) In accordance w/ intl. provisions 2557-2560[13].
Downlink	1596	0.1	1559-1610	"Radionavigation Satellite (space-to-Earth)." (1550-1645.5 MHz) used by some nations for fixed services.
	2200	1.0	2200-2290	"Earth Exploration Satellite Service (uplink & downlink) In accordance w/ intl. provisions 2557-2560.

Table 2.2 GeoBeacon Candidate Frequency Allocations and Current Status

[11]Personal communication.
[12]Code of Federal Regulations, Title 47, Chapter 1, Part 2, Subpart B, 1988.
[13]These provisions list the allowable power flux-densities at the Earth's surface from artificial satellites.

2.3.2 Uplink Antenna

Signals at the two uplink allocations will be transmitted through a simple wide-beamwidth antenna to the satellites. In this study, an optimal antenna beam pattern was not selected. However, any candidate beam pattern should be (i) symmetrical about the vertical axis, (ii) have maximum gain at a zenith angle between 40° and 60°, and (iii) have low gain at very low elevation angles, in order to minimize multipath interference. One pattern which meets these criteria is that of Counselman's MITES antenna design[14]:

$$G \begin{cases} \cong 1.23\,(1 + \cos(z))^2 \sin^2\left(\frac{3\pi}{4}\cos(z)\right) & 0° \le z \le 90° \\ \cong 0 & z > 90°,\ z = \text{zenith angle} \end{cases} \qquad (2.1)$$

The MITES antenna pattern has a peak gain at an elevation angle of ~50°. The sharp drop-off in Equation 2.1 at low elevation angles provides protection against horizontal multipath interference. This pattern has the characteristics desired in a GeoBeacon transmitter antenna, and will be used to provide sample antenna gain values for the link calculations. The worst case scenario for the link budgets is a satellite being viewed at a minimum elevation angle of 15°.

The location- and time-dependency of multipath phase perturbations is not included in this link budget. By using an antenna such as the MITES antenna, with a ground plane, and at unobstructed sites, it should be possible to minimize cases of large phase distortions.

2.3.3 Propagation Losses

Under normal atmospheric conditions, a 2 GHz signal transmitted at an elevation

---

[14]Counselman, C. C. and Shapiro, I. I., "Miniature Interferometer Terminals for Earth Surveying," *Bulletin Geodesique*, vol. 53, pp. 139-163, 1979.

angle of 15° is attenuated on the order of 0.1 dB, due primarily to H_2O absorption. This loss will increase under heavy precipitation conditions, but the contribution can still be neglected in the link calculations. For example, based on a rain attenuation model by Lin[15], a signal at 2 GHz propagating at an elevation angle of 15° through rain falling at a rate of 100 mm/h is attenuated by approximately 0.2 dB.

2.3.4 Orbit Altitude

There are two reasons to keep GeoBeacon satellite orbits as high as possible: (i) to view networks with the same inter-continental size baselines as GPS-based networks, and (ii) to keep the orbit accuracy requirements the same as that for GPS satellites. In this study, however, there are two limits upon the GeoBeacon satellite orbital altitude. One limit stems from the desire to use an inexpensive launch vehicle, such as Pegasus, to place the satellites into orbit. Based on information used by NASA's Jet Propulsion Laboratory in designing their missions (see Figure 2.1), it appears that the maximum circular orbit altitude for a Pegasus is launch-limited to 1000 km, though no reason is given for that upper bound. Also, as orbit altitude increases from 1000 km, the spacecraft will encounter higher levels of trapped charged particles, which can degrade the performance of satellites without adequate protection. Protection against this hazard would add to the GeoBeacon mission costs, so for both strawman designs, the maximum satellite altitude considered is 1000 km.

---

[15]Ippolito, L. J., *Radiowave Propagation in Satellite Communications*, Van Nostrand, Chapter 5, 1986.

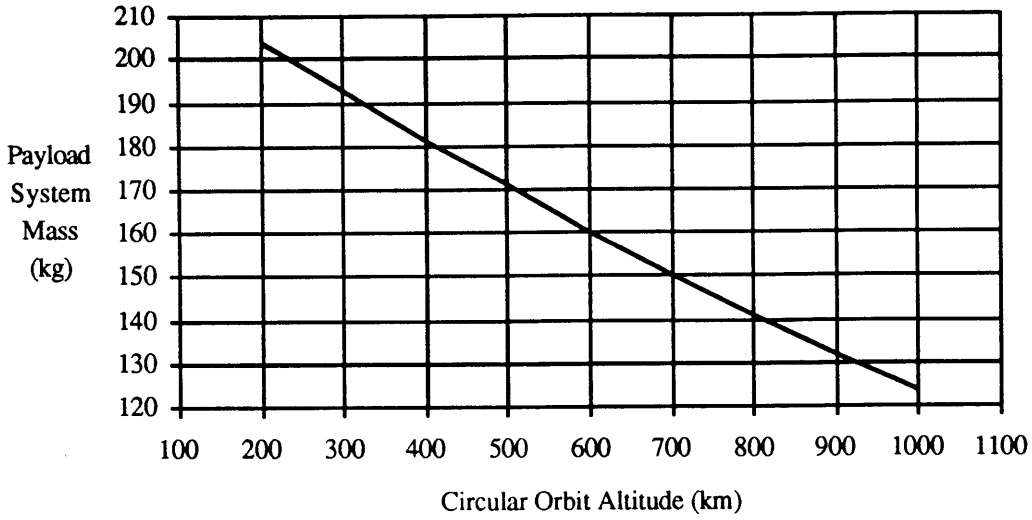

Figure 2.1 Pegasus Payload Capabilities to Circular Polar Orbit[16]

2.3.5 Constellation Selection

In this section, two GeoBeacon satellite arrangements are presented. The first arrangement, the '2-sat' configuration, has only two satellites, the absolute minimum number for geodetic measurements to be performed. In this configuration, a difference in mean motion between the two satellites guarantees periods of mutual visibility from the ground. The mean motions of the orbits are set so that meaningful observations can be made on one day every two weeks. In the second configuration, the 'Multi-sat' configuration, the large number of satellites result in the possibility of making observations every day. A third constellation possibility is also considered.

2.3.5.1 Use of Relative Mean Motion

In order to minimize space hardware costs, there are no plans to include propulsion systems on GeoBeacon satellites for orbit plane changes and station keeping. For both

[16]Bayer, T. J., *et al.*, "Expendable Launch Vehicles Summary for JPL Mission Planning," JPL D-6936, Rev. A, p. 2-21, February 1991.

configurations, all satellites are deployed in coplanar orbits. Without station keeping, they will drift in orbital longitude, relative to each other, in an uncontrollable manner. In order to be visible simultaneously from any site on the Earth's surface, two satellites must be separated by a geocentric angle of less than ~36° (for 1000 km altitude orbits, assuming a 15° minimum elevation angle; see Figure 2.2). In order to guarantee recurrence of opportunities when two satellites can be observed simultaneously, one satellite could be placed in a slightly lower orbit than the other, to create a difference in the mean motions. As the lower satellite periodically overtakes the higher satellite (hereafter referred to as an 'lapping event'), the geocentric angle between the two satellites varies between 0° and 180° linearly with time . Thus, for one fifth of the time, the satellite footprints will intersect on the Earth's surface.

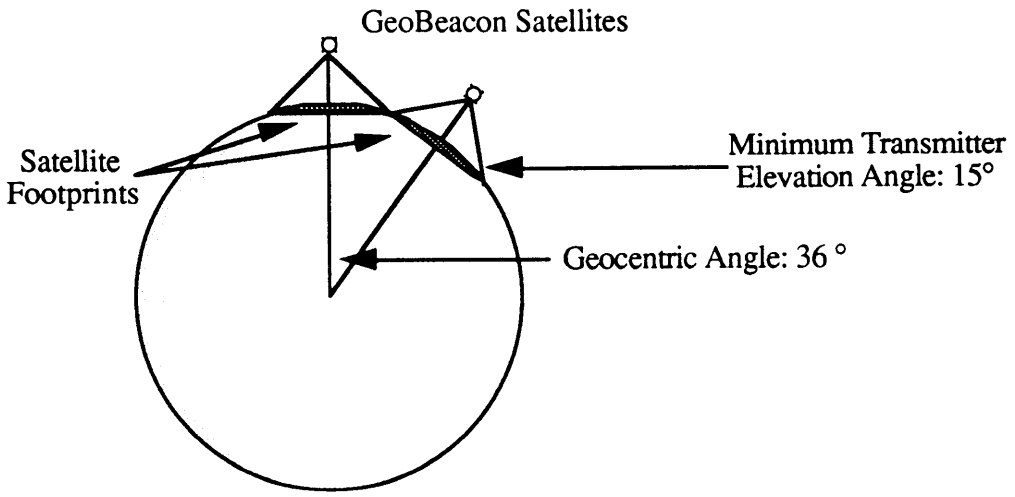

Figure 2.2 Footprints from Two GeoBeacon Satellites

Before continuing, it is necessary to define three terms to help describe GeoBeacon satellite observation opportunities (see Figure 2.3). From a ground site, the episode of simultaneously viewing two satellites rise and fall in the sky is known as a simultaneous pass. The duration of a simultaneous pass, for satellites in 1000 km altitude orbits, depends on the geocentric angle between the two satellites. For two such satellites spaced closely together, a pass can have a maximum duration of 10 minutes.

For non-zero inclination orbits, the earth rotates through the orbit plane. The satellite ground tracks shift westward from one pass to the next. A set of consecutive simultaneous passes resulting from the earth rotating beneath the same northbound (or southbound) orbit arc are called a set of passes. With 1000 km altitude orbits, there is an approximately 1 h 45 m wait between consecutive passes of a set.

A group of sets (alternating between north- and south-bound sets) associated with the same satellite 'lapping' event is known as a session of passes. For high inclination orbits (the reason for considering these orbits is discussed later in the chapter), successive sets are spaced approximately twelve hours apart.

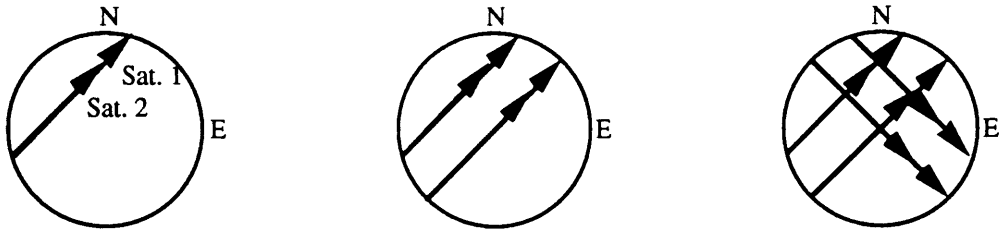

A 2-Satellite Simultaneous Pass Duration: 0-10 min.

A Set of 2 Northbound Passes Time Span: ~ 2 hr.

A Session of 2 Sets Time Span: ~ 12 hr.

Figure 2.3 Sky Plots Illustrating a Two-Satellite Pass, Set, and Session
(Satellites in high inclination circular orbits; orbit altitude = 1000 km)
(Circle in sky plot defines local horizon)

Now that we have defined these terms, we can address the question: By how much should the mean motion of the two GeoBeacon satellites differ? The choice of time interval between satellite 'lapping' events is a tradeoff between (i) the frequency of observation sessions and (ii) number of sets and passes per session. Increase the number of passes and sets per session, and the time between sessions (positioning opportunities) becomes too long. Increase the frequency of observation sessions, and the lower satellite may overtake the higher one so quickly that a ground observer may not be guaranteed even one pass during that session.

Figure 2.4 shows the number of passes and sets that can be expected on average as a function of time between 'lapping' events. As an example, if one wanted to have a lower satellite overtake a higher, 1000 km altitude satellite once every two weeks, the lower satellite would have to be deployed at an altitude of approximately 975 km. There will be on average three sets of passes, that is, three opportunities to view passes, during one 'lapping' event. A ground observer can expect four passes during these fortnightly sessions. Two weeks between sessions appears to be as frequent as one can get and still ensure multiple sets of passes (with an additional set for insurance). Therefore, the '975 km - 1000 km altitude orbit' pair will be used for the '2-sat' configuration.

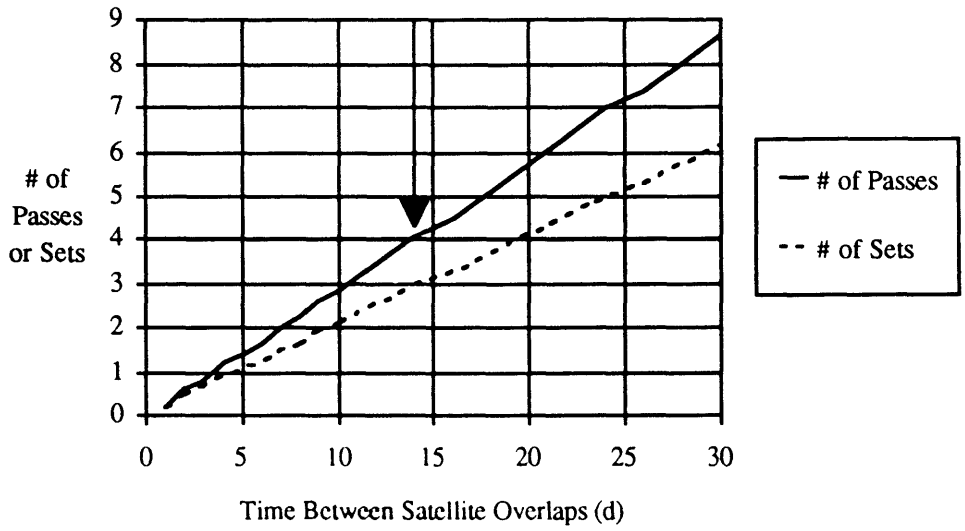

Figure 2.4. Number of Passes & Sets of Passes Versus Satellite Overlap Time
(Arrow denotes '975 km - 1000 km' satellite pair biweekly overlap time.)

2.3.5.2 Polar Orbits

Changing the semi-major axis of one satellite relative to another, as in the '2-sat' configuration, introduces a problem. The Earth's oblateness (and to a lesser extent, the Moon and Sun) causes satellite orbit planes to precess. At a 1000 km altitude, the oblateness effect dominates the lunar and solar effects by several orders of magnitude. The

negative rate of advance of the longitude of the ascending node due to oblateness is a function of orbit semi-major axis, inclination, and eccentricity:

$$\dot{\Omega}_{oblate}(deg/day) \cong -2.065(10^{14})\, a^{-7/2} \cos i\, (1 - e^2)^{-2} \quad \text{(a is in kilometers)} \qquad (2.2)$$

$$\cong -5.99 \cos i \ \text{(deg/day)} \quad \text{(1000 km altitude circular orbits)}$$

The planes of satellites in 975 km and 1000 km altitude orbits precess with respect to each other at a rate of $\Delta\Omega = 26\ (\cos i\ )$ (deg/yr). The simplest way to eliminate the difference in $\dot{\Omega}$ between GeoBeacon satellites in different altitude orbits, while keeping the orbits coplanar, is to launch them all into polar orbits.

2.3.5.3 Probability of Favorable Observation Conditions with Multiple Satellites

There is a second method by which the simultaneous visibility of two satellites can be essentially guaranteed. Instead of placing two satellites into coplanar polar orbits of differing altitudes, one could deposit several satellites into approximately the same orbit. The satellites would be deployed from the launch vehicle payload assembly with springs. By varying spring coefficients, each satellite could be given a slightly different orbital energy, and therefore a different period. Within a few months, the satellites would be randomly distributed throughout the orbit. This arrangement has been named the 'Multi-sat' configuration.

How many satellites would one then need to perform geodetic measurements? In order to perform doubly differenced phase measurements, both ends of the baseline need to be within the boundary on the Earth's surface defined by the overlap of at least two satellite footprints (see Figure 2.5). Let's assume that random perturbations to the satellite orbits are quasi-statically slow, i.e. the dimensions of the overlap region stay relatively constant over a few hours. For the sake of simplicity (and in order to reach a lower bound on the number of satellites needed), let us also assume that the dimensions of the network are

negligible compared to the overlap region.

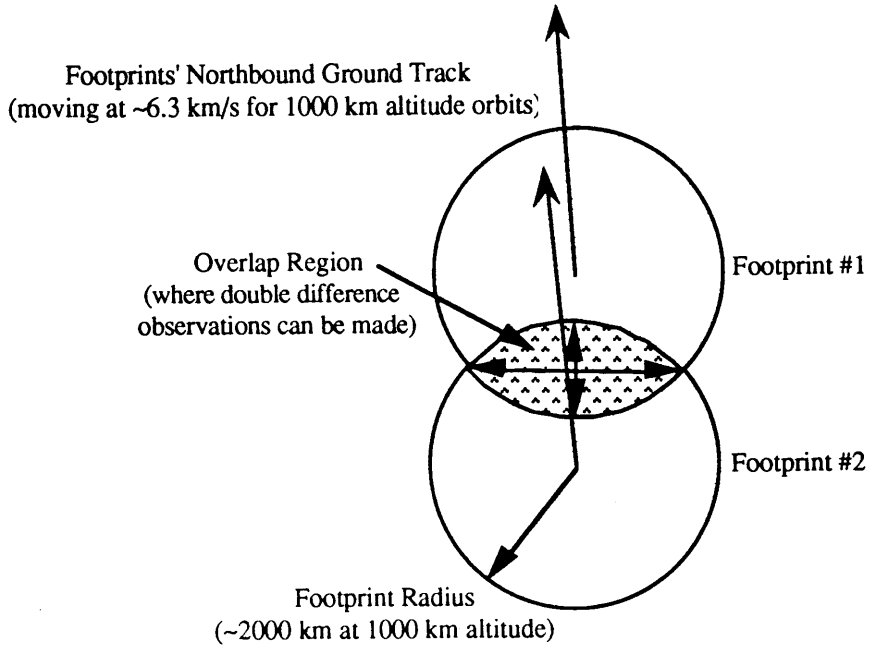

Figure 2.5 Ground Track of Overlapping Satellite Footprints

The transmitters and central site of the ground network need to be within the lenticular shaped footprint-overlap for a length of time long enough that the transmitter signals can be acquired and sufficient observations be made at the central site. Satellite footprints are scattered around the Earth circumference defined by the constellation orbit plane. The probability of having footprints from satellites i and j overlap is denoted by P(i,j). With three satellites, the probability of having the first and second, as well as the first and third footprints overlap, is written P(1,2; 1,3), and so forth. For example, the probability of having at least two satellites overlap, given three randomly distributed satellites throughout the orbit arc, is expressed as:

$$P_3 = P(1,2) + P(1,3) + P(2,3)$$
$$- P(1,2;\ 1,3) - P(1,2;\ 2,3) - P(1,3;\ 2,3) + P(1,2;\ 1,3;\ 2,3) \qquad (2.3)$$

For n satellites independently scattered throughout the orbit we have

$$P_n = \sum_{r=1}^{m} (-1)^{r+1} \binom{m}{r} P(1,2;\ 1,3;...;1,r); \qquad m = \frac{n(n-1)}{2}. \tag{2.4}$$

The probability P(1,2;1,3; ... ;1,r), and consequently, P_n, depend upon f_d, the ratio of the maximum geocentric separation of two satellites that would allow geodetic positioning, to the entire orbit circumference:

$$P(1,2;\ 1,3;...;\ 1,r) = (2\,f_d)^r \qquad P_n = 1 - (1 - 2\,f_d)^m \tag{2.5 a,b}$$

How do we define this range of 'suitable' geocentric angles? The partial derivative of the double-difference observation (introduced in the Chapter 1 overview) with respect to a station's position vector **x** is the difference of unit vectors to the satellites $\hat{s}$ which make up this observation:

$$\frac{\partial(\text{Double Difference Observation})}{\partial \mathbf{x}} = \Delta\hat{\mathbf{s}} \tag{2.6}$$

These partial derivatives are incorporated into the normal equations along with $\Delta\hat{s}$ vectors from other times in that particular pass, as well as other passes, to generate the position-correction estimate formal standard errors. The ratio of the three-dimensional position-correction estimate rms error to the (double-difference) measurement rms error

$$\text{PDOP} = \frac{\sqrt{\sigma_{\text{Lat.}}^2 + \sigma_{\text{Long.}}^2 + \sigma_{\text{Vert.}}^2}}{\sigma_{\text{Msmt.}}} \tag{2.7}$$

characterizes the strength of the ability of a particular satellite constellation to provide accurate position estimates. This ratio is commonly referred to as the Position Dilution of Precision (PDOP). In studies involving satellite constellations such as GPS, PDOP is considered to be an instantaneous value, a function of the satellites currently in view. In this study, since GeoBeacon satellites lie in a single plane, instantaneous PDOP cannot be defined. Therefore, one PDOP value will be calculated for all the observations made by a

particular satellite configuration. In order to focus on the strength of the orbit geometry, and not the number of measurements, the ratio obtained throughout the passes is multiplied by the square root of the number of observations made (N; see Chapter 1). Hereafter, the definitions in equations (2.8 a-c) will be used for horizontal, vertical, and position dilutions of precision (HDOP, VDOP, and PDOP, respectively). The original, conventional definition of PDOP will not be used in this study.

$$HDOP=\sqrt{N}\frac{\sqrt{\sigma_{Lat.}^2+\sigma_{Long.}^2}}{\sigma_{Msmt.}} \quad VDOP=\sqrt{N}\frac{\sigma_{Vert.}}{\sigma_{Msmt.}} \quad PDOP=\sqrt{HDOP^2+VDOP^2} \quad (2.8\ a\text{-}c)$$

Code was written to calculate observations opportunities for a particular combination of satellites and ground stations. Observations were simulated for a range of geocentric angles between two GeoBeacon satellites. 100 days of observations were used in order to determine the average dilution of precision that could be expected. Figure 2.6 shows how HDOP, VDOP, and PDOP vary with geocentric angle for two 1000 km altitude satellites.

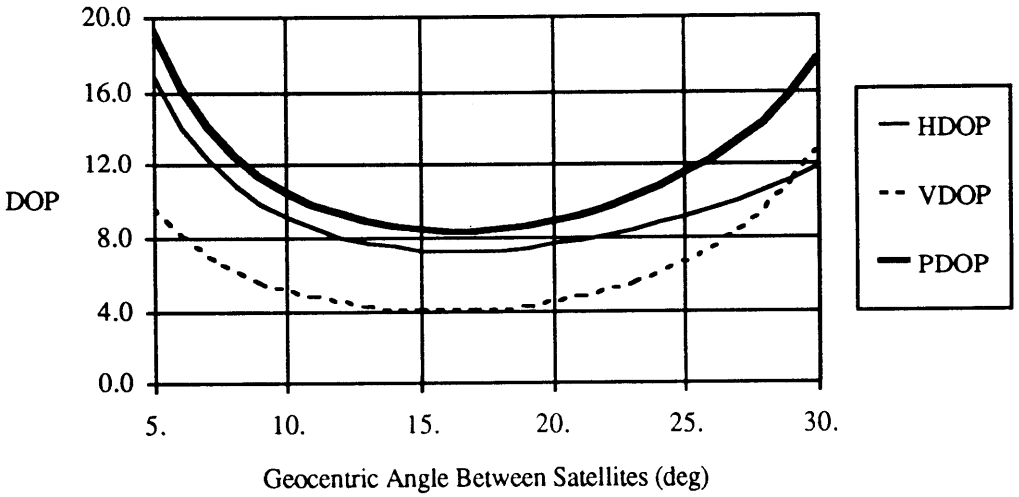

Figure 2.6 GeoBeacon PDOP Versus Satellite Geocentric Angle of Separation

The range of geocentric angles which yield PDOPs below a particular value selected reflect a tradeoff between (i) station coordinate sensitivity to the double difference observable and (ii) robustness of the distribution of coordinate partial derivatives. If the satellites are spaced closer together in orbit, the pass duration increases (see Figure 2.7), but the size of the $\Delta\hat{s}$ vectors (the station partials defined in equation 2.6) decreases, resulting in a higher PDOP. If the satellites are spaced farther apart, the $\Delta\hat{s}$ vectors in each pass rotate through less of an angle within the plane defined by that pass. As a result, the VDOP and PDOP increase (see Figure 2.6).

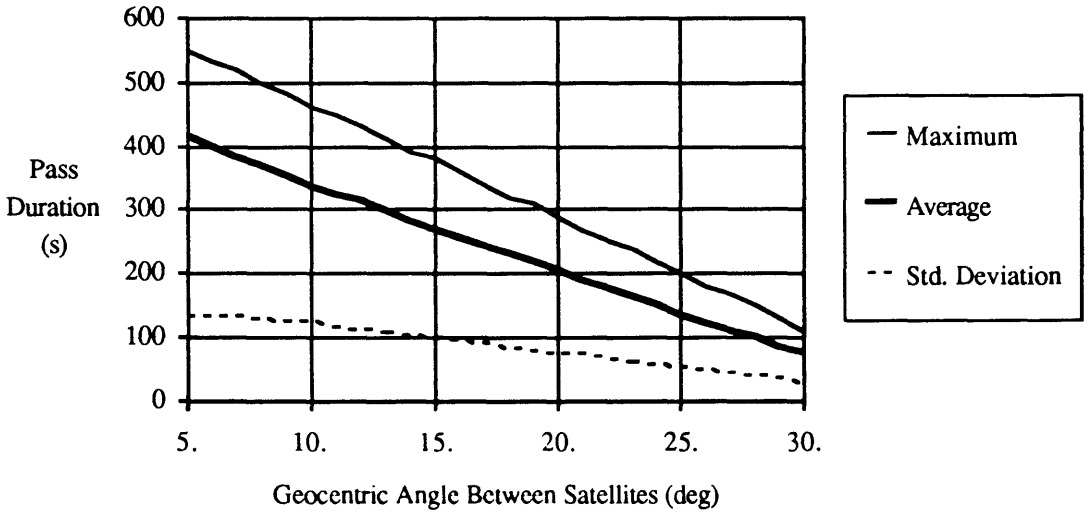

Figure 2.7 Two-Satellite Pass Duration Versus Geocentric Angle of Separation

For a particular maximum PDOP, one can use Figure 2.6 to see what ranges of geocentric angles are acceptable. These ranges (as a fraction of the entire orbit arc) can be incorporated into Equation (2.5 b) to estimate how many satellites would be needed to position ground sites at that PDOP level or better. The number of satellites needed is also a function of the probability that no two of these satellites are spaced adequately.

	$PDOP_{max}$	10	12	14	16	18	20
Probability	50%	6	5	4	4	4	4
That Adequate	10%	9	8	7	7	7	6
Satellite	1%	13	10	10	9	9	9
Spacing Is Not	0.1%	15	12	12	11	11	10
Encountered	0.01%	17	14	13	13	12	12
	0.001%	19	16	15	14	14	13

Table 2.3. Number of Satellites Required (to Perform Geodetic Positioning) Versus Maximum Allowable PDOP and Probability That Adequate Satellite Spacing Is Not Encountered

In May 1990, Jan King, representing the Orbital Sciences Corporation, showed the GeoBeacon group how at least 16 Microsats could be placed into 1000 km altitude orbits with one launch of the Pegasus vehicle. Since this number of satellites provides a low PDOP and high probability of adequate spacing, the 'Multi-sat' configuration will be assumed to carry 16 satellites. Since relative precession does not affect this configuration, these satellites could be placed into one sun-synchronous orbit plane (with $i = 99.5°$ for a 1000 km altitude orbit). The advantage of this orbital inclination is that eclipsing of the Sun by the Earth can be eliminated. Eclipsing complicates the power requirements for the transponder, and results in a non-constant solar radiation force upon the satellite, which can potentially result in larger orbit estimate errors.

2.3.5.4 Another 2-Satellite Constellation Possibility

Using polar orbits is not the only solution to keeping different orbits coplanar. Eccentricity can also be varied to compensate for changes in $\dot{\Omega}$ from orbit size. By matching $\dot{\Omega}$ values (see Equation 2.2) for a pair of satellites with semi-major axes (a_1, a_2) and eccentricities (e_1, e_2), we obtain the following condition, which ensures essentially

coplanar orbits:

$$\left(\frac{a_2}{a_1}\right)^{\frac{7}{4}} = \frac{1 - e_2^1}{1 - e_2^2} \tag{2.9}$$

This relation can be expressed in terms of T', the period between satellite overlaps:

$$T' = \frac{2\pi\, \alpha^{3/2}\, a^{3/2}}{\sqrt{\mu}\,(1 - \alpha^{3/2})} \qquad \text{where} \qquad \alpha = \frac{a_2}{a_1} = \left(\frac{1 - e_1^2}{1 - e_2^2}\right)^{4/7} \tag{2.10 a,b}$$

For example, if one satellite has a 1000 km circular orbit, and T' is set to two weeks, then the second satellite would orbit about 25 km lower, as before. However, the first satellite would need an eccentricity of ~0.08 to match the precession rate of the second satellite. This results in a perigee altitude of $r_{p1} \approx 410$ km and an apogee altitude of $r_{a1} \approx 1600$ km. This variation in altitude causes the area of the effective footprint to vary by a factor of 6. Since the argument of perigee of the eccentric orbit also changes, there would be windows where larger baselines could not be observed. Therefore, if only two satellites are to be deployed, they should be in a polar orbit.

2.3.6 GeoBeacon Satellite Requirements and Microsat Spacecraft

In 1990, the Amateur Radio Satellite Corporation of North America (AMSAT-NA) launched 6 lightweight satellites, placing them on a shelf below the main payload of an Ariane-4 launch of a sun-synchronous satellite[17]. The AMSAT satellites (see Figure 2.8) each weighed between 10 - 12 kg, and were placed into sun-synchronous orbits at an ~800 km altitude.

[17]Loughmiller, D. and McGwier, B., "Microsat: The Next Generation of OSCAR Satellites," QST Magazine, June 1989.

Design qualified for launches on:	Ariane 4, Atlas, Delta 2, Pegasus
Standard Spacecraft Size:	23.5 cm x 23.0 cm x 23.0 cm
Power from Solar Arrays:	13 W peak, 5.8 - 6.5 W average
Antenna Gain Patterns:	~Omni-directional
Attitude Control System:	Passive Magnetic Stabilization

Table 2.4 AMSAT Microsat Spacecraft Characteristics[18]

Many of these characteristics (see Table 2.4) are compatible with the requirements of a low-Earth orbiting GeoBeacons satellite. However, there is a design change that should be considered, since it may result in a cost savings to the geodesist. While the Microsat architecture is compatible with GeoBeacon satellite requirements, by altering the (i) antenna design and (ii) pointing accuracy requirements, it may be possible to lower the ground transmitter power requirement and cost.

2.3.6.1 Antennas

The satellite uplink and downlink antenna pattern requirements are considered identical for this study. If the satellite could keep one face constantly pointing towards the Earth's surface, a directional antenna pattern symmetric about the satellite-Earth center line could be used instead of the omni-directional pattern used in past Microsat spacecraft. Directionality of the spacecraft antennas should reduce the uplink and downlink transmitter power requirements. Peak gain should occur at the edge of the satellite's defined footprint, where ground transmitters would view the satellite at an elevation angle of 15 degrees.

[18]King, J. A., *et al.*, "The In-Orbit Performance of Four Microsat Spacecraft," presented at the Fourth USU Conference on Small Satellites, Logan, Utah, 1990.

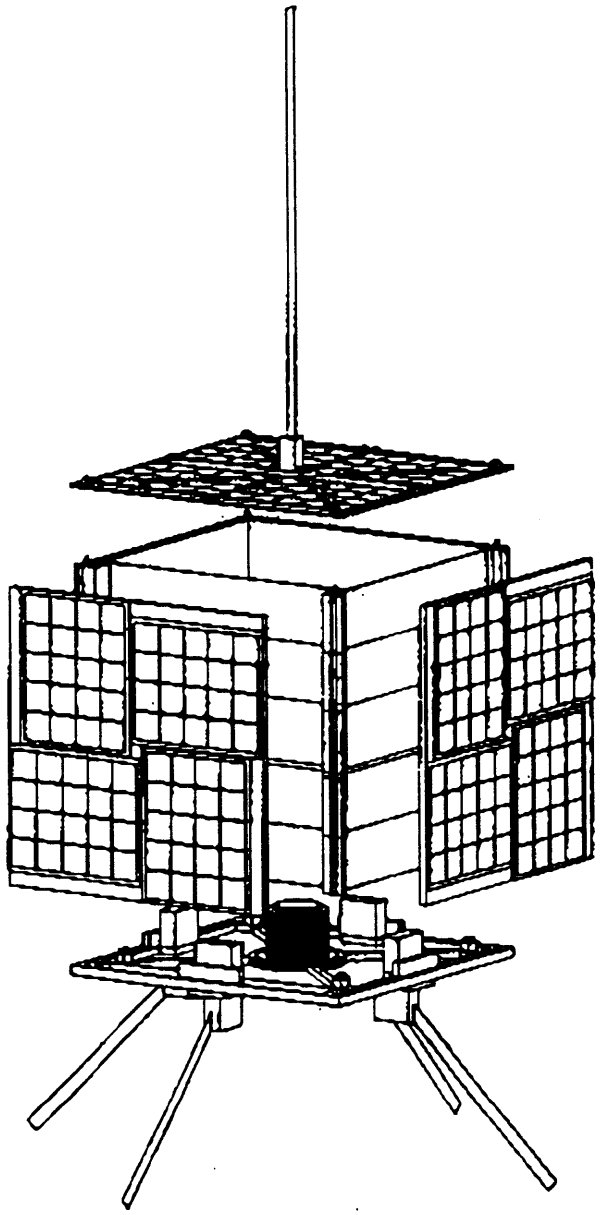

Figure 2.8 Standard Microsat Exploded View

In Figure 2.9, we consider transmitters on the Earth's surface farther and farther away from the sub-satellite point (increasing geocentric angle). The satellite antenna gain needed to offset the increase in path loss is defined as P_c. For the case of a satellite in a 1000 km altitude circular orbit, and a minimum elevation angle of 15 degrees, the MITES

antenna gain pattern described in Equation (2.1) appears to adequately compensate for the variation in slant range to the earth's surface. Table 2.5 also shows that in a large fraction of the footprint the satellite is viewed at low elevation angles. By providing sufficient antenna gain at low elevation angles, one can insure that most of the footprint will be adequately compensated. For the link calculations we will use a satellite gain of 4.4 dB (see Table 2.5 and Figure 2.10). As in the selection of the ground transmitter antenna, the MITES pattern is <u>not</u> optimal, but it does have the azimuthal symmetry desired and provides a simple example of a gain pattern to compare against the ideal path-loss compensation.

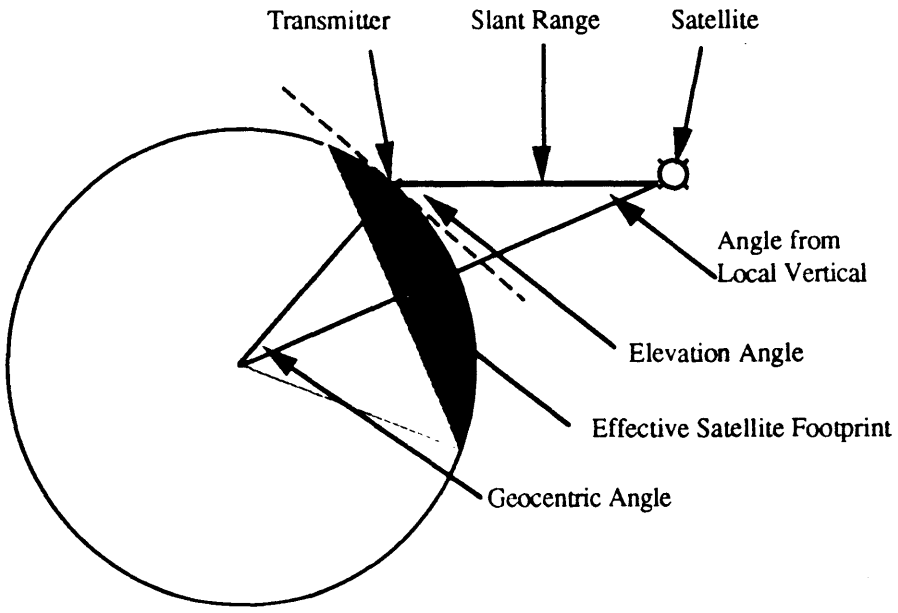

Figure 2.9 Satellite Footprint and Ground Transmitter Diagram

Geocentric Angle (deg)	Transmitter Elevation Angle (deg)	Angle from Local Vertical (deg)	Slant Range (km)	% of Total Footprint Area	Ideal Path Loss Compensation (dB)	MITES Pattern Gain (dB)
0	90.0	0	1000	0	-2.6	3.9
2	75.5	12.5	1030	1.2	-2.4	4.3
4	62.3	23.7	1110	4.8	-1.7	5.0
6	51.2	32.8	1230	10.7	-0.8	5.5
8	42.1	39.9	1380	19.1	0.2	5.6
10	34.7	45.3	1560	29.8	1.2	5.5
12	28.7	49.3	1750	42.8	2.2	5.3
14	23.6	52.4	1950	58.2	3.2	5.0
16	19.4	54.7	2160	75.9	4.0	4.7
18	15.7	56.4	2370	95.9	4.9	4.4
18.4	15.0	56.6	2410	100.0	5.0	4.4

Table 2.5. MITES Antenna Gain Pattern Versus Required Against Path Loss Compensation

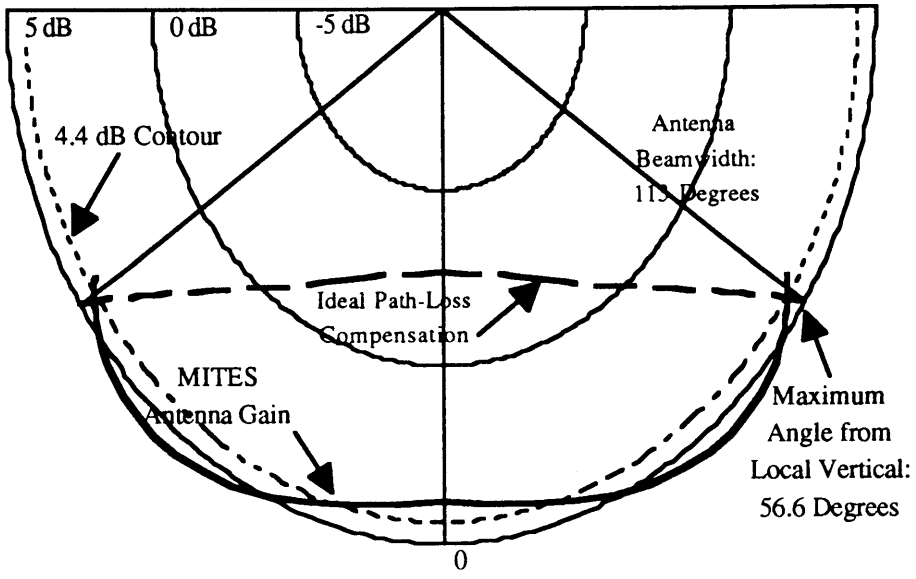

Figure 2.10. MITES Antenna Gain Pattern vs. Required Path-Loss Compensation

2.3.6.2 Pointing Requirements

The AMSAT Microsat spacecraft use magnetic stabilization, by aligning permanent magnets installed within the spacecraft to the Earth's magnetic field. Because of the variation in magnetic field vector orientation with latitude, the polar orbiting Microsats do not keep the same face pointed towards the Earth's surface. They rotate twice per orbit, which aids in minimizing thermal gradients within the spacecraft [19].

There is another potentially low-cost option for GeoBeacon spacecraft stabilization. Gravity gradient stabilization could be used in order to keep the MITES design antennas pointed at the Earth's surface. Since the MITES antenna beamwidth is fairly wide, the allowable pointing error is large compared to that of most communications satellites, on the order of 10 degrees. With the satellite antenna gain pattern being considered, an error of this magnitude would result in a gain loss of 2.5 dB.

Either stabilization scheme is adequate to counter expected destabilizing torques. For the gravity-gradient approach, solar radiation and the Earth's magnetic field are expected to be the largest destabilizing forces (Aerodynamic drag is several orders of magnitude lower than the other sources listed). The spacecraft with magnetic stabilization is assumed to have the same structure as the Microsat spacecraft. For the spacecraft with gravity-gradient stabilization, a boom is added to provide the required stabilization torque (see Figure 2.11).

[19]In the Microsat design, the four blades of the omni-directional antenna are painted black on one side and white on the other. This arrangement allows the sun to impart a torque about the local vertical axis, further reducing the thermal gradient across the spacecraft.

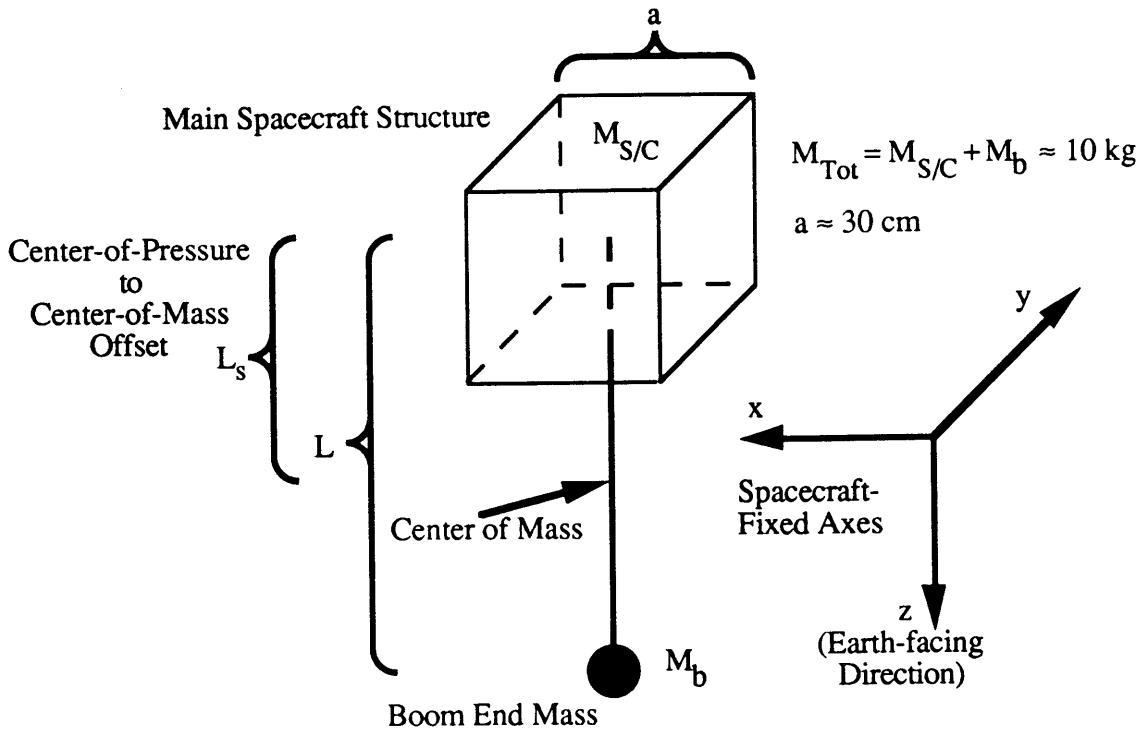

Figure 2.11 Spacecraft Diagram

The objectives of this section are to show that (i) the boom and end mass needed to overcome destabilizing torques is not prohibitively large nor heavy, and (ii) the magnetic stabilization used in the AMSAT Microsat spacecraft is suitable for the GeoBeacon orbits considered. The magnitude of the gravity gradient torque, T_g, is

$$T_g = \frac{3\mu}{2R^3}|I_z - I_y|\sin(2\theta) \tag{2.11}$$

where μ is $GM_\oplus$, R is the orbit radius, I_z and I_y are the moments of inertia about the z and y (or x, because of symmetry) axes, and θ is the deviation of the z axis from the local vertical (in radians). For the main spacecraft structure, the assumption that the mass is distributed across the faces of the cube will yield the most conservative estimates of T_g.

The expression for torque resulting from solar radiation, T_s, assumes specularly reflective surfaces:

$$T_s = P_s A_s L_s (1 + q) \cos i \tag{2.12}$$

P_s is the solar flux, A_s is the surface area of the main spacecraft structure, L_s is the offset between the spacecraft's centers of mass and pressure, i is the solar angle of incidence (assumed to be 90° for the worst case), and q is the reflectance factor which ranges from 0 to 1 (q = 0.6 will be used in the estimates[20]).

The torque applied to the spacecraft by the Earth's magnetic field is expressed as

$$T_m = 10^{-7} DB \tag{2.13}$$

where B is the magnetic field strength in Oersted (1 Oersted = $(1/4\pi)(10^3)$ (Amp.) m^{-1}), and D is the residual dipole of the vehicle in pole·cm (1 pole·cm = $4\pi(10^{-10})$ kg m^3 $(Amp.)^{-1}$ s^{-2}). For small spacecraft the residual dipole can be as low as 200 pole·cm, and with permanent magnets installed, the AMSAT Microsat dipole moment is estimated to be at least 50,000 pole·cm.

In Figure 2.12 the correcting torque magnitudes are shown for booms of varying length with one and five kilogram end masses. Boom lengths on the order of three to five meters are needed to offset the expected magnetic torque disturbance. By installing permanent magnets in the spacecraft, the magnetic correcting torque magnitude can be increased by orders of magnitude, as is the case in the AMSAT Microsat spacecraft.

In conclusion, both stabilization techniques provide adequate torque to overcome expected destabilizing torques. As will be shown in the tradeoff performed at the end of the chapter, neither system results in prohibitively large power requirements in the ground transmitters or GeoBeacon satellite. There is no strong reason to discard either stabilization scheme, assuming that the gravity gradient boom can be incorporated into the Microsat

---

[20]Wertz, J. R., and Larson, W. J., eds., *Space Mission Analysis and Design*, Chapter 11, 1991.

spacecraft design without significantly increasing the volume of.the spacecraft onboard the launch vehicle.

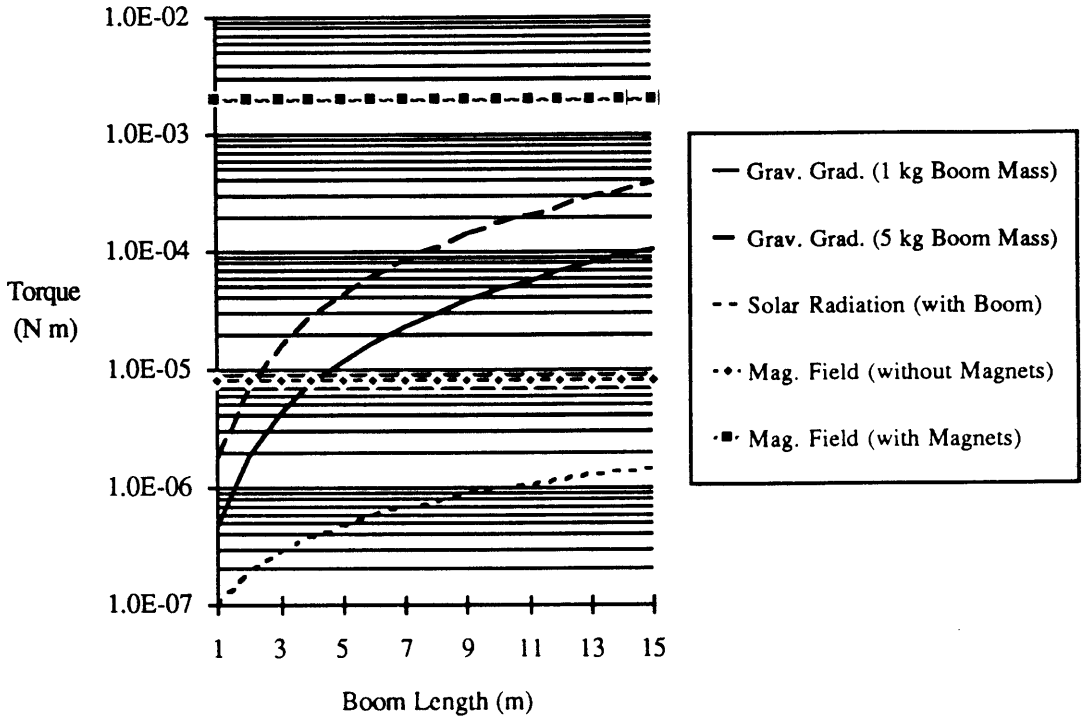

Figure 2.12 Torque Magnitudes vs. Satellite Boom Length

2.3.7 Carrier-to-Noise Ratio

The sources of the noise density No can be grouped into two categories: (i) contributions from both natural and man-made sources, and (ii) the interference received at the central site from other GeoBeacon transmitters in the acquisition of the signal of a particular transmitter. Therefore, the uplink carrier-to-noise density ratio has two components, the 'carrier-to-receiver noise' density ratio, $(C/No)_m$, and the carrier-to-interference ratio, (C/I). In the following three sections these noise contributions will be further defined and their relative contributions estimated.

2.3.7.1 Natural Noise Sources

For frequency bands between ~400 MHz and ~20 GHz, the primary source of natural noise is reradiation of surface thermal radiation. In the earlier study of GeoBeacons, a conservative upper limit of 290 K[21] was established for the signal frequencies considered in Table 2.2.

2.3.7.2 Man-Made Noise Sources

One conclusion of the feasibility study of GeoBeacons was that there was a need to understand better the terrestrial radio noise environment as seen from Earth orbit. The man-made noise component appears to be large compared to the natural noise component. In contrast to the natural noise signature, man-made noise levels vary greatly with measurement location, time of day, density of electrical equipment at source, and frequency band.

Unclassified evidence which might be used to arrive at an estimate can be sorted into three groups:

(i) Estimates using models of interfering sources on the Earth's surface

(ii) Measurements made from aircraft

(iii) Measurements made from Earth orbiting spacecraft

There are two caveats to these sources of information. One is that these noise estimates are made by integrating noise power density levels over bandwidths of different sizes. One must keep this bandwidth difference in mind when estimating the expected noise level across the GeoBeacon signal bandwidths. The second factor is the year that the estimates are made. As frequency allocations change and radio activity continues to grow, one

---

[21]Ippolito, Chapter 7.

should expect an ongoing increase in the average noise level. However, there is one set of limited measurements that suggests no significant increase in noise level has taken place between the years 1972 - 1990[22].

The study that has covered the largest portion of the spectrum was performed by Skomal[23]. In this study, the man-made noise environment was estimated by using measurements of the radio noise environment made in metropolitan areas. The distribution of these urban areas across the Western Hemisphere was modeled, and the total electromagnetic power was calculated for an antenna in geosynchronous orbit. The result was an estimate of the man-made noise temperature over a large part of the radio spectrum. In addition, Skomal attempted to confirm the estimates made, using actual measurements from the LES-5 satellite[24]. The results of the measurements were inconclusive, but a minimum value for the total ambient noise temperature was reported to be at about the natural noise temperature, 290 K.

The study by Cudak and Swenson[25] was the repeat of a 1972 incidental radio noise experiment. Measurements were made with a broad beam antenna mounted on an airplane flying at an altitude of 700 m over metropolitan areas in Illinois. Measurements were made at 144, 222, and 412 MHz. Another study by Herman[26] took account of all registered transmitters on frequency bands from 117 - 154 MHz to make estimates of the noise power levels in 1 MHz bandwidth segments.

In Figure 2.12, the results of these studies were scaled to approximate the total

---

[22]Cudak, M. C., and Swenson, G. W., "Airborne Measurements of Incidental Radio Noise from Cities," *Radio Science*, Vol. 26, No. 3, pp. 773 - 781, May - June 1991.
[23]Skomal, E. N., "Analysis of Spaceborne VHF Incidental Noise Over the Western Hemisphere," *IEEE Transactions on Electromagnetic Compatibility*, Vol. EMS-25, No. 3, pp. 321 - 328, August 1983.
[24]Ward, W. W., *et al.*, "The Results of the LES-5 and LES-6 RFI Experiments," *IEEE Transactions on Aerospace and Electrical Systems*, Vol. AES-11, No. 6, pp. 1059 - 1066, November 1975.
[25]Cudak, Ibid.
[26]Herman, J. R., "The Radio Noise Environment in Near Space: A Review," *Proc. IEEE International Symposium on Electromagnetic Compatibility*, June 20 - 22, 1978.

radio noise temperature expected by the GeoBeacon antenna in a 1000 km altitude orbit. In the case of the city noise measurements made by Cudak, *et al*, demographic information from Skomal was used to calculate the density of city noise seen from Earth orbit.

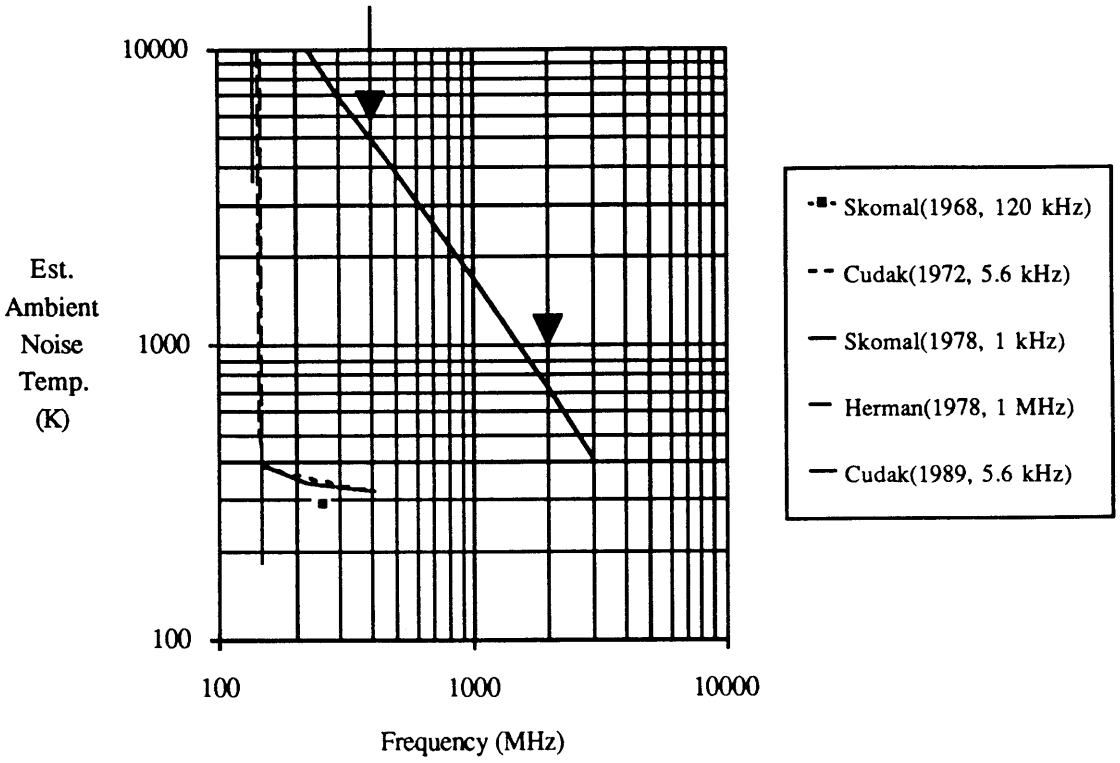

Figure 2.13 Estimated Ambient Noise Temperature as Seen from 1000 km Altitude (extrapolated from measurements and estimates; listed by source author, date, and bandwidth considered) (Arrows denote GeoBeacon signal frequencies (f_1 = 401 MHz, f_2 = 2036 MHz).)

The plots shown do not provide conclusive estimates of the noise power level as seen from Earth orbit. But there are two conclusions that can be drawn. First, from the Skomal estimates, there appears to be a general downward trend in noise power with frequency. Second, from the Herman estimates, there are large (~3 orders of magnitude) variations in noise power over small changes (~1 MHz) in signal frequency. Since the Skomal estimates are based upon actual measurements, that plot will be referenced for the antenna noise temperature values. The only other source at present which lends credibility to this decision is the amateur satellite community, which reports a noise temperature of

3000 - 4500 K operating in the 144 - 146 MHz band.[27]

2.3.7.3 Crosstalk Among Transmitters

(C/I) is estimated by calculating the number of operating ground transmitters in the satellite footprint. It is assumed that on average the power received from an interfering transmitter is equal to the power received from the transmitter of interest. It is also assumed that all transmitters are operating on a 100% duty cycle, a worst case scenario (in order to aid in signal acquisition during the pass, this may turn out to be the case). In Figure 2.14, the Carrier-to-Interference ratio for one interfering transmitter, $(C/I)_1$, is calculated. The correlation of the wanted and unwanted signals with a replica of the wanted transmitter's code results in $(C/I)_1 = R_c / (2\ B_i)$, where R_c is the code chip rate and B_i is the integration bandwidth (the inverse of the integration time span). Since all of the transmitters operate independently, the results from one interfering transmitter can be multiplied by the total number of transmitter signals received at the central site to estimate the interference from all the transmitters operating simultaneously.

[27]King, Ibid.

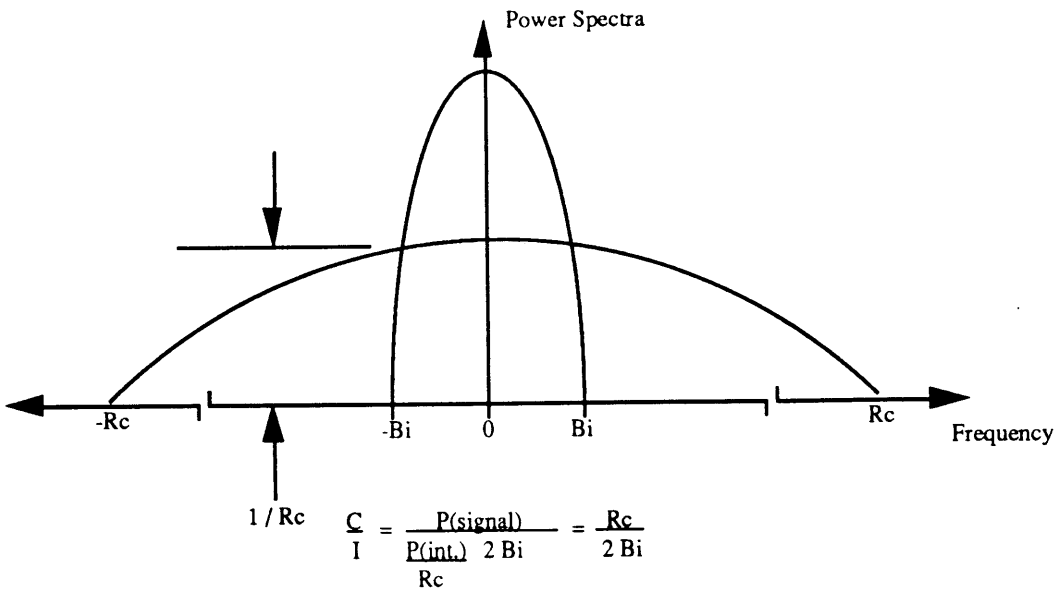

where P(signal) = Total Signal Power within Integration Bandwidth
P(int.) = Power in 'Interfering Signal correlated with Desired Signal ' within Integration Bandwidth
Rc = Code Chip Rate

Figure 2.14 Crosstalk Interference Diagram

2.3.8 Required Carrier-to-Noise Density Ratios

There are two factors which immediately affect the required carrier-to-noise density ratios. One is the need for sufficiently small phase errors of the recovered carrier of the transmitted signal. The second factor is the need to guarantee that the signal can be acquired in an amount of time small compared to the pass duration. In work done by Cheng *et al*[28], estimates are made for the mean acquisition time of a noisy signal coherently correlated against a copy of the original code, in the presence of Doppler shift. In the study, the crosscorrelation is sampled and placed through a Fast Fourier Transform. The parameters which are sought are code-phase offset, code-frequency offset, and carrier-frequency offset. The crosscorrelation function is characterized as a non-central χ^2-distribution with two degrees of freedom. By integrating this probability distribution, the

[28]Cheng, U., *et al.*, "Spread-Spectrum Code Acquisition in the Presence of Doppler Shift and Data Modulation," *IEEE Trans. on Communications*, Vol. 38, No. 2, February 1990.

probability of detection is calculated. The mean acquisition time (T_{acq}) is given as

$$E\{T_{acq}\} = \frac{(K+1)}{P_D} T_I \tag{2.14}$$

where T_I is the coherent integration time, P_D is the probability of detection, and K is a factor to account for verification searches (in this case, K is set to 1). The variance of T_{acq} is

$$\sigma^2_{T_{acq}} = \frac{1 - P_D}{P_D^2} (K + 1)^2 T_I^2 \tag{2.15}$$

Figure 2.15 shows the mean acquisition time and its standard deviation for the two GeoBeacons signals. The choice of required carrier-to-noise density ratio reflects a tradeoff between long acquisition times and unnecessary high $(C/N_0)_{req}$. The chosen $(C/N_0)_{req}$ values for the two signals (24 dB Hz for the 401 MHz signal, and 20 dB Hz for the 2.036 GHz signal) are noted with arrows in the figure.

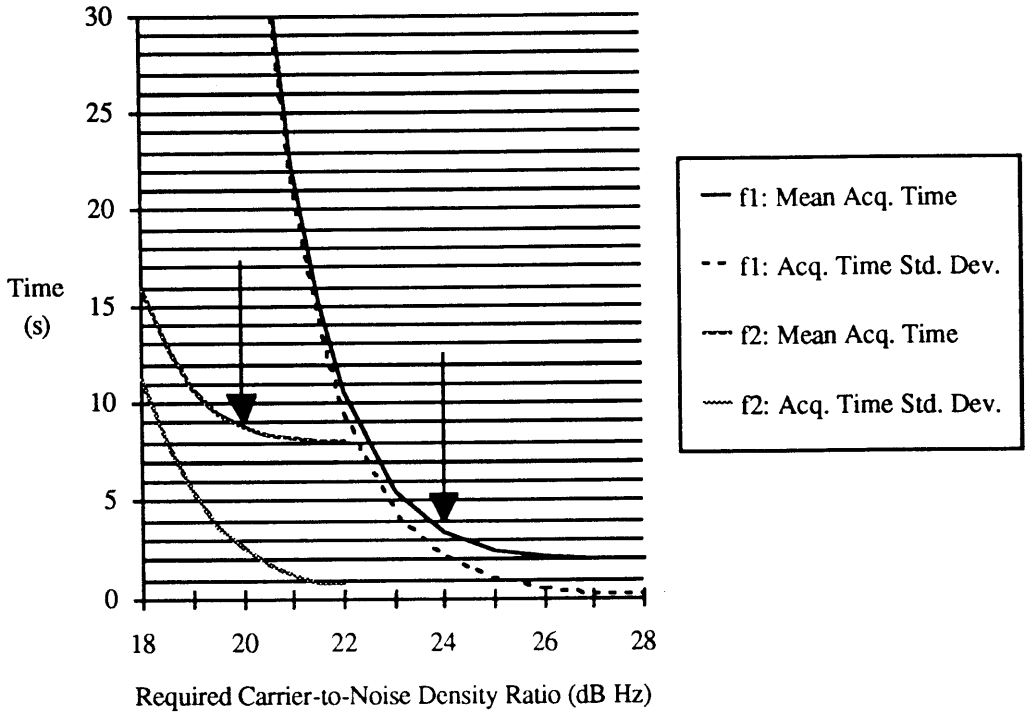

Figure 2.15 Mean Acquisition Time and its Standard Deviation versus $(C/N_0)_{req}$
(uncertain carrier-frequency range = 1 kHz, 10^{-4} chip slips during integration,
two searches (initial acquisition and verification), code length: 16384)
(f_1 (401 MHz): T_I = 1 s, Carrier Frequency Resolution = 1 Hz;
f_2 (2036 MHz): T_I = 4 s, Carrier Frequency Resolution = 0.25 Hz)

2.3.9 Required Transmitter Power

In order to choose the ground transmitter and satellite transmitter values, it is necessary to establish the relative importance of the costs of three items: the ground transmitters, the satellites, and the receiving dishes at the central site. Of the three, the receiving dish costs are least important, since they are inexpensive compared to the satellites, and only a few are needed (in contrast to the thousands of ground transmitters likely to be involved). It would be desirable to have small receiver dishes on the order of a few meters in diameter.

The ground transmitter and satellite costs are both sensitive to the power

requirements, but in different ways. It is important to ensure that the satellite transmitter power requirements are within the bounds available with the Microsat spacecraft, approximately 4 watts[29]. If the satellite needed to be resized to accommodate a larger power requirement, the satellite construction costs would rise, and the possibility of deploying the constellation with a single launch would be in jeopardy. On the other hand, these is no strong need to bring the satellite transmitter power requirement to an absolute minimum. Since one launch will be needed anyway, and it has already been established that at least 16 Microsat spacecraft can be deployed from a small payload launcher, there is little cost savings in downsizing the satellites (to Nanosats). For the ground transmitters, it would be cost-effective to make the power requirement as low as possible.

Figure 2.16 shows the tradeoff between satellite and ground transmitter power requirements for different receiving dish sizes, using the link power budgets (shown in detail in Appendix A). Arrows mark the power values selected at the two signal frequencies, for both the gravity gradient and passive magnetic stabilization systems (see Table 2.6).

	Gravity Gradient Stabilization		Passive Magnetic Stabilization	
	f_1	f_2	f_1	f_2
Ground Transmitter	85 mw	30 mw	40 mw	30 mw
Satellite Transmitter	270 mw	244 mw	227 mw	215 mw

Table 2.6 Required Ground and Satellite Transmitter Powers
(f_1: Lower Frequency Allocations, f_2: Higher Frequency Allocations)

The power requirements for the gravity gradient case are slightly greater than those for the passive magnetic stabilization case. This is due to a conservative approach to the link calculations. For the gravity gradient case, we assumed a satellite pointing error of 10

[29]King, *ibid.*

degrees. The uplink signal was being received at a lower gain than expected, but the noise power from the Earth was being received at the same gain (the main beamwidth lobe is still pointed in the direction of the Earth). In the magnetic stabilization case, the signal and noise power levels received by the satellite are essentially independent of the satellite attitude.

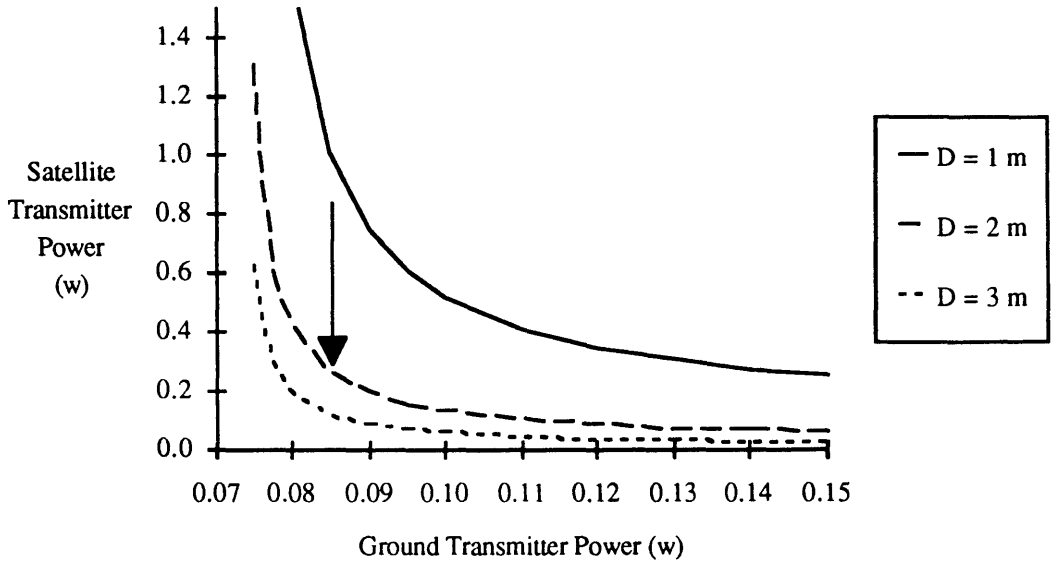

(a) Lower up-and downlink allocations; Gravity Gradient Stabilization

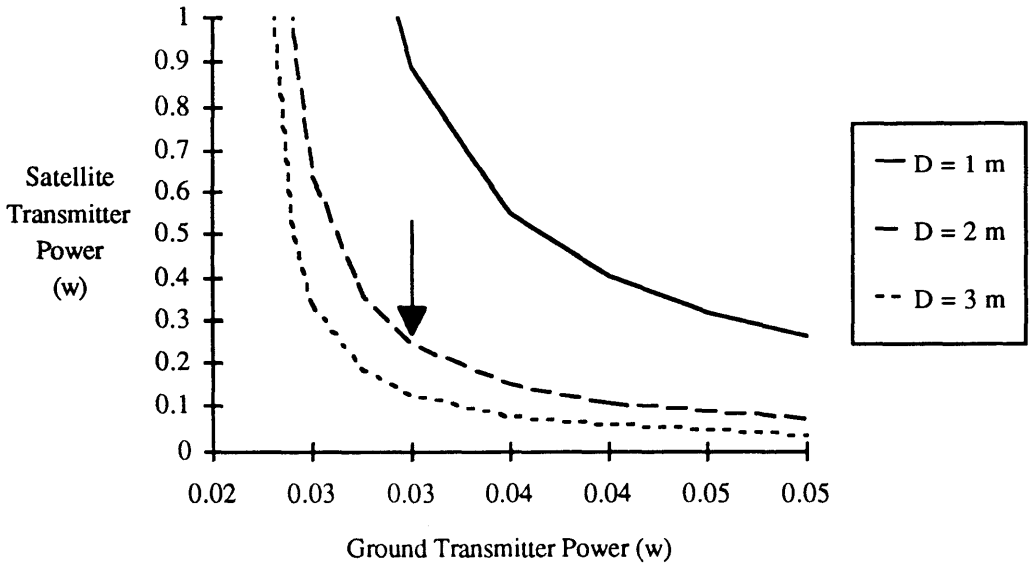

(b) Higher up-and downlink allocations; Gravity Gradient Stabilization

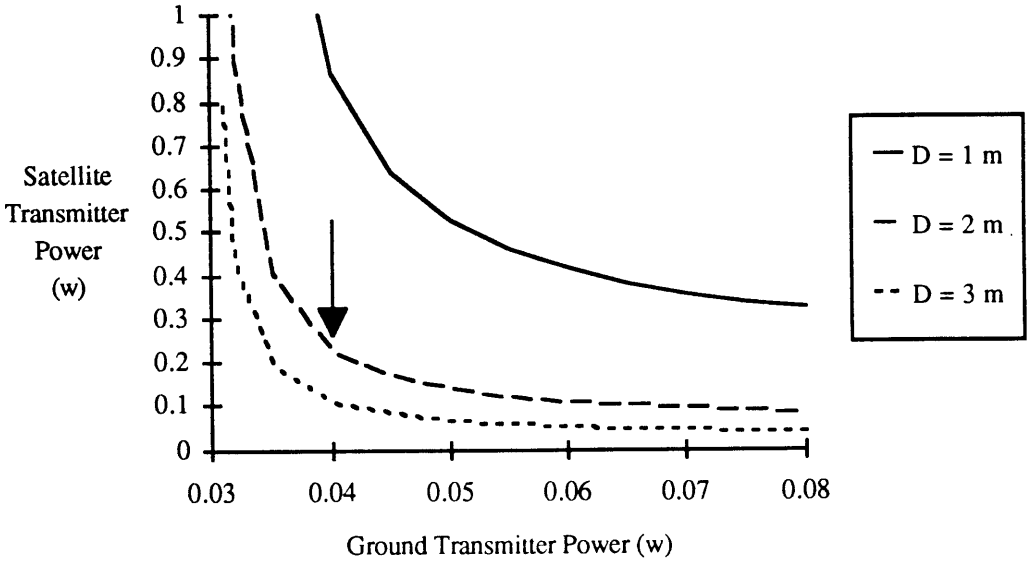

(c) Lower up-and downlink allocations; Passive Magnetic Stabilization

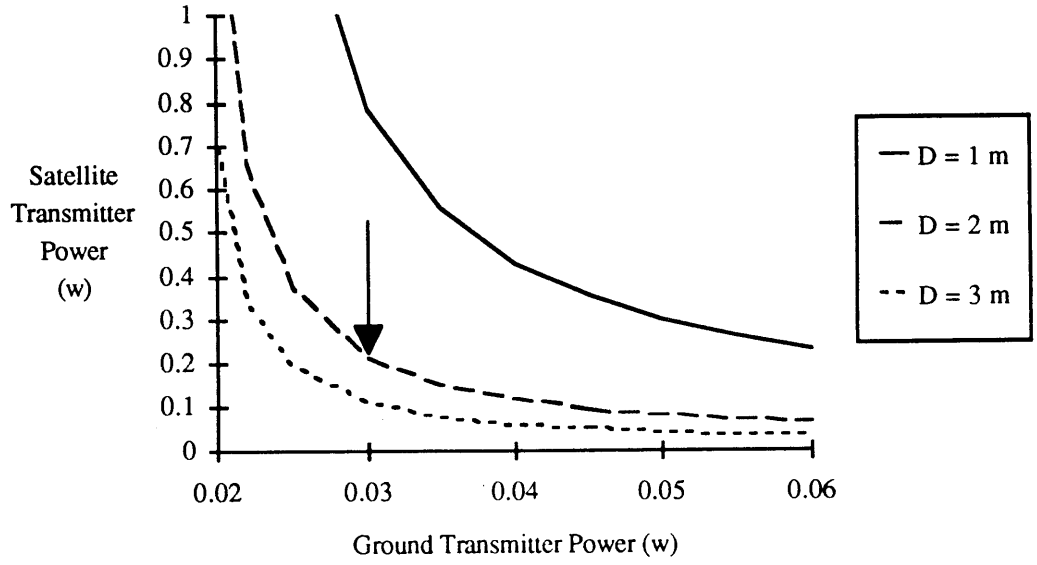

(d) Higher up-and downlink allocations; Passive Magnetic Stabilization

Figure 2.16 (a,b, preceding page; c,d, this page)
Satellite Transmitter Power versus Ground Transmitter Power and Receiving Dish Diameter (D)

3. Comparison of GeoBeacons and GPS Positioning Capabilities

In the previous chapter, two baseline configurations were defined for a possible GeoBeacons-based network. Both GeoBeacons- and GPS-based geodesy rely upon the same radio signal measurement, the double difference phase observable. However, the GeoBeacon and GPS satellite constellations differ in number of satellites, orbit size, and number of orbit planes. In this chapter, the effect of these differences upon positioning capability is examined.

Four figures of merit are defined and calculated to compare the geodetic positioning capabilities of the baseline GeoBeacon systems against a GPS-based network. The first figure of merit involves PDOP as defined in Chapter 2. The variation of station PDOP with network latitude, for small networks, will be presented. The second figure of merit also involves PDOP, in a comparison of simulated positioning capabilities for a network in California. This figure of merit was created in order to introduce a plausible network arrangement into the comparison. By varying the observation duration, changes in the geometric strengths of GeoBeacons and GPS constellations can be compared. The third figure of merit is the maximum length baseline whose ends can be observed simultaneously, including the variation of these lengths with latitude. This figure of merit reflects the ability of a particular satellite constellation to accommodate large geodetic networks over the Earth's surface. The final figure of merit is the maximum network spatial and temporal measurement density, which helps compare the systems' resolution of the crustal motion 'signal' which is being studied. For the GeoBeacon case, the '2-sat' and 'Multi-sat' configurations are considered, and the '18+3 spare' satellite constellation is used to represent the full capabilities of GPS. In this constellation, the satellites are launched into six different orbit planes (see Table 3.1).

The code used in Chapter 2 to study PDOP as a function of satellite geocentric angle of separation was used to compare GPS and GeoBeacon network-constellation scenarios. For the GPS case, valid measurements were counted when a station was in view of the same two satellites. For the GeoBeacon case, valid measurements were counted when a particular station and the central station were both in view of the same two satellites.

Orbit Plane #	Right Ascension Node	Argument of Latitude
1	0°	0°, 120°, 240°, 30° (Spare #1)
2	60°	40°, 160°, 280°
3	120°	80°, 200°, 320°, 170° (Spare #2)
4	180°	0°, 120°, 240°
5	240°	40°, 160°, 280°, 310° (Spare #3)
6	300°	80°, 200°, 320°

Table 3.1 GPS Constellation ('18 + 3 Spare' Arrangement)[1]

3.1 PDOP Comparison for Small Networks

In this comparison of the three systems, orbits were simulated and the DOPs were calculated for a station in a small network, in the manner illustrated in section 2.3.5.3. Enough simulated observations were generated for each case such that adding more observations would not change the DOP values. For the '2-sat' configuration, seven satellite overlap events were included, spanning 100-day observation sessions.

The full GPS constellation provides a PDOP about equal to 5 for a network at low or mid-latitudes (see Figure 3.1 a). The increase in PDOP at polar latitudes results from a higher VDOP, brought about by a poorer distribution of the 55° inclination GPS satellites in elevation. Both GeoBeacon configurations (see Figures 3.1 b, c) have about the same

[1]Wells, David, *Guide to GPS Positioning*, Canadian GPS Associates, Fredericton, N.B., Canada, 1986.

VDOP. In both cases the distribution of the vertical component of the $\Delta\hat{s}$ vectors (defined in Equation 2.6) are the same. Also, both configurations have a horizontal $\Delta\hat{s}$ distribution which improves with increasing latitude, leading to an improvement in PDOP. The difference in the positioning capability of the two configurations is that, with 16 satellites, there are always at least two satellites suitably spaced (as covered in Section 2.3.5.3) when a network is passing under an orbit arc. Therefore, there is a more even horizontal distribution of $\Delta\hat{s}$ with the larger configuration.

To illustrate the change in GeoBeacon positioning capability with latitude, Figures (3.2 a, b) show a typical series of GeoBeacon passes at a mid-latitude and at a high latitude site. The $\Delta\hat{s}$ vectors from any one pass essentially lie in a plane defined by the site and the satellite sky tracks. For the polar-orbiting GeoBeacon '2-sat' configuration, the $\Delta\hat{s}$ vectors have strong vertical and North-South components, but poor distribution in the East-West direction at mid-latitudes. For a network at a high latitude, the passes are more frequent and better distributed in local azimuth, leading to a drop in HDOP without any sacrifice in VDOP.

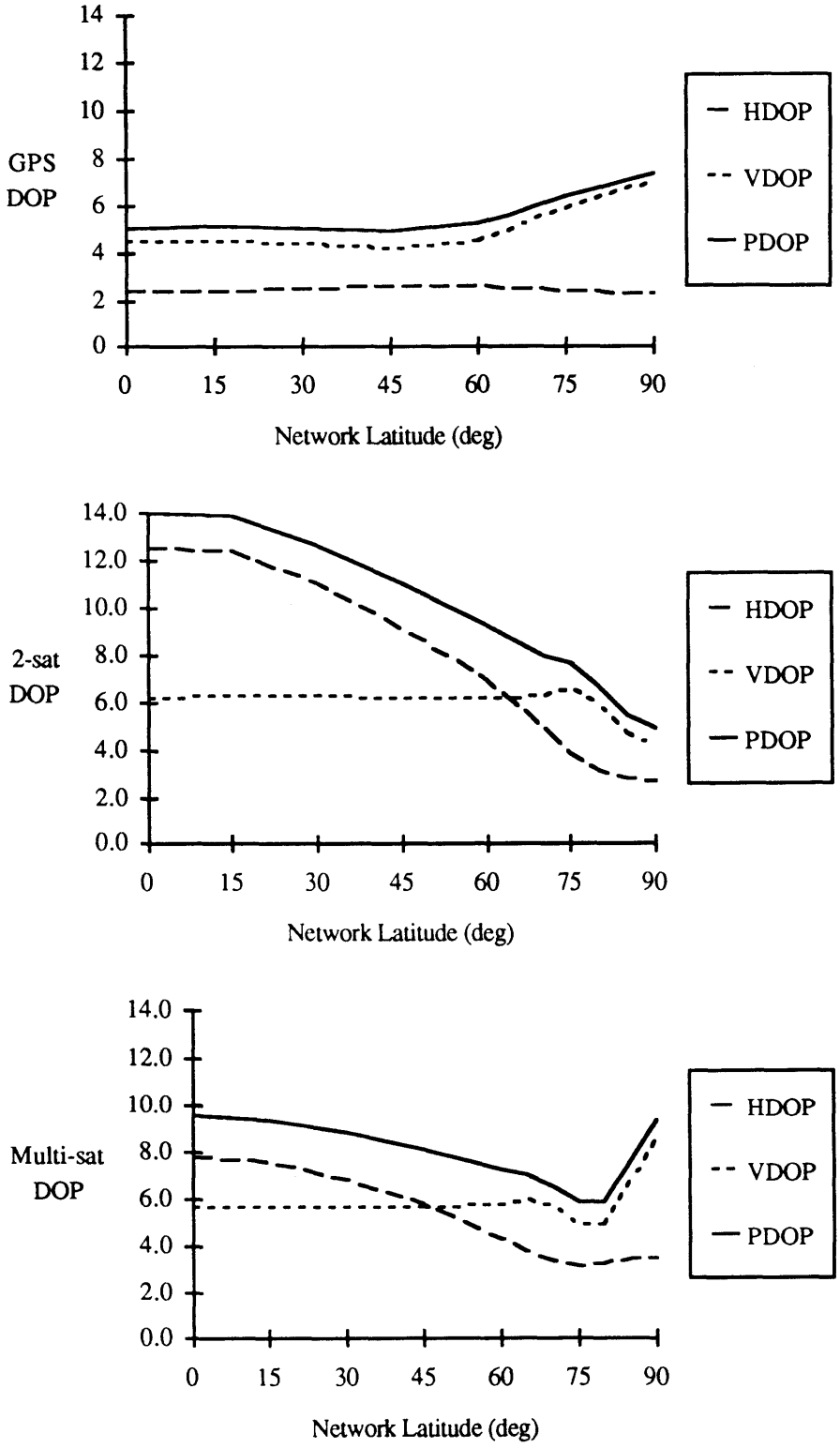

Figures 3.1(a-c) DOP vs. Network Latitude
(a, Top) GPS (33 d runs, 60 s intervals)
(b, Middle) GeoBeacons '2-sat' Configuration (100 d runs, 10 s intervals)
(c, Bottom) GeoBeacons 'Multi-sat' Configuration (10 d runs, 10 s intervals)

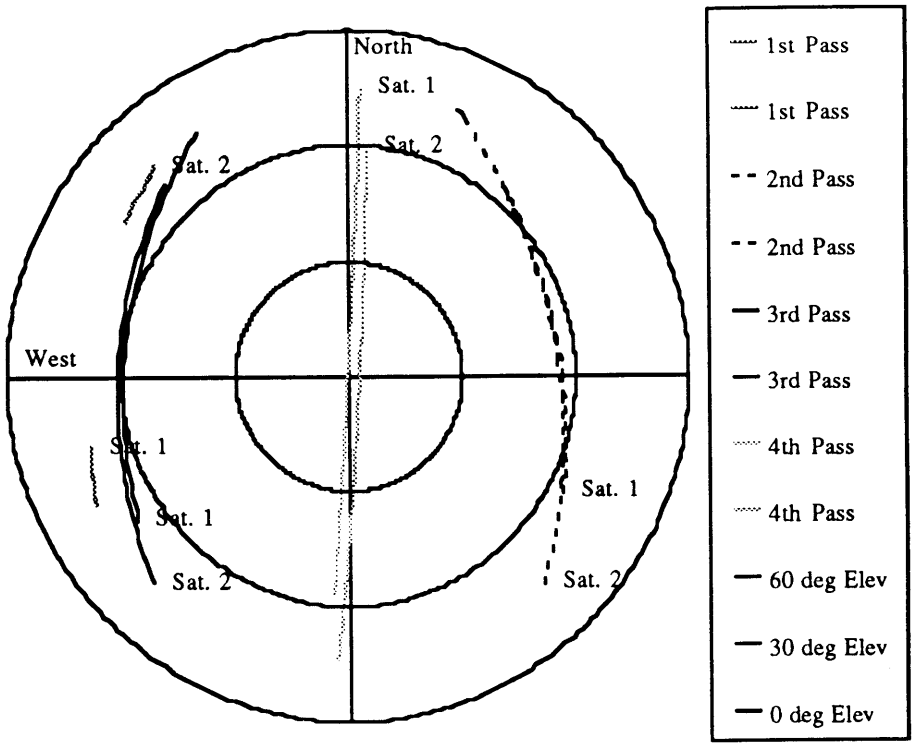

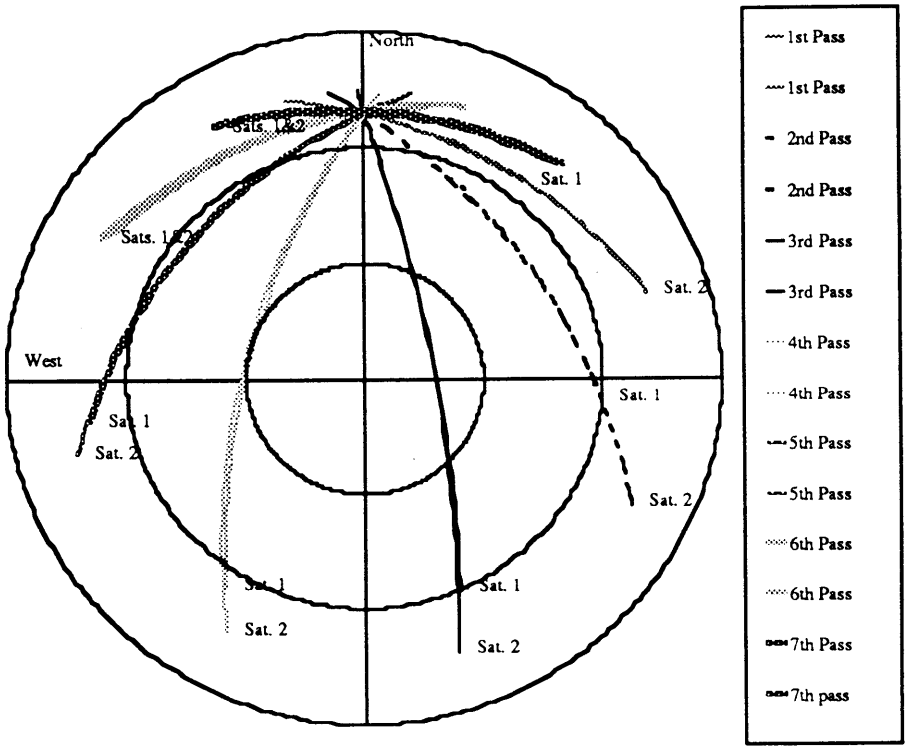

Figures 3.2(a,b) Sky Plots of 2 Simultaneously Visible GeoBeacon Satellites
(a, Top) Network Latitude: 35° N (24 h sample of passes);
(b, Bottom) Network Latitude: 75° N (12 h sample of passes)

3.2 PDOP Comparison for a California Network

The objective of this particular comparison is two-fold. First, it is necessary to compare GeoBeacon and GPS positioning capabilities for a realistic network. The intent of this comparison is to see if the overlapping GeoBeacon footprints can cover remote sites and the central site in a plausible scenario. Second, it is important to know how long it would take for a particular PDOP level to be achieved.

It was decided to simulate an 8-station network in southern California. Though the station deployment (see Figure 3.3) does not coincide with any existing geodetic network, the sites roughly encompass a well-monitored portion of the San Andreas fault. Should either GeoBeacon configuration ever be put into operation, California would be an ideal place to first deploy a network. The positioning accuracy of a GeoBeacon network would be relatively easy to verify with existing VLBI, GPS, and ground-to-ground laser ranging stations.

In these simulated observation sessions, the highest, lowest, and network average PDOP values were calculated and presented.

Figure 3.3 Sites Considered for 'California' Network
(Maximum Baseline Distance: San Francisco - San Diego (739 km))

Due to the large number of satellites always present in the sky with the full GPS constellation, only a few hours of observations are needed for the minimum PDOP level to be reached (see Figure 3.4 a).

For the '2-sat' configuration, it is important to know when the next satellite overlap event will take place. The network must not only be beneath an orbital arc, the two satellites must be near each other for suitable measurements to be made. For this reason, in Figure 3.4 b the station PDOP values are plotted against the time after the overlap event, which occurs every two weeks in this configuration. The arrows in the chart mark the times of six passes. After the first pass, there is no meaningful PDOP to report, since good 3-d positioning cannot be established with one pass. Starting with the second pass, each successive pass improves the PDOP obtained.

For the 'multi-sat' configuration, there is always an adequately spaced pair of satellites appearing over the network twice a day. In Figure 3.4 c the network PDOP drops quickly every twelve hours, reaching the limit shown in Figure 3.1 c after two days of observations. The fact that the limit is reached indicates that the GeoBeacon satellite footprint size does not handicap GeoBeacon positioning capability in this California network.

However, for short term observation sessions (~1 d), there appears to be a spread of GeoBeacon PDOP values among the stations that GPS PDOP values never exhibit. This GeoBeacon PDOP distribution reflects a difference between the GeoBeacons and GPS system data retrieval architectures. In GPS surveying, only the baseline ends need to view the same satellites, while with GeoBeacons, the baseline ends and central station need to view these satellites, in order to perform measurements. With GeoBeacons, the station farthest from the central site will generally have the highest PDOP, and a transmitter at the central site itself should have the lowest PDOP. This was the case for the GeoBeacon configurations, with San Francisco having the highest and Bakersfield the lowest PDOP values.

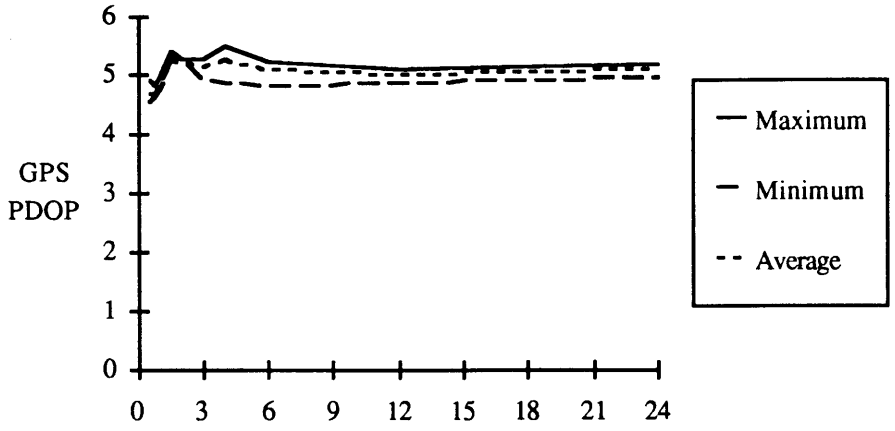

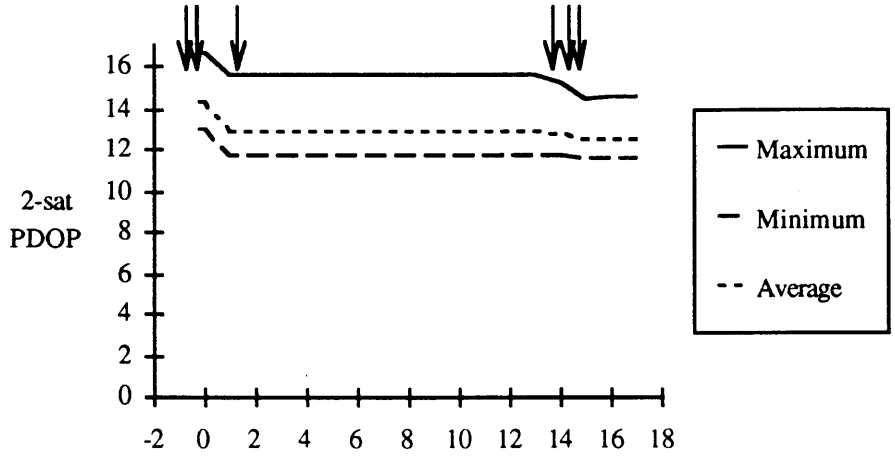

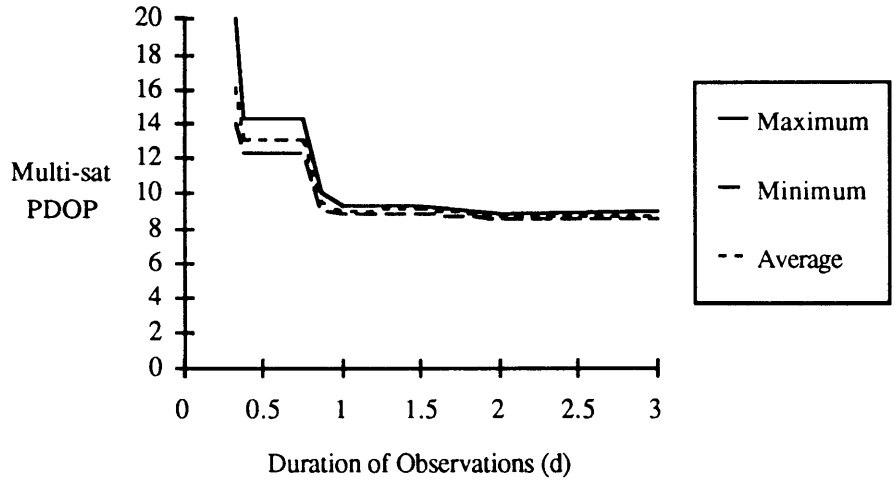

Figures 3.4(a-c) PDOP Versus Observation Duration
(a, Top) GPS (60 s intervals)
(b, Middle) GeoBeacons '2-sat' Configuration (10 s intervals)
(c, Bottom) GeoBeacons 'Multi-sat' Configuration (10 s intervals)

The results for each of the three cases also confirms that the duration of the computer runs in section 3.1 was long enough to yield the asymptotic PDOP limit for each latitude.

3.3 Maximum Length Baseline in a Network

In order to estimate the length of the maximum length baselines measurable with each satellite system, observations were simulated for a one-baseline network. One station was located at the central site, and the other station was considered to be the remote site. These stations (both north-south and east-west baselines were examined) were separated in successive simulations until the PDOP for the remote station exceeded the 'small station' (~0 length baseline) PDOP by 50%. Figure 3.5 a confirms that the GPS constellation provides intercontinental baseline measurement capability, especially at low latitudes. The GeoBeacon '2-sat' configuration (Figure 3.5 b) can observe baselines up to about 1500 km in length over most latitudes. There is a more even distribution of inter-satellite spacing in the multi-sat configuration. This distribution provides a better opportunity to obtain a large overlapped footprint zone, allowing longer east-west baselines to be measured.

Although the GeoBeacon baselines are significantly shorter than what is attainable with GPS, GeoBeacon baseline capability is more than enough for dense local networks (for example, the length of the state of California is ~1200 km).

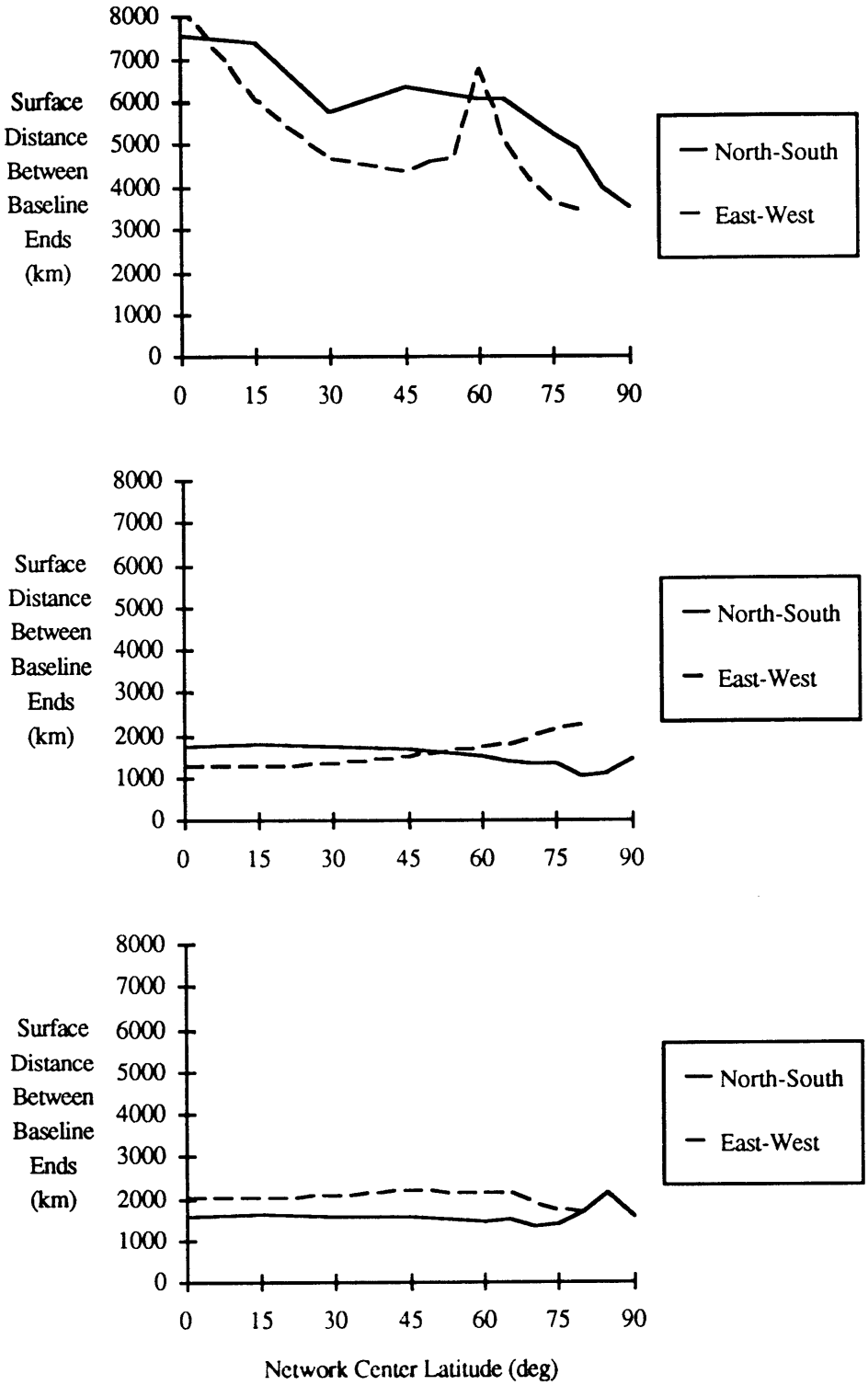

Figures 3.5(a-c) Maximum Baseline Length vs. Network Latitude
(a, Top) GPS (10 d runs, 180 s intervals)
(b, Middle) GeoBeacon '2-sat' Configuration (100 d runs, 20 s intervals)
(c, Bottom) GeoBeacon 'Multi-sat' Configuration (5 d runs, 20 s intervals)

3.4 Maximum Measurement Density

Comparisons between an existing and a proposed system are risky. Failure to recognize unforeseen limitations in strawman designs, such as the GeoBeacon configurations, make any subsequent performance comparisons to GPS unfair. The objectives of this section are to identify the factors which are expected to limit the spatial and temporal measurement density of GPS and GeoBeacon networks, and to estimate these limits.

3.4.1 Spatial Density

If one possessed the capability to easily collect measurements from remotely sited GPS receivers, there would be no physical limit to site density in a network. Assuming that the GPS receivers are engineered to minimize RF interference, they are passive devices and do not interfere with one another. At present, however, the largest GPS networks in existence (or soon to be deployed) have on the order of 200 stations, spaced an average of 50 - 100 km apart. Surveys of such a network use on the order of 10 to 20 receivers at one time.[2] Measurement data at present are usually brought back to the processing center along with the receivers themselves. The spatial limit at present appears to be the number of GPS receivers that can be collected and deployed at one time by the sponsoring organization.

As mentioned in Chapter 1, one large advantage of monitoring large networks of ground transmitters is that one need not revisit stations after the initial deployment. While GeoBeacons is not expected to have logistics-related limits on spacing, there will be a limit brought about from the crosstalk interference from all the transmitters simultaneously in view. In Appendix A, both GeoBeacon configurations assumed that 10 000 transmitters were in view. The estimated crosstalk interference was large compared to the expected

[2]From a survey of papers presented at the 1991 Fall AGU meeting.

radio noise density from other sources for the lower uplink frequency allocation. As mentioned in the power budget calculations, this number of transmitters deployed over an area the size of California would result in an inter-station spacing on the order of 6 km, resulting in an areal density about two orders of magnitude greater than that currently achievable with GPS.

3.4.2 Temporal Density

Once the full GPS constellation is in place, measurements can be made continuously. With the GeoBeacons '2-sat' configuration, positioning opportunities will recur every two weeks, with sets of passes appearing every twelve hours over 36 to 48 hours (see Figure 3.4b). With the 'multi-sat' configuration, positioning opportunities would occur twice a day, about twelve hours apart, every day (see Figure 3.4c).

4. Comparison of GeoBeacons and GPS Costs

We have described a new positioning system and have shown it to have a positioning capability adequate for monitoring dense intra-continental networks. In the final section of Chapter 3, we noted that GeoBeacon networks do not have a data-retrieval constraint upon measurement frequency as do existing GPS networks. Before seeking funding for continued studies, it is also important to study other factors affecting the systems' costs. Estimates of overall project and user costs of large GPS and GeoBeacon geodetic networks will be presented in this chapter. The objective is to determine the break-even point, that is, the minimum number of ground sites needed for a GeoBeacon-based system to be cost-competitive with GPS.

4.1 Initial Cost Assumptions

As was done in Chapter 2, a set of assumptions will be made to facilitate the costing analysis, without unnecessarily restricting the effectiveness of this system comparison. For example, since both GPS- and GeoBeacon-based positioning use the same doubly differenced phase observable, data storage and processing costs should be essentially identical for networks of the same size. Therefore, all costs associated with storing and processing phase measurements after they are collected at the central site in both cases will be neglected. Since this commonality also appears in the deployment of the network receivers / transmitters, those deployment costs will not be included in the comparison.

Another consideration which must be made is to recognize the difference between paying for the entire system and paying for a service provided by a constellation of satellites. In this study, project costs will include that of all required hardware (ground and space-based) and mission operations. User costs include the costs of only ground based hardware.

From the comparisons made in Chapter 3, it is evident that only the 'Multi-sat' configuration has a positioning capability comparable to that of GPS. Therefore, the main comparison in this chapter will be between the full GPS constellation and the 16 satellite GeoBeacon constellation. However, it is possible to perform positioning with as few as two satellites (provided each carries transponders operating at the same two frequency bands). With the increasing trend towards multi-satellite communications projects, an opportunity to use two existing satellites in a GeoBeacons test network may arise in the future. Therefore, the user costs of a '2-sat' configuration will also be included, keeping in mind its potentially poor positioning capability. Also, in all cases, the hardware and project lifetime is on the order of ten years.

Finally, a data retrieval system needs to be chosen for the candidate GPS network. In order to make this an objective comparison between the two systems, a method must be selected to bring back the one-way phase measurements to a central site (laboratory, computing center) inexpensively without changing the measurement capabilities inherent in the GPS constellation. Data retrieval systems can be grouped into the following four categories:

(i) Manual Retrieval: Since GPS receivers are seldom left in the field at present, phase measurements are usually retrieved with the receivers at the end of an observation session. For large (> 1000 site networks), it is extremely doubtful that the sponsoring organization would want to deploy and retrieve the receivers at every site between measurement campaigns. Even if the hardware could be left unattended, it would still be difficult for a university or government laboratory to employ enough people to retrieve data, especially from remote sites.

(ii) Phone Link: If the receiver could be permanently deployed, and a phone line installed to the site, the site need not be visited again except for possible maintenance. However, using phone links favors networks near developed

areas. Costs between networks in California and Alaska, for example, would widely vary.

(iii) Ground Radio Link: Installing a ground radio link at each site would eliminate the need for site visits and the bias towards the selection of developed sites. However, since this radio network does not exist at present, it would have to be designed and built, adding to the project and user costs.

(iv) Satellite Radio Link: A network of GPS receivers with satellite radio links to the central site sounds suspiciously like the fusion of the GPS and GeoBeacon systems. In the GPS case, however, only the phase measurement values would be relayed to the central site. If an existing satellite constellation could be used for this purpose, it would offer all the advantages of a ground radio link and eliminate additional development costs.

It appears that there will soon be a satellite system that will inexpensively meet our data retrieval needs. A mobile communications service named ORBCOMM is expected to go into operation by mid-1994. It is made up of an Earth-based message processing center and 20 low-earth orbiting satellites. The system is targeted to serve users with low data rate needs and high geographic distribution, by minimizing the cost per data bit[1]. Figure 4.1 lists the type of customers targeted by ORBCOMM. Our geodetic needs appear to be matched by the service they will provide. At present, user equipment costs are estimated to range between $50 - $400 / unit, and service will be offered at an annual rate of $30 - $400 / yr.

[1]Dr. Antonio Elias, Orbital Sciences Corporation, personal communication.

Emergency Services	Road Service Search and Rescue Medical
Data Acquisition	Environmental Monitoring Industrial and Utilities Monitoring Remote Asset Monitoring
Tracking	Boxcars and Containers Property Recovery Animal Tracking Customs and Shipment Security
Messaging	Personal Business Trucking

Table 4.1 Examples of Services To Be Provided by ORBCOMM[2]

This proposed system meets our data retrieval needs. The total cost per site of using ORBCOMM is a fraction of the cost of the GPS receiver itself. Therefore, the ORBCOMM system will be used to represent the costs of a GPS network data retrieval system.

4.2 Total Network Cost Comparison

The selection of ORBCOMM eliminates development costs for a GPS network. Hardware costs include the ORBCOMM transmitters, GPS receivers, and the interface between the two. Geodetic GPS receiver costs have been dropping consistently now for about a decade, and it is believed that they will reach the $500 - $1000 range within a few years. The ORBCOMM costs are presented above, and the interface costs would roughly double the ORBCOMM transmitter cost.

In the GeoBeacon network, the function of the ground transmitter is similar to that of existing ELTs. Therefore, the cost per transmitter is estimated to be in the $100 - $200

[2]This information was presented at an ORBCOMM review, November 1991.

range. Additional network costs include satellite construction and launch, as well as the dishes and correlators at the central site. The correlators are needed in order to identify one-way phase measurements from each of the transmitters.

Estimates for the construction cost of a AMSAT-class Microsat range from $400,000[3] to $1,000,000[4] per satellite ($US 1990). The launch costs are essentially independent of the number of satellites, since only one launch is needed. At the high end, a Pegasus launch costs about $8,000,000 ($US 1990)[5]. On the other hand, the AMSAT community has launched up to four Microsats at a time by "piggy-backing" them onto the payload platform of an Ariane-4. It is possible to place up to eight microsats on one launch, at a cost of ~$100,000 per satellite[6].

At the central site, two antennas would be needed for the '2-sat' configuration, and four dishes should meet the viewing requirements of the 'Multi-sat' configuration. In this comparison, the costs of the hardware needed to track these satellites is also included. Our estimate of the tracking hardware costs come from descriptions of rigs used by amateur radio enthusiasts to track OSCAR (Orbiting Satellite Carrying Amateur Radio) satellites, in the $1000 - $5000 range. Finally, the cost of the correlator ($1.25 to $2.5 million) comes from an estimate of the purchase or joint use of a MARK-III correlator currently used in VLBI.

In Figure 4.1, we incorporate all the costs mentioned and present them as a cost per site per year, as a function of number of sites being monitored. Keep in mind that these estimates only include costs not held in common by the different systems. The 'Multi-sat'

---

[3]Wertz and Larson, Chapter 22. These satellites were built with student and faculty support.
[4]Based upon the proposal made by Drs. Clark and Counselman (of the GeoBeacons group) to obtain funds from the NASA / Goddard Director's Discretionary Fund.
[5]Wertz and Larson, Chapter 20.
[6]Clark and Counselman, *ibid.*

network appears to become competitive with GPS-based networks at about the 10,000 station level, and the '2-sat' network breaks even around the 1,000 station level.

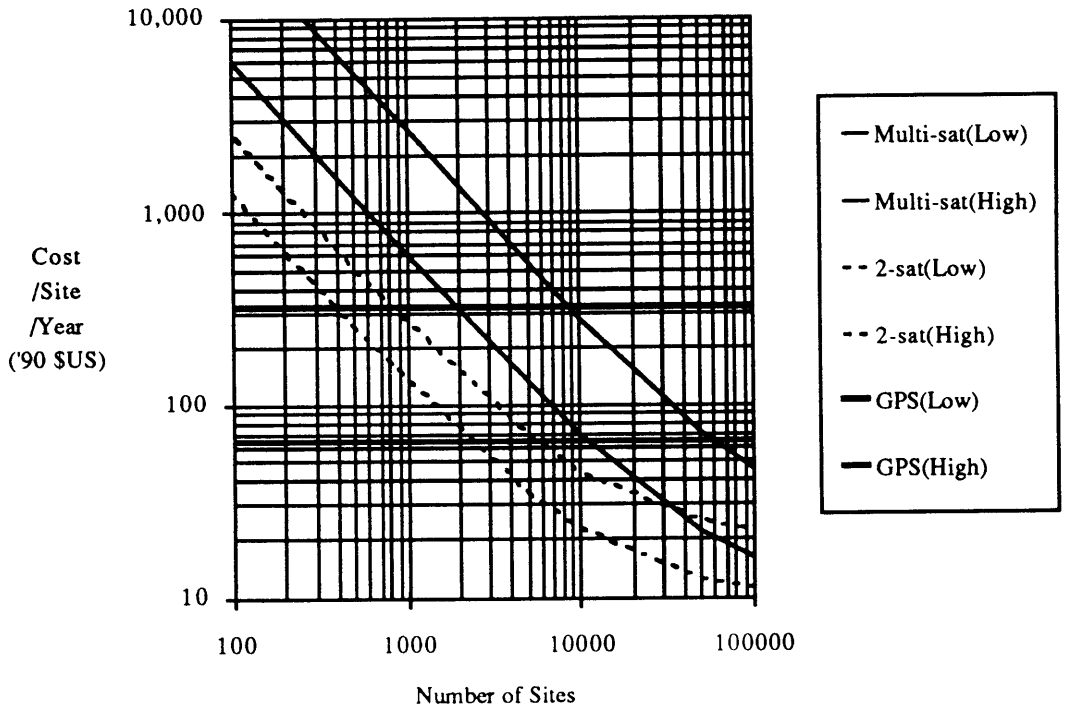

Figure 4.1 Comparison of GPS and GeoBeacon Total System Costs

4.3 User Cost Comparison

As was mentioned in the description of the ORBCOMM system, many groups of users will share the entire cost of the system. It is plausible that groups of institutions could unite to share the costs of implementing a GeoBeacon system. As mentioned in Chapter 2, this type of project could become an Explorer class experiment, and be funded through NASA. In that case, the GeoBeacon user costs would drop significantly compared to the GPS-based system, and the number of stations required to breakeven is on the order of 1,000 stations for all GeoBeacon configurations.

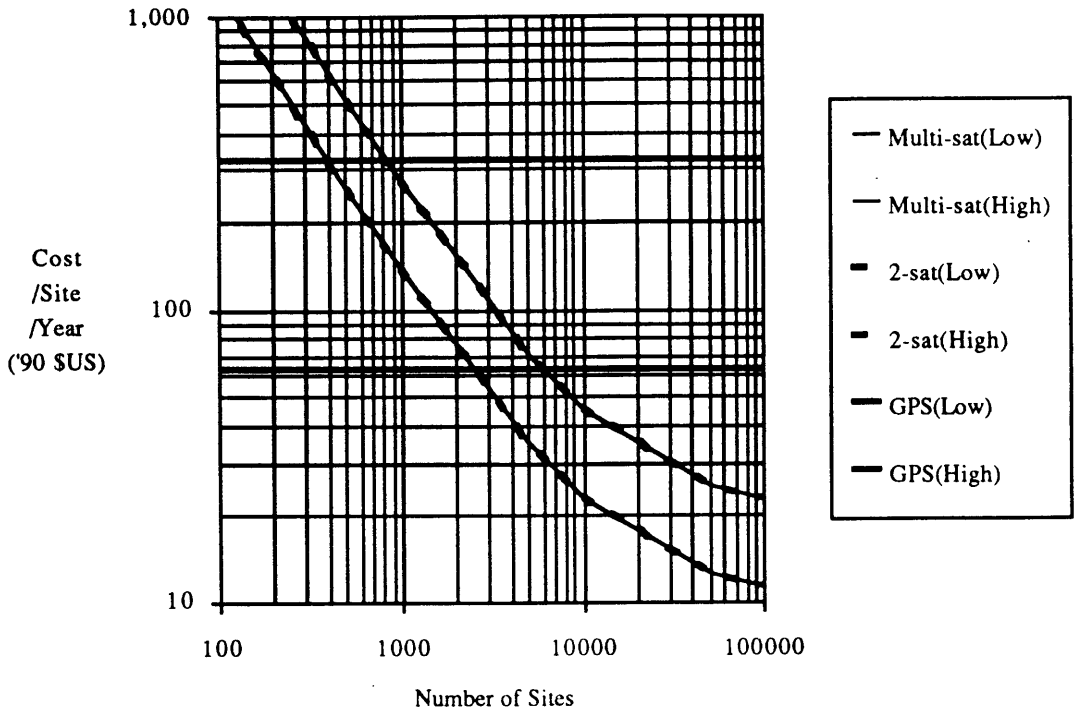

Figure 4.2 Comparison of GPS and GeoBeacon User Costs

5. Demonstration Experiment

As mentioned in introductory chapter, the GeoBeacon group commenced work on a demonstration experiment to imitate as closely as possible the components of the GeoBeacon system (see Figure 1.1) and demonstrate its usefulness as a geodetic tool. The GeoBeacon group (including the author) believes that a successful demonstration of the concept is necessary before a permanent, more capable system could be funded. Presented here is a summary of work completed to date on the experiment design, including the uplink and downlink power calculations, selection of transmitter codes and transmitter sites, and the simulation of the experiment itself.

5.1 Experiment History

In November 1989, a proposal for a GeoBeacons demonstration experiment was submitted by Prof. Charles Counselman of MIT and Dr. Tom Clark of NASA / Goddard to the Director's Discretionary Fund at NASA / Goddard, and accepted. From November 1989 through the summer of 1990, members of the GeoBeacon group worked on various parts of the experiment, and their progress was recorded in a series of reports. By the fall of 1990, when funding for the experiment ended, the GeoBeacons team had not yet performed the experiment, but had made much progress in its design. Some hardware had been purchased for the transmitter and receiver systems (for more details on the chronology of the project status, copies of the progress reports are available from the author).

The link calculations, code selection, network selection, and covariance simulation results which follow do not represent the total effort made by the GeoBeacons group. However, these sections represent the diversity of issues that need to be addressed by those who wish to perform this experiment.

5.2 Experiment Configuration

In this section, the satellite choices and initial transmitter arrangement are presented, along with a detailed explanation of the bias-fixing strategy (introduced in section 1.1.5) used to improve the orbit determination.

The experiment was to have been conducted at the NASA / Goddard Optical Research Facility (GORF) test range in Greenbelt, Maryland. From the GORF test range, up to four GOES satellites are visible (see Table 5.1 and Figure 5.1).

Satellite	a (km)	e (-)	i (deg)	Ω (deg)	ω (deg)	M (deg)	Average Elevation (deg)	Average Azimuth (deg)
GOES 2	42163	$4.74(10^{-4})$	8.42	-4.67	205.	101.	41.	152.
GOES 5	42182	$1.40(10^{-4})$	3.91	0.99	225.	12.5	26.	237.
GOES 6	42136	$8.43(10^{-4})$	2.56	6.15	202.	20.3	19.	246.
GOES 7	42166	$4.89(10^{-4})$	0.12	1.60	259.	352.	35.	223.

Table 5.1 Orbital Elements (and Elevation, Azimuth Angles from GORF Range (39° N, 77° W)) for GOES-2, 5, 6, and 7[1]

[1]The elements are from the 1950.0 Vernal Equinox frame, and the epochs (not shown) range from Julian day 332 to 338 in 1990. The orbital elements, from the NASA Prediction Bulletin, were obtained through the Celestial Bulletin Board Service, (513) 427-0674, (operates at 300, 1200, or 2400 baud, 8 data bits, 1 stop bit, no parity). The system administrator is Dr. T. S. Kelso of the Air Force Institute of Technology, Wright Patterson Air Force Base, OH, as of the spring of 1992. The orbital elements are consistent to within 5 km in position.

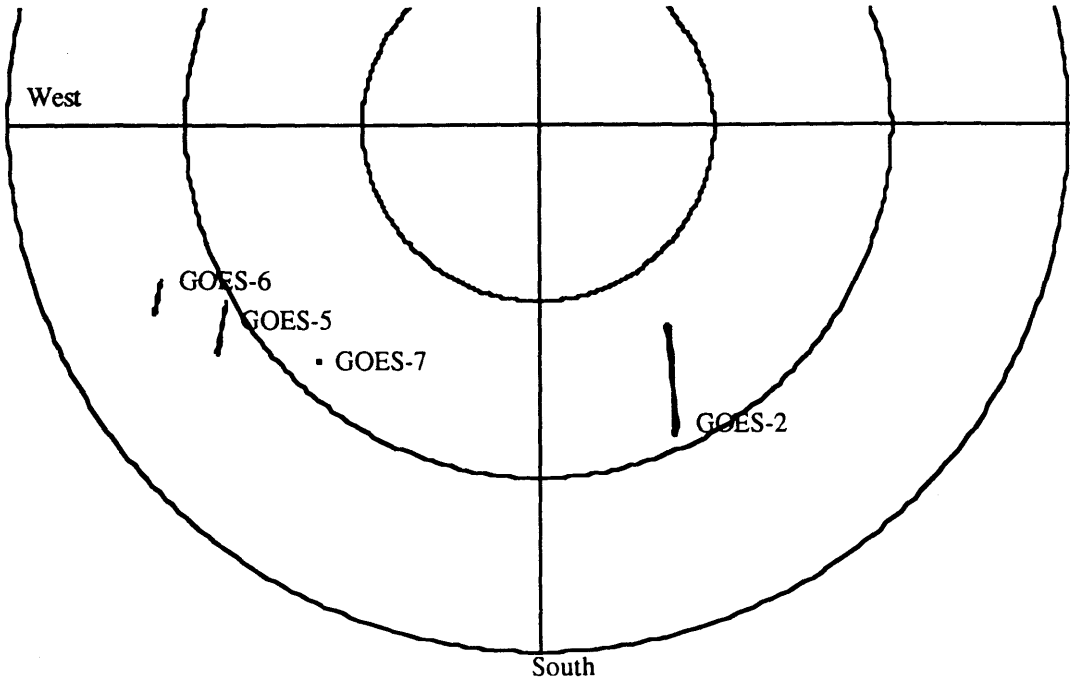

Figure 5.1 Sky Plots for GOES-2, 5, 6, and 7 as seen from the GORF Range (24 hr of observations).

5.2.1 Network Geometry

Since only one frequency allocation is available on the GOES transponders, the ionospheric phase contribution can not be solved for in this demonstration. In order to limit this contribution to the differenced phase measurements, the baselines will have to be limited in length to 1 km. It is known from GPS survey work, that for baselines on the order of 1 km in length, the residual ionospheric effect is less than five parts per million of the baseline length. The close transmitter spacing also aids in canceling the tropospheric phase contribution.

Now that the spatial scale of the network has been established, the number and arrangement of transmitters needs to be decided. In order to demonstrate the usefulness of the GeoBeacon concept, it would be necessary to be able to solve for at least the following parameters:

-satellite orbits

-integer-cycle biases of the doubly differenced phase observations

-station coordinates[2]

One goal of the experiment is to solve for all three coordinates of one station. In order to establish a coordinate frame for determination of these coordinates, the outermost stations' coordinates will be pre-determined through a GPS survey, and their coordinates will stay fixed in the least squares solution.

In order to facilitate the estimation of the integer-cycle biases (which will be explained in section 5.2.2), the ground transmitters will be arranged in a nautilus-shaped spiral (see Figures 5.2 a,b), with station separation increasing by a factor of 2 as one proceeds outward from the innermost transmitter. The resulting network is asymmetrical, having dimensions in the ratio of about 2:1. How should the spiral be oriented? As was shown in Chapter 2, the partial derivative of station position with respect to the double difference observable is the difference of unit vectors from that station to the satellites considered. Therefore, the network orientation does not depend upon site positioning performance. A covariance analysis (which will be explained in section 5.5) showed that the longest network dimension should be oriented along the arc defined by the satellites. This orientation minimizes the magnitude of orbit parameter estimate variances. Therefore, the network's longest baseline (stations 10 & 12) is oriented in an east-west direction. The longest dimension of this network is ~1100 m.

[2]The coordinates of at least three stations (the outer three stations) are left fixed in order to establish a coordinate frame for the remaining stations.

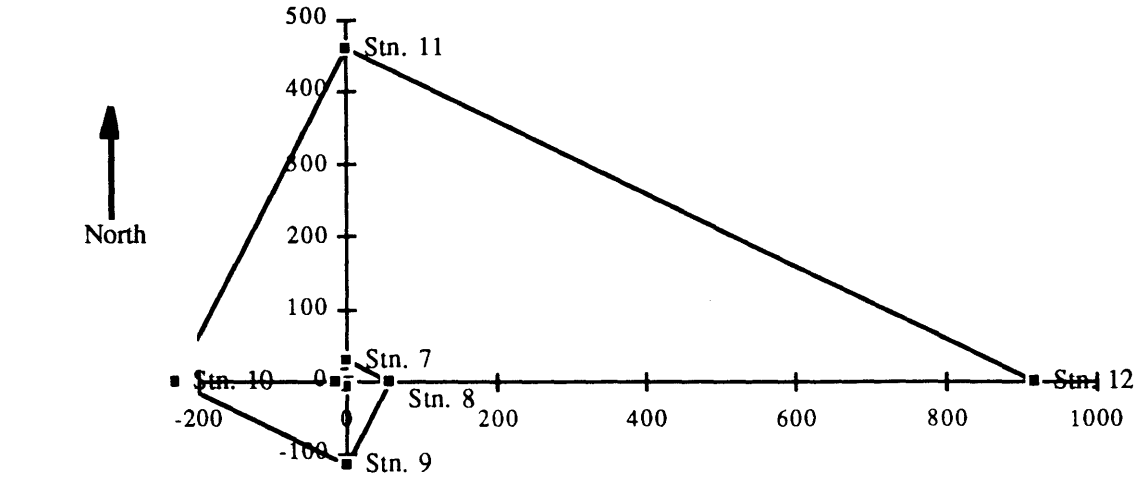

(a)

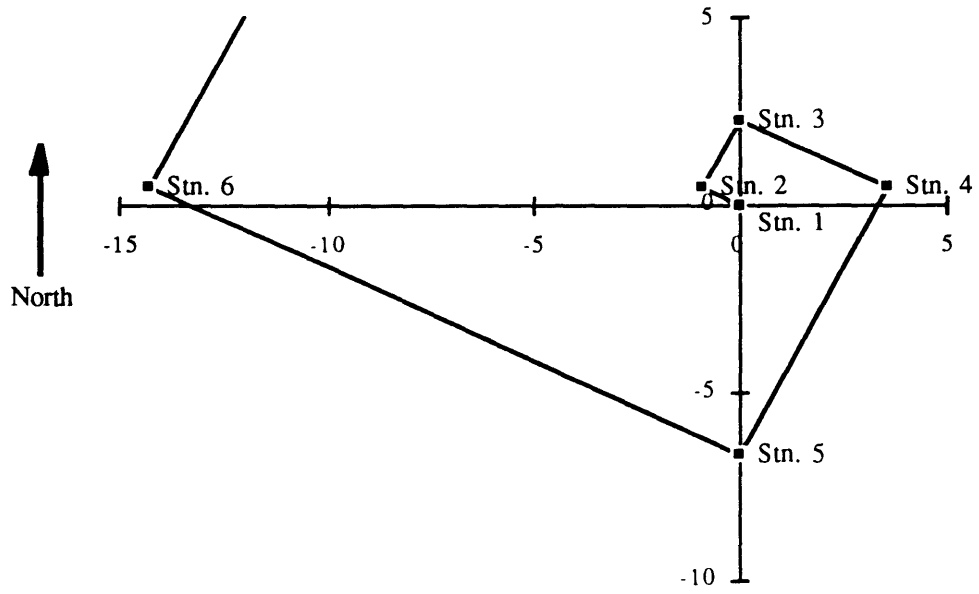

(b)

Figures 5.2 (a,b) Layout of Ground Transmitters for Demonstration Experiment
(E-W and N-S Axes in meters)

5.2.2 Bias-Resolution Strategy

In section 1.1.5, the nautilus network was reported to aid in fixing biases and obtaining precise orbit parameters without additional information from outside sources (once a coordinate-system had been defined). In this experiment, the same strategy will be employed. The purpose of this exercise is to determine how many stations the nautilus

spiral needs. In the covariance analysis, we start with a 12-station spiral. There is nothing special about having twelve stations, except that it provides a series of baselines with lengths increasing by a factor of two, from 1 m to 1024 m. We will solve for the initial position and velocity of each of the satellites observed, for all biases, and for the three coordinates of the innermost station (#1). If all the biases can be fixed through the application of bootstrapping (which will be introduced in section 5.5.2) to this station configuration, station 2 will be removed from the network, and the covariance determination software re-executed. If the bootstrapping continues to aid in fixing all remaining biases, stations 3, 4, 5, etc. are removed in successive runs until it is no longer possible to bootstrap to a complete solution, i.e. solve for all the biases.

5.3 Link Calculations

Table 5.2 lists the uplink and downlink power budgets for the demonstration experiment. The satellite transponder bandwidth, losses, and transmitter power are already determined; there is flexibility in the choices of ground receiving dish diameter and ground transmitter equivalent isotropically radiated power (EIRP).

Uplink:

(i) Transmitter E.I.R.P.	P_T	dBm	Objective: min(P_T)
(ii) Vacuum Path Length Loss	190.6	dB	40 000km @ 2029.1 MHz
(iii) Satellite Receive G/T	-17.1	dB/K	
(iv) Boltzmann's Constant	-198.6	dBm/HzK	
(v) Uplink Input C/N_0	(P_T - 9.1)	dBHz	= (i) - (ii) + (iii) - (iv)

GOES Transponder:

(vi) Hard Limiter Losses	1.5	dB	Assumed

Downlink:

(vii) Transmitter E.I.R.P.	53.0	dBm	dominated by uplink noise
(viii) Transponder Bandwidth	69.1	dBHz	8.2 MHz wide
(ix) Vacuum Path Length Loss	189.0	dB	40 000km @ 1687.1 MHz
(x) Receiving Antenna Gain	G_R	dB	
(xi) Received Noise Density (N_{0S})	(G_R-205.1)	dBm/Hz	= (vii) - (viii) - (ix) + (x)

Ground Receiver:

(xii) Receiver Noise Temperature	20.0	dBK	100 K
(xiii) Receiver Noise Density (N_{0R})	-178.6	dBm/Hz	kT_{sys}

Table 5.2 Uplink and Downlink Power Budgets for Demonstration Experiment

In order to demonstrate the tradeoff between receiver dish size and transmitter E.I.R.P., we start with the carrier-to-noise ratio at the ground receiver. This ratio is a function of uplink carrier-to-noise density ratio, receiver and downlink noise densities:

$$\left(\frac{C}{N_0}\right)_{TOT} = 20.0 \text{ dB (objective)} = \left(\frac{C}{N_{0S} + N_{0R}}\right) = \frac{1}{1 + F}\left(\frac{C}{N_0}\right)_{UP} \tag{5.1}$$

where $F = \frac{N_{0R}}{N_{0S}}$ (fraction of receiver noise density to downlink total noise density).

Substituting expressions (xi) and (xiii) for F in (5.1) yields:

$$G_R(dB) = 10 \log_{10}\left(\frac{513.}{P_T(w) - 1.15}\right) \tag{5.2}$$

Assuming an aperture efficiency of 50%, we can express the ground receiver antenna diameter (d) as a function of transmitter E.I.R.P.:

$$d(ft) = \frac{5.95}{\sqrt{P_T(w) - 1.15}}. \tag{5.3}$$

One cannot obtain sensible dish sizes for $P_T < 1.15$ w because below that level, one cannot even achieve an uplink carrier-to-noise ratio of 20.0 dB. Figure 5.3 shows the dish diameter required to achieve the desired SNR.

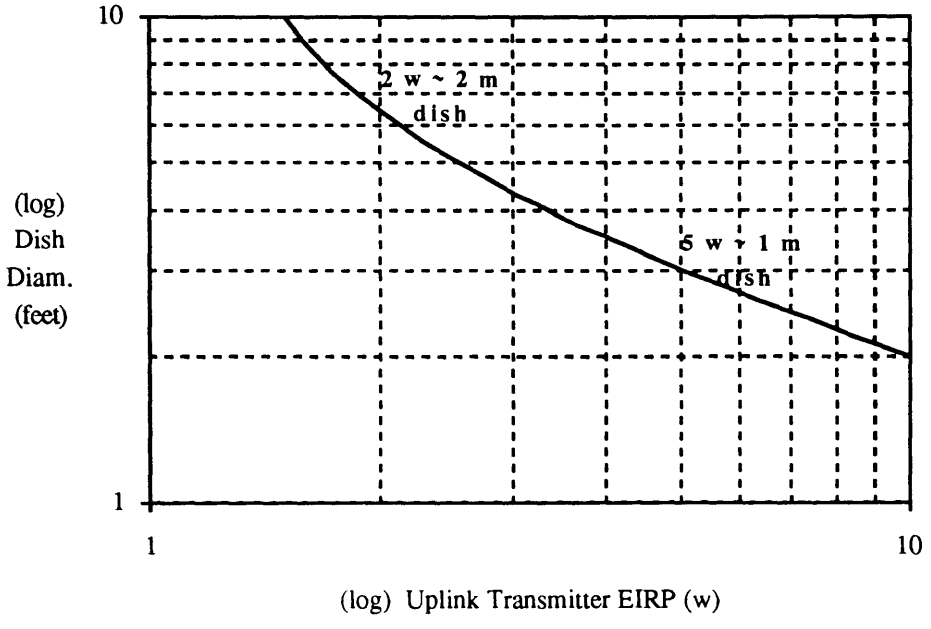

Figure 5.3 Downlink Dish Diameter Versus Uplink Transmitter EIRP Tradeoff

5.4 Transmitter Code

Although no hard decision was made on code period (repetition time interval), chipping rate (number of chips per period), or type of code, we have been assuming that (i) the received-signal-processor's carrier phase tracking loop bandwidth will be about 1 Hz, corresponding to a coherent-integration or code-correlation time of 1 second; and (ii) in this integration time, the code should have about $2^{12} - 1 = 4095$ chips. The 4095-chip estimate is derived from consideration of the crosstalk from the five other GeoBeacon transmitters whose signals will be present in addition to the signal desired to be tracked by a particular code-correlating loop. (Due to cost considerations, we had planned to use six transmitters in our initial experiments.) To facilitate code delay search during initial signal acquisition, we also assume that the code will be periodic with a period no greater than the integration time. So our baseline design calls for an approximately 4095-bit pseudorandom code sequence to be transmitted at a rate of about 4095 bits per second and correlated in the receiver for about 1 second.

What kind of code should we use? Something like the GPS C/A codes seems an obvious possibility. The GPS C/A codes[3] are 1023-bit Gold codes, and are known to have good crosscorrelation properties, i.e., the crosscorrelation between any two different code sequences in the set, or "family," is small. Unfortunately, for a bit period of $2^n - 1$, when n is a multiple of 4, there is no Gold code with quite the same crosscorrelation properties as those described in Spilker[4]. However, there are other families of codes known to have low crosscorrelations. For this study, five such sets were examined (see Table 5.3). Each of these sets may be defined in the following way[5]:

---

[3] Spilker Jr., J. J. , "GPS Signal Structure and Performance Characteristics," *Global Positioning System, Navigation, Journal of the Institute of Navigation*, Vol. 25, No. 2, 1978.
[4] Ibid.
[5] Sarwate, D. V., and Pursley, M. B., "Correlation Properties of Pseudorandom and Related Sequences," *Proceedings of the IEEE*, Vol. 68, No. 5, May 1980.

$$G(u,u[k]) \equiv \{u,\ u \oplus u[k],\ u \oplus T(u[k]),\ u \oplus T^2(u[k]),\ ...,\ u \oplus T^S(u[k])\} \qquad (5.4)$$

where u is a binary maximum-length linear feedback shift-register sequence (hereafter referred to as an M-Sequence, see Figure 5.4 for an example). The symbol $\oplus$ denotes modulo-2 addition for the (0,1) binary sequences; u[i] is the sequence (u_i, u_{2i},u_{3i}, ...), in which u_i is the i^{th} bit, modulo 4095, of the sequence u; $T^i(u)$ is the shifted sequence (u_{1+i}, u_{2+i}, u_{3+i}, ...); and (s + 2) is the total number of sequences in the set.

Set/Family Name	Set Definition	# in Set (s+2)	Values taken by X-Correlation Function
M-Sequence	G(u,u[127])	4097	-65, -1, 63, 127
Reciprocal M-Seq.	G(u,w)	4097	-127,..., 129
Gold-Like	G(u,u[129])	4096	-129, -65, -1, 63, 127
Dual-BCH	G(u,u[3])	4096	-129, -65, -1, 63, 127
Small Kasami	G(u,u[65])	64	-65, -1, 63

Table 5.3 Candidate Pseudorandom Sequences for Demonstration Experiment

In the case of the Reciprocal M-Sequence, the sequence w is the m-sequence generated by the polynomial for u with the order of the shift register feedback taps reversed.

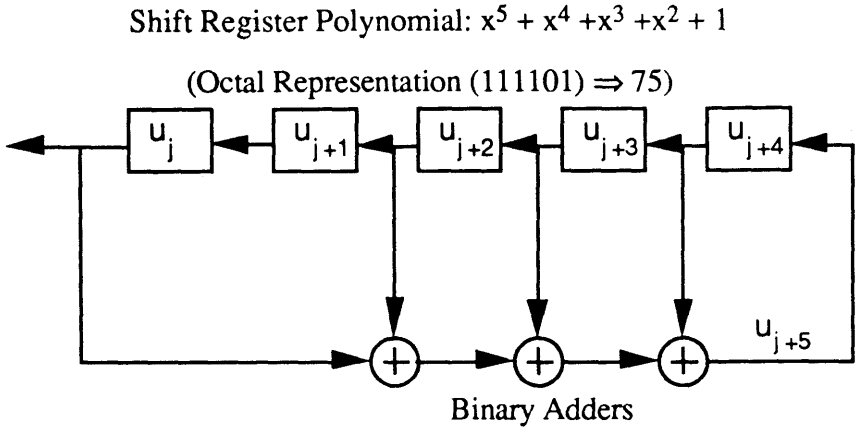

Figure 5.4 Maximal Length Linear Feedback Shift-Register[6]

It appears from Table 5.3 that the Small Kasami set of codes may provide the lowest overall crosscorrelation performance. The maximum magnitude of the normalized crosscorrelation between two Small Kasami codes is never greater than (65/4095), about 0.016.

This value of the crosscorrelation assumes that cross-multiplication and summation is carried out over exactly one period, 4095 bits, of the code. The possibility that the hardware may not perform a full-period correlation must be considered. If the correlation time is slightly less than a period, for example, because some 'dead' time must be allowed for unloading and loading registers, then the crosscorrelation properties of a family of codes can be degraded. GPS receivers have been observed to have a dead time of about 6% of the C/A code period of 1 ms.[7] For a pair of codes from each candidate set (the "u" and "u ⊕ T(u[k])" sequences), crosscorrelations were computed for correlation times from 93% to 100% of the code period. Figures 5.5 (a,b,c,d) show how the average magnitude, the standard deviation, the peak positive value, and the peak negative value of the crosscorrelation varied as the correlation time dropped from a full period. The relatively low magnitudes of the peak positive and negative crosscorrelations as well as the low

---

[6]Ibid.
[7]Prof. Charles Counselman III, personal communication.

standard deviation of the crosscorrelation value found for the Small Kasami set make this set look like the best choice. The average value, or absolute value, of the Small Kasami crosscorrelation is slightly higher than that of the other code families, but this statistic does not appear to be so meaningful. Curiously, the average-magnitude statistics of the Small Kasami sequences are quite insensitive to incompleteness of the crosscorrelation period (see Figure 5.5 (a)). There are only 64 different codes in the Small Kasami set, but this should be more than enough for a small-network experiment.

The GOES satellites will appear essentially stationary in the sky at the ground sites. Therefore, the effect of Doppler shift upon code correlation and thus, signal acquisition, has not been considered.

Average Magnitudes of Partial Correlations

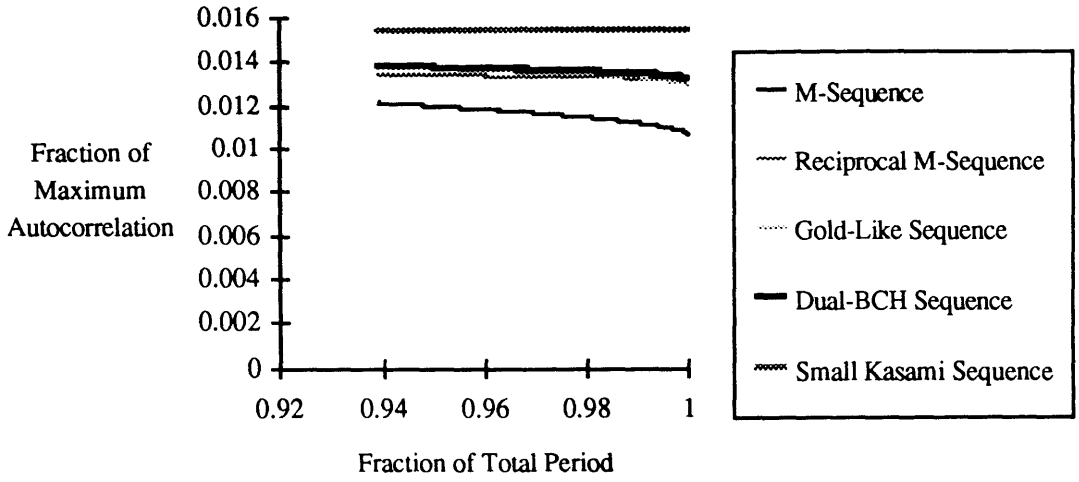

(a)

Standard Devations of Partial Correlation Values

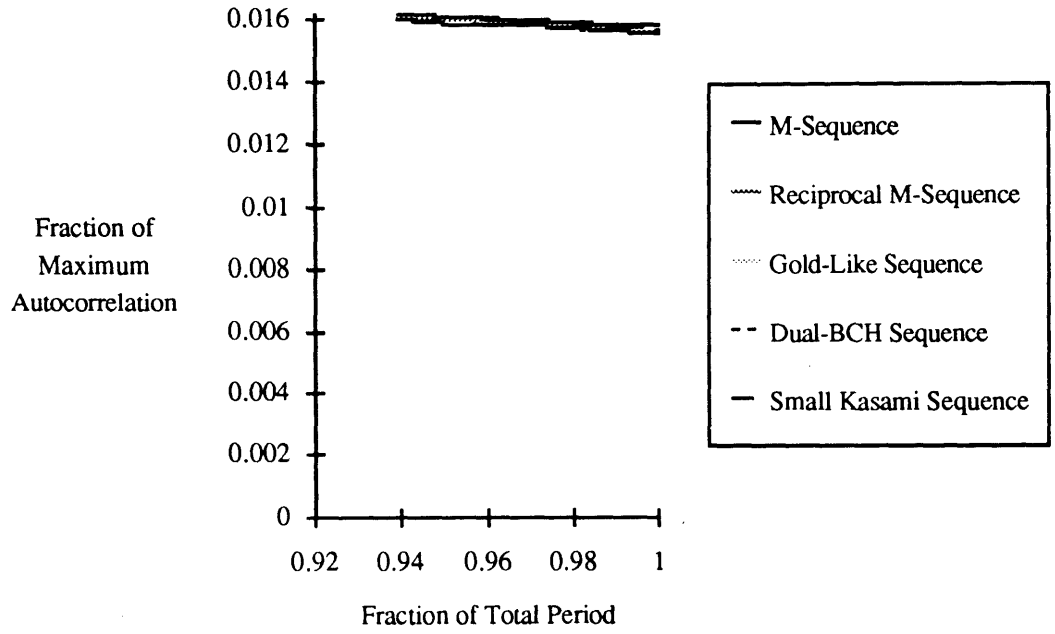

(b)

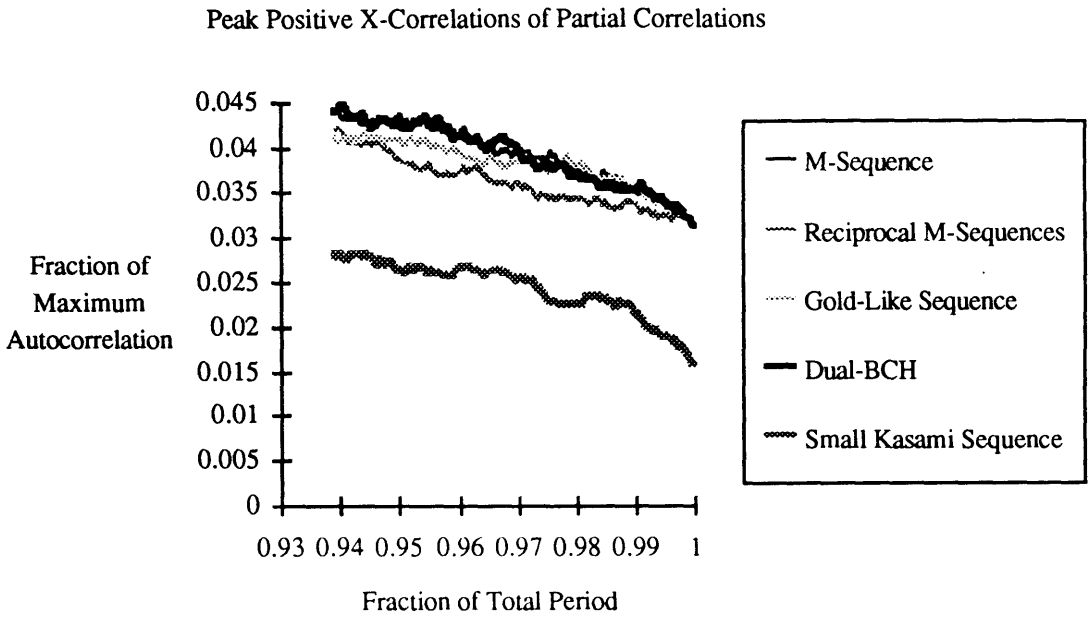

(c)

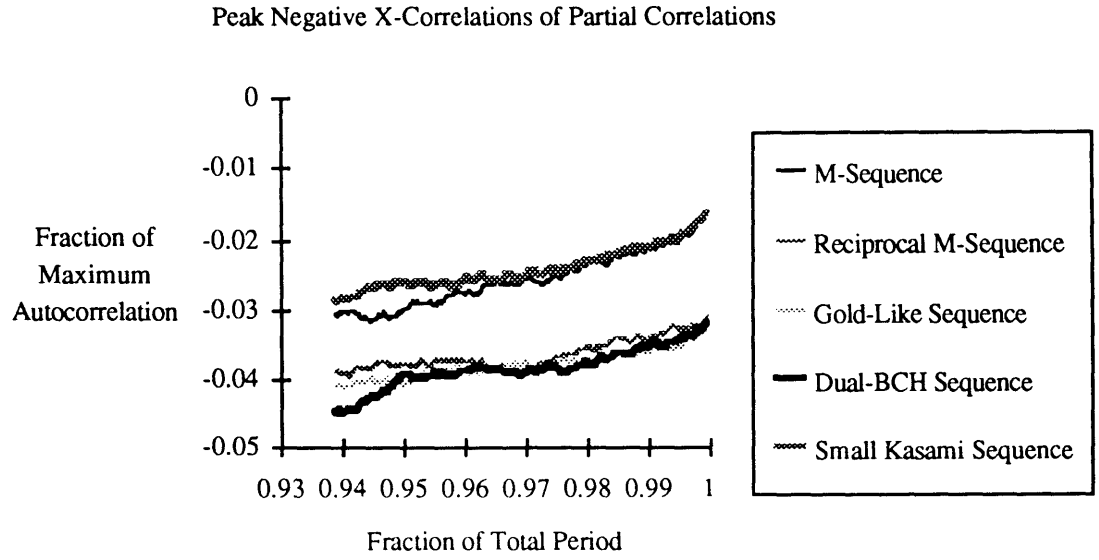

(d)

Figures 5.5 (a,b, preceding page; c,d, this page) Partial Crosscorrelations of Candidate Sequences

The polynomial which generates u for the Small Kasami set is $u(x) = x^{12} + x^6 + x^4 + x + 1$, or in a shorthand octal notation, 10123. The sequences u[i] also have corresponding polynomials, and in the Small Kasami set, $u[65] = x^6 + x^5 + 1$, or 00141.

The outputs of these two polynomials are modulo-2 added, which is the same as multiplication if the (0,1) sequences are replaced by (-1, 1) sequences. So the final polynomial which generates these sequences is $f(x) = x^{18} + x^{17} + x^{11} + x^{10} + x^9 + x^7 + x^6 + x^5 + x^4 + x + 1$, or 1407363. Care must be taken in initializing this sequence, so that the codes take on the values dictated in Equation 5.4, and do not reach an 'all zeros' state instead.

5.5 Covariance Analysis

The objectives of the covariance analysis are to (i) convince ourselves that this enactment of the GeoBeacon concept will yield meaningful results, and (ii) help us decide the ground transmitter geometry for the experiment.

5.5.1 Partial Derivatives With Respect to Non-Bias Parameters

The software for this covariance analysis sets up and evaluates equations (1.8) and (1.10). The partial derivatives of one-way phase measurements with respect to a bias parameter are either 1 or -1. In order to obtain the partial derivatives with respect to non-bias parameters, we must refer back to (1.3), dropping time and frequency indices for clarity.[8]

$$\frac{\partial \phi^{i}_{jk}}{\partial x} = -f_k \frac{\partial \tau^{i}_{j}}{\partial x} \qquad (5.5)$$

Here 'x' represents any non-bias parameter. The signal propagation time (in vacuum), τ, is obtained from the range vector $\mathbf{R}$

$$\tau^{i}_{j} = \frac{1}{c}\left|\mathbf{R}^{i}_{j}\right| \qquad \mathbf{R}^{i}_{j} = \mathbf{s}^{i} - \mathbf{r}_{j} \qquad (5.6\ a,b)$$

---

[8]King, R. W., *et al.*, *Surveying With GPS*, Monograph 9, School of Surveying, The University of New South Wales, Kensington, N.S.W. Australia, 1985.

where **s** and **r** are the satellite and ground station vectors, respectively. The chain rule is then used to obtain the required partials:

$$\frac{\delta \tau_j^i}{\delta x} = \frac{1}{c} \frac{\delta \left| \mathbf{R}_j^i \right|}{\delta \mathbf{R}_j^i} \cdot \frac{\delta \mathbf{R}_j^i}{\delta x} \quad . \tag{5.7}$$

In the case of ground site coordinates, the ground vector is differentiated with respect to coordinates whose axes rotate with the Earth. These coordinates need to be transformed in order to obtain the partial derivatives with respect to an inertial frame (which is the frame used to represent the $\mathbf{R}_j^i$ vector and to obtain the satellite partial derivatives).

$$\frac{\partial \mathbf{R}_j^i}{\partial x} = -\frac{\partial \mathbf{r}_j}{\partial x} \tag{5.8}$$

$$\frac{\partial \mathbf{r}_j}{\partial \phi} = \begin{bmatrix} -\nu \cos(\lambda) \sin(\phi) \\ -\nu \sin(\lambda) \sin(\phi) \\ \nu \cos(\phi) \end{bmatrix} \qquad \frac{\partial \mathbf{r}_j}{\partial \lambda} = \begin{bmatrix} -\nu \sin(\lambda) \cos(\phi) \\ \nu \cos(\lambda) \cos(\phi) \\ 0 \end{bmatrix} \qquad \frac{\partial \mathbf{r}_j}{\partial \nu} = \frac{\mathbf{r}_j}{\nu} \tag{5.9}$$

where ϕ, λ, and ν are geocentric latitude, east longitude, and radius, respectively[9]. The satellite orbit parameters, in this case, the position and velocity vectors at epoch, are obtained by differentiating the satellite position vector.

$$\frac{\partial \mathbf{R}_j^i}{\partial x} = \frac{\partial \mathbf{s}^i}{\partial x} \tag{5.10}$$

In most geodetic software, the orbit-parameter partial derivatives are obtained from a numerical integration of the orbits throughout the time span where observations will take place. If unperturbed two-body orbital motion is assumed, it is possible to obtain analytical expressions for the orbits and their partials. These expressions are derived in Appendix B,

[9]The station partials must be rotated to the same inertial frame used to describe the satellite orbits, in this case the 1950.0 Vernal Equinox frame.

and incorporated into the software. Neglecting perturbations to the orbits of the GOES satellites should not change the conclusions reached concerning the feasibility of the demonstration experiment. At the same time, using these expressions eliminates the need to integrate orbits and substantially reduces the running time of the covariance determination software.[10]

5.5.2 Covariance Analysis Results

For the simulated observation session, 24 h of measurements were used in order to take full advantage of the geosynchronous satellites' motion in the sky. One-way phase measurements were made once every six minutes, with a phase error variance of (1.0 mm of phase)^2. In the software, the necessary condition for fixing a bias parameter is that its formal standard error be less than 0.1 cycle.

The formal standard error criterion for bias fixing, the measurement frequency, and the rms measurement error are intended to represent realistic values. These assumed values however, warrant justification. Since the bias parameters are fixed as integer values, an rms error of 0.1 cycle should eliminate most ambiguities between choices of integers. The rms phase error and measurement frequency directly influence the parameter estimate variances and the number of stations required. The measurement frequency is chosen to be similar to that used by GPS receivers, and the rms phase error is primarily due to radio noise power in the receiver. Other error sources, such as multipath and small-scale variations in the troposphere and ionosphere, are not included in this analysis.

It is conceivable that through poor transmitter placement, multipath errors could exceed the 1.0 mm level, and the lack of satellite motion in the sky will prevent the cancellation of multipath errors that occurs with GPS satellite motion in the sky. In times

---

[10]The GAMIT software, which uses numerical integration to calculate the orbit history and partial derivatives, was used to check the software written for this demonstration experiment.

of high ionospheric activity, the ionospheric phase contribution could vary by over 1.0 mm over a 1 km baseline, and even abrupt changes in weather could introduce equally large phase errors. However, since the objective of this exercise is to demonstrate the validity of this technique for determining the required number of ground transmitters, the rms phase error value is set at 1.0 mm, along with the caveats presented above.

The relative lack of motion of GOES-7 results in orbit parameter partials that do not change with time. Thus, the orbit parameters become nearly indistinguishable from the bias parameters. Therefore, two cases are presented: (i) observations including the use of only GOES-2, 5, and 6; and (ii) observations including GOES-2, 5, 6, and 7. In the three-satellite case, it is possible to have as few as six stations (numbers 1, 8, 9, 10, 11, and 12 from Figure 5.2) and still be able to fix all the biases by bootstrapping. Five iterations are required to complete the bias fixing (see Figure 5.6 a). When all four satellites are included, only three iterations are needed (see Figure 5.6 b), but two additional stations (numbers 6 and 7 from Figure 5.5) are required in order to fix all the biases. Therefore, the number of ground transmitters required for the experiment, with respect to bias fixing, increases when including satellites with little apparent motion in the sky.

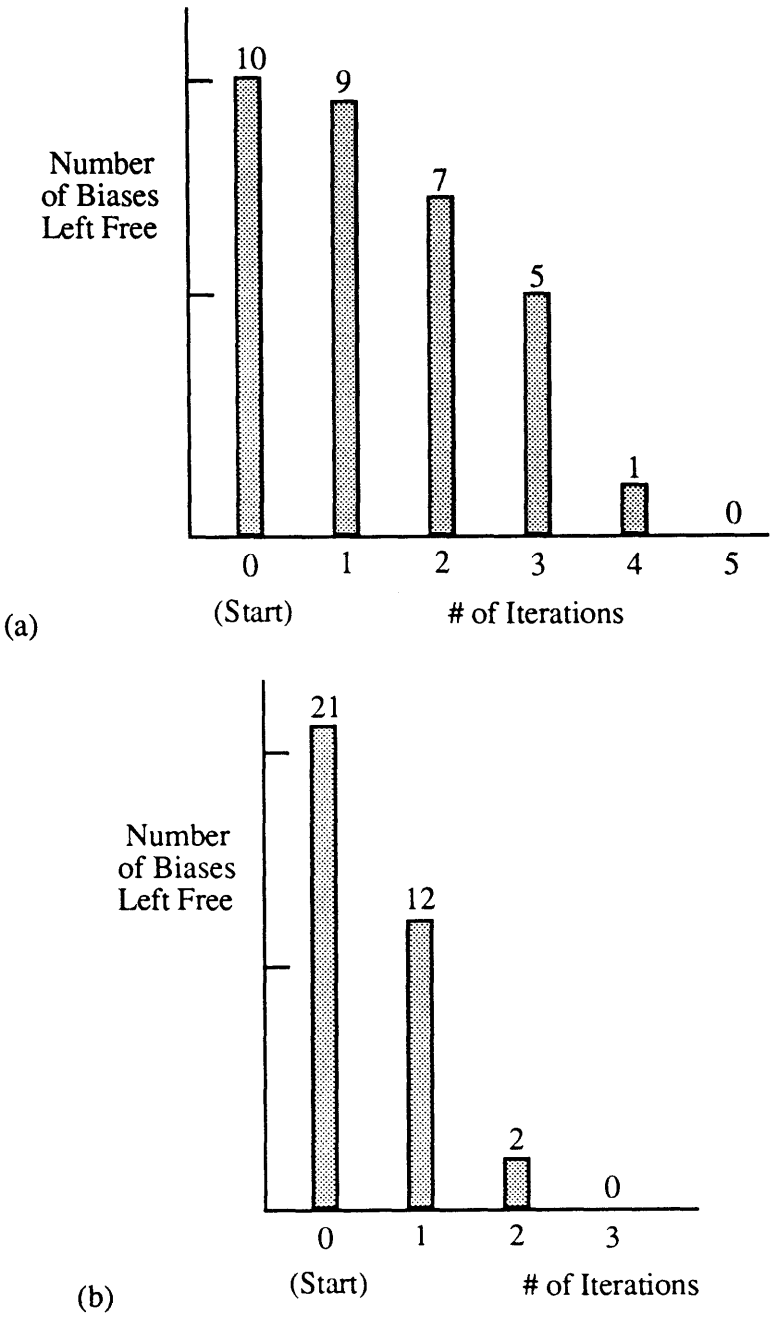

Figure 5.6 (a,b) Bias Fixing through Multiple Iterations
(a, Top) Six Station Network (GOES-2, 5, and 6 observed)
(b, Bottom) Eight Station Network (GOES-2, 5, 6, and 7 observed)

In Figure 5.7, the eigenvectors of the formal standard error ellipse are shown for the three-satellite case. This 1-σ error ellipsoid has a volume corresponding to a spherical error probable (SEP) of 0.562 mm. As expected, the principal eigenvector is normal to the plane defined by the differences of unit vectors from the station to the three satellites

(hereafter referred to as $\Delta\hat{s}$ vectors; the relation between $\Delta\hat{s}$ vectors and positioning errors was addressed in Chapter 2). In this case, the $\Delta\hat{s}$ are predominantly in an East-West direction.

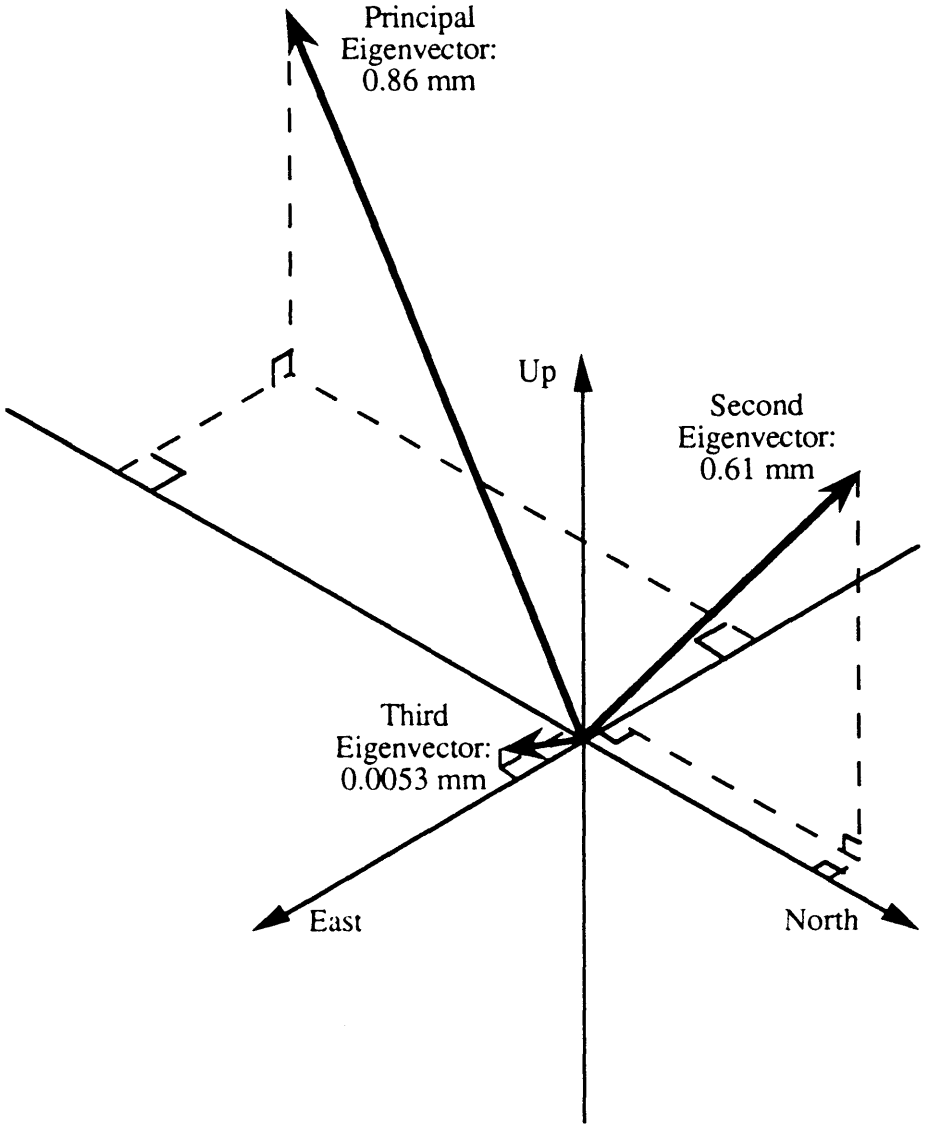

Figure 5.7 Transmitter Position Formal Error Eigenvectors[11] (GOES-2, 5, and 6)
(based on observations using six ground transmitters; all biases fixed. Not drawn to scale.)

In the four-satellite case (see Figure 5.8), the addition of GOES-7 reduces the magnitude and reoriented the position error eigenvectors. The (SEP) in this case is now

[11]In Figures 5.7 and 5.8, the eigenvector magnitudes do not represent anticipated rms error values. These error eigenvectors are intended to demonstrate the geometrical strength of the GOES constellation.

0.25 mm. The $\Delta\hat{s}$ vectors now include vectors with a large component in the direction of the primary eigenvector in the first case.

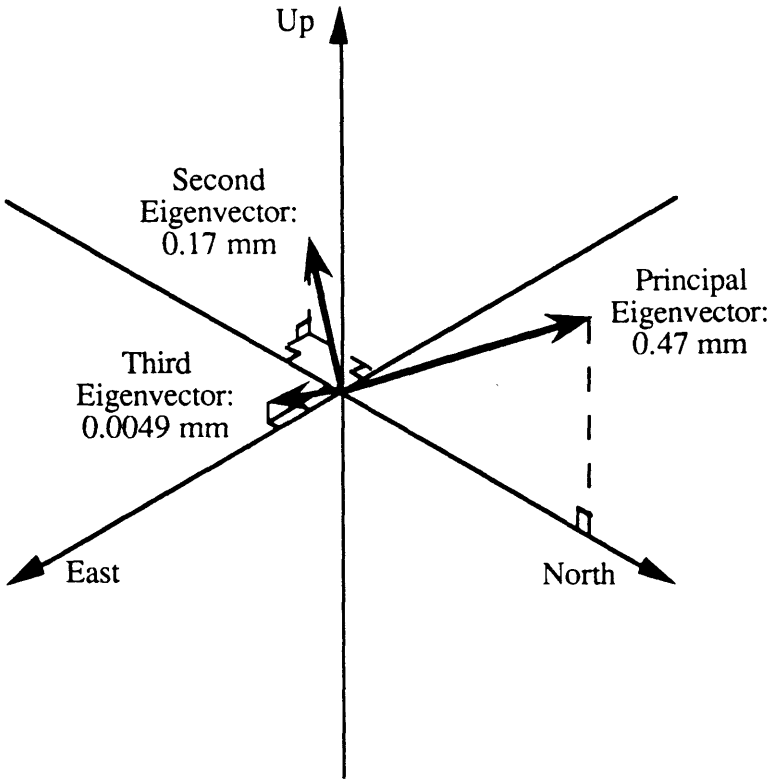

Figure 5.8 Transmitter Position Formal Error Eigenvectors (GOES-2, 5, 6, and 7)
(based on observations using eight ground transmitters; all biases fixed. Not drawn to scale.)

As a rough check that the order of magnitude of the calculated variances is numerically consistent, the orbit and ground station parameter formal standard errors should obey the following rule-of-thumb relation used in GPS geodesy

$$\frac{|\vec{dB}|}{|\vec{B}|} = \frac{|\vec{ds}|}{|\vec{\rho}|} \tag{5.11}$$

$$\frac{0.078 \text{ mm}}{60 \text{ m}} \stackrel{?}{=} \frac{100 \text{ m}}{40000 \text{ km}}$$

$$1.3(10^{-6}) \sim 2.5(10^{-6})$$

where $|\vec{ds}|$ is the orbit error, $|\vec{\rho}|$ is the transmitter-satellite range, $|\vec{b}|$ is the baseline length and $|\vec{db}|$ is the resulting baseline error.

These formal standard errors, however, reveal a difference between the demonstration experiment and the geodetic positioning typically performed using GPS satellites. The magnitude of the formal standard errors of orbital position (see Figures 5.9 (a,c)) are about 2 orders of magnitude larger than typical GPS orbit errors. This is a result of the unusually small size of the network. In both cases, the cross-track (out of orbit plane) components of orbital position and velocity error are the largest.

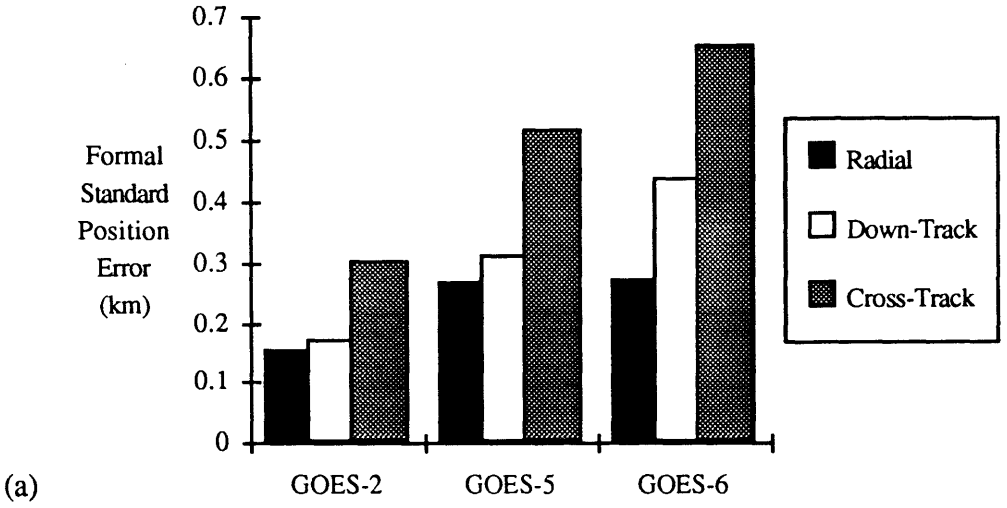

(a)

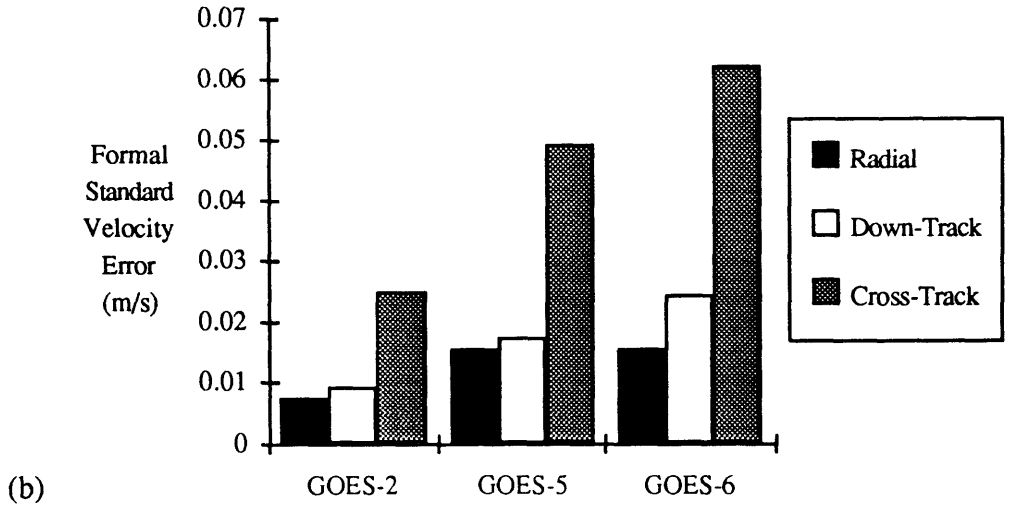

(b)

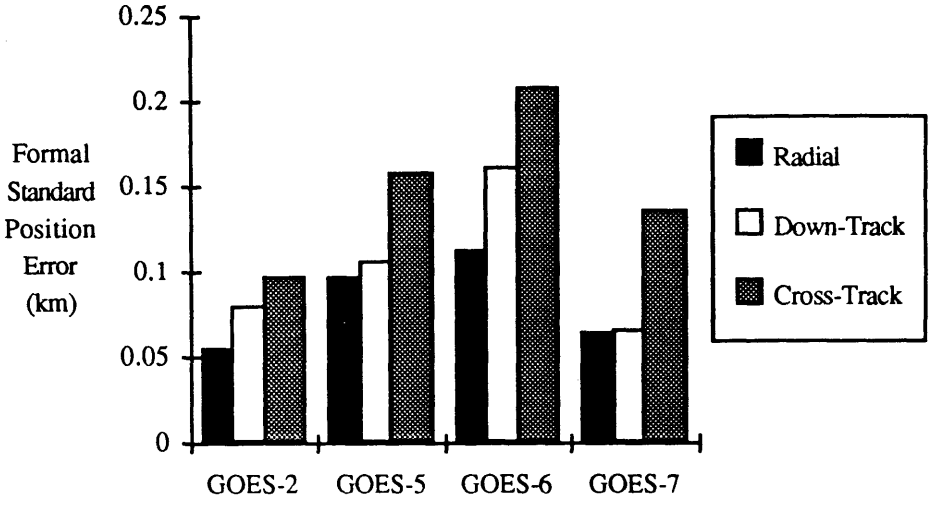

(c)

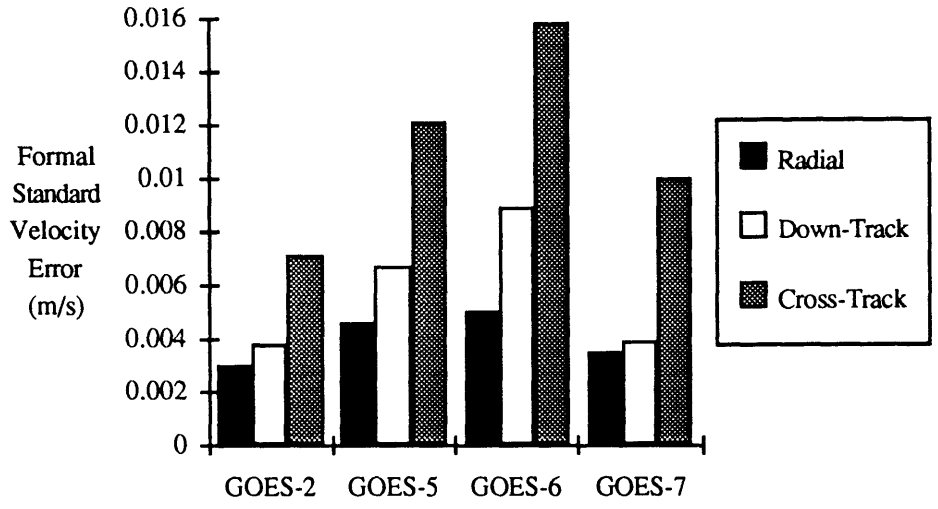

(d)

Figures 5.9 (a,b, preceding page; c,d, this page) Satellite Position and Velocity Errors (all Biases Fixed). (a,b) GOES-2, 5, and 6, six ground transmitters, (c,d) GOES-2, 5, 6, and 7, eight ground transmitters

5.5.3 Consequences of Satellite and Network Selection

It is difficult to express concisely the exact relations governing the relative sizes of orbit errors of different satellites. However, since the sky plots of these satellites are relatively easy to model, covariance analyses were performed to characterize the sensitivity of parameter variances to changes in ground site location and geosynchronous satellite selection. If someone wishes to demonstrate the GeoBeacon concept with geosynchronous

satellites in the future, there may be different satellites available. Therefore, it is important to study the effect of satellite choice upon positioning and orbit-determination capability.

For this purpose, simulations were performed with a four-station network, consisting of three stations in an equilateral triangle, $10\sqrt{3} \sim 17$ m on a side, with a fourth station located at the centroid of the triangle. Three geosynchronous satellites were used; see Figure 5.10 for the sky plot and orbital elements. The orbit inclinations alternate between 1° and -1° in order to ensure that the $\Delta\hat{s}$ vectors span 3-d space.

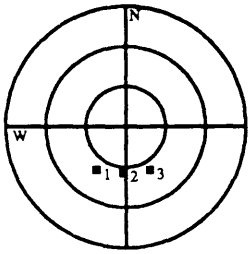

Satellite #	a (km)	e	i (deg)	Ω (deg)	ω (deg)	M (deg)
1	42164.09	0.	1.	-15.	0.	0.
2	42164.09	0.	-1.	0.	0.	0.
3	42164.09	0.	1.	15.	0.	0.

Figure 5.10 Nominal Keplerian Orbital Elements and Sky Plots for Geosynchronous Satellite Covariance Investigation (Note: ω not defined for circular orbits)

In these simulations, all biases were fixed through the bootstrapping method of Section 5.4.2. As in the demonstration experiment simulation, the satellite orbits and center station coordinates were the parameters which were estimated. The time-span of observations was 24 h, as before, with the same measurement error and the same bias-fixing criterion. The parameters which were varied include: satellite inclination, inter-satellite spacing, satellite longitude location, mean network latitude, network east-west distance, and network north-south distance. The results are summarized in Table 5.4.

The effect of these variations upon position variances can be verified through examination of the $\Delta\hat{s}$ vectors in the network. The relation between orbit errors and these variations cannot be verified as easily, but a few conclusions can be drawn. In order to minimize orbit estimation errors, one should select satellites with higher inclinations, well spaced across the sky. The network should be low in latitude, centered beneath the satellites selected if possible, with baseline lengths as large as possible in both latitude and longitude.

Variation in Satellite Orbits (or Ground Transmitters)	Resulting Change in Sky Plots (or Network)	Effect Upon Orbit Parameter Formal Standard Errors	Effect Upon Station Position Formal Standard Errors
Increase in Orbit Inclination	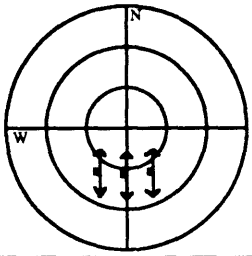	All errors decrease, especially cross-track and along-track position and velocity.	Longitude error essentially unchanged, but latitude and altitude errors decrease.
Increase in Inter-Satellite Spacing in Longitude	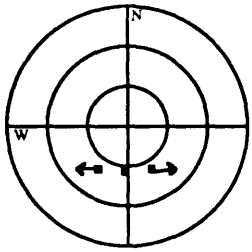	All errors decrease, but cross-track position and velocity errors remain relatively high.	Errors in all three coordinates decrease, but level out for spacings of 30 degrees or more.
Increase Longitude of Ascending Node of All Satellites	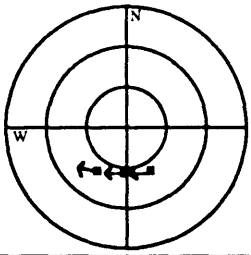	Cross-track errors remain the same. Errors increase as satellite nears horizon.	Longitude errors increase, altitude errors decrease.
Increase Network Latitude	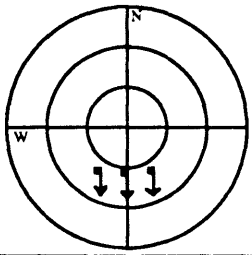	All errors increase except cross-track position and velocity.	Latitude errors decrease, longitude and altitude errors increase.
Increase Network East-West Distance	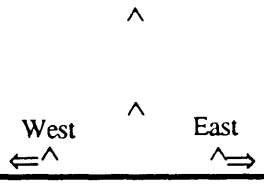	Cross-track position and velocity errors decrease the most.	No change.
Increase Network North-South Distance	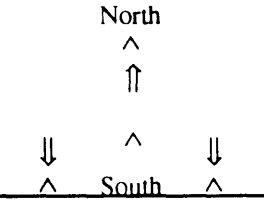	Errors of all components decrease.	No change.

Table 5.4 Effects of Satellite and Network Variations Upon Orbit and Station Estimation Errors

6. Recommendations for Further Research

A low-cost GeoBeacon system has been outlined and compared to a GPS-based system. This study, however, merely introduces the concept of performing geodesy with repeater satellites. Many other system-level questions warrant examination. One topic is the orbit determination strategy for GeoBeacon satellites. Another topic which deserves further attention is the possibility that another multi-satellite application may have satellites that meet the technical requirements (in availability, repeater frequency, and geometry) for a prototype GeoBeacons system. Yet another topic worthy of attention is the application of the GeoBeacons concept to other bodies in the solar system.

6.1 Orbit Determination of Proposed GeoBeacon Satellites

In the rule-of-thumb (Equation 2-11) that describes the relation between orbit and ground station parameter errors, it is assumed that the location of satellites in the sky relative to each other appears to be the same at both ends of the baseline. In a low-earth orbiting system such as GeoBeacons, with baseline lengths approaching the satellite-station range, this 'no-parallax' assumption no longer holds. For a simple 2 satellite, 2 station case, the sensitivities of station position error (Δr_1,Δr_2) and satellite position error (Δs^1,Δs^2) to the double difference observable are

$$\Delta\vec{r}_2 \cdot \left(\hat{\rho}_2^2 - \hat{\rho}_2^1\right) - \Delta\vec{r}_1 \cdot \left(\hat{\rho}_1^2 - \hat{\rho}_1^1\right) = \Delta\vec{s}^2 \cdot \left(\hat{\rho}_2^2 - \hat{\rho}_1^2\right) - \Delta\vec{s}^1 \cdot \left(\hat{\rho}_2^1 - \hat{\rho}_1^1\right) \qquad (6.1)$$

where $\hat{\rho}_i^j$ is a unit vector from station i to satellite j. Up to the present, with VLBI and GPS geodesy, the vector differences ($\hat{\rho}_2^2$ - $\hat{\rho}_2^1$) and ($\hat{\rho}_1^2$ - $\hat{\rho}_1^1$) have been essentially identical.

Therefore, the baseline error ($\Delta B = \Delta r_2 - \Delta r_1$) is relatively insensitive to satellite position (or quasar location) error, compared to "single-point" positioning.

As position errors become more sensitive to satellite errors, it is more important to examine the sources of satellite errors. Due to the simplicity of the GeoBeacon satellite design, orbit changes due to stationkeeping maneuvers are non-existent. The lack of large flexible solar panels will make the solar radiation pressure model much simpler than that of the GPS satellite. Another major difference in the GeoBeacon satellite environment is the sensitivity of the 1000 km altitude orbit to variations in the geopotential. For example, the secular rate of change of orbital elements due to the J_2 term in the geopotential expansion for 1000 km altitude orbits is on the order of 100 times greater than that for GPS (20,000 km altitude) orbits. Since the primary cause of satellite error is Earth-related instead of spacecraft-related, GeoBeacon satellite orbit determination might yield much more information about the local geopotential than GPS surveys.

In addition to the change in error sources, the GeoBeacon satellite pass duration is a much smaller fraction of the orbit period than that of a GPS satellite. Two passes (often separated by several hours) are needed for good 3-d positioning. Considering the short pass duration, perhaps the satellite positions at epochs during each pass can be approximated by short arcs, instead of trying to determine orbital elements for the entire duration between the two passes (which is never observed.)

Some orbit determination work has already been performed for low-Earth orbiting satellites carrying GPS receivers[1]. If the addition of these receivers greatly enhances GeoBeacon positioning capability, they could be added to the spacecraft design without much additional complexity in the design.

---

[1]Wu, S. C., *et al.*, "Reduced Dynamics Technique for Precise Orbit Determination of Low Earth Satellites," *Journal of Guidance, Control, and Dynamics*, Vol. 14, No.1, pp;. 24-30, January-February 1991.

6.2 Feasibility of Using Existing Satellite Repeaters in a GeoBeacon System

The largest costs in any configuration of the GeoBeacon system are the construction and launch of the satellites. If these expenses could be absorbed by another space-based application, GeoBeacons would appear much more attractive for monitoring large networks.

The '2-sat' configuration presented in Chapter 3 illustrates the three hard technical requirements of any satellite system to be considered for use in a GeoBeacon system:

Requirement	Reason
At least two satellites in view simultaneously at both ends of a baseline	Need to Double Difference to eliminate transmitter clock errors
Repeaters operating at two different uplink bands	Need to eliminate first-order ionospheric phase
Sufficient distribution of $\Delta\hat{s}$ vectors in three dimensions	Need three-dimensional position fixes

Table 6.1 Technical Requirements for Satellites used in the GeoBeacon System

The third requirement prohibits relying solely upon geostationary satellites, due to their apparent lack of motion in the sky. There aren't many repeater satellites at GPS-orbit altitudes, but there is much interest in deploying communications-oriented satellite constellations in low earth orbit (see Table 6.2). These projects will be mostly intended to provide data and voice communication to remote users around the world. In these applications, only one satellite is needed in view at any time. However, there will be times when multiple satellites are visible across a baseline; the schedule of these viewing events should be investigated. Of particular interest are the Aries, Globalstar, and Odyssey systems, which meet the 'two-uplink band' requirement.

System	Proposing Company	Number of Satellites	Orbit Planes	Orbit Altitude (km)	Up- & Down-link Frequencies (MHz)	Services
Leosat	Leosat Inc., Ouray, CO	18	3	1000	148-149 up 137-138 down	Two-way communication and radio-location for intelligent vehicle highway system
Orbcomm	Orbital Communications Corp., Fairfax, VA	20	3 inclined, 2 polar	970	148-148.9 up 137-139, 400.1 down	Two-way communication and radio-location; slow, low-cost data transmission
Starnet	Starsys Inc., Washington, D. C.	24	24 random	1300	148-149 up 137-138 down	Global two-way communication, data, radio location
Vitasat	Volunteers in Technical Assistance (VITA), Arlington, VA	2	Single, circular	800	149.8 up 400.2 down (or 137.7 down, 400.2 up)	Data services and file transfer primarily for developing nations
Aries	Constellation Communications, Herndon, VA	48	4 polar	1018	1610-1625.6 up 2483.5-2500 down 5150-5216 down 6525-6541 up	Position determination and reporting, two-way telephony, dispatch voice, facsimile, and data collection, distribution, and control services
Ellipso	Ellipsat, Washington, D. C.	24	3 highly elliptical	2903 by 426	1610-1626.5 up 2483.5-2500 down	Will connect to a cellular phone to convert 800 MHz cellular to the 2.5 / 1.6 GHz RDSS bands
Globalstar	Loral Cellular Systems Corp., New York, NY	48	8	1389	1610-1625.6 2483.5-2500 5199-5216 6525-6541 all bidirectional	RDSS, voice, data communications
Iridium	Motorola Inc., Chandler, AZ	77	11	765	1610-1626.5 bidirectional 27.5-30 up 18.8-20.2 down	Worldwide cellular telephony and portable phone service
Odyssey	TRW Inc., Redondo Beach, CA	12	3 inclined circular	10370	1610-1626.5 up 2483.5-2500 down 19700-20000 down 29500-30000 up	Voice, radio location, messaging, data services

Table 6.2 Proposed Low Earth Orbit Mobile-Satellite Communication Systems[2]

[2]Pattan, Bruce, *WARC-92: Issues for U.S. International Spectrum Policy*, Federal Communications Commission, Office of Technology Assessment, November 1991.

6.3 Extending the GeoBeacon Concept to Other Bodies in the Solar System

While the Global Positioning System is able to effectively disseminate accurate clock and individual position information to users, GeoBeacons efficiently provides the user with positions of many remote sites. In addition to Earth-crustal monitoring, GeoBeacon systems could be used to study the crustal dynamics of other planets, such as Venus and Mars, as well as the Moon. In addition to monitoring stationary transmitters, these systems could track vehicles moving on the surface or through the atmosphere. Atmospheric and other scientific data could be carried by the spread-spectrum signal, further enhancing the merit of these stations. The doubly differenced phase observable has already been used in the past to track a vehicle on the Moon[3] and probes in the Venusian atmosphere[4].

Planning of projects to send vehicles to bodies in the inner solar system should include studies of the benefits of using doubly diffeenced phase data for positioning purposes. For example, using the concept proposed by Draim[5] for continuous global double satellite coverage, a 6-satellite constellation could continuously provide 2 satellites in view at the Martian surface. Table 6.3 shows the lowest possible constellation (where all satellites have the same orbit size, eccentricity, and inclination) which provides double coverage on Mars. The two moons of Mars, Phobos and Deimos, could also be viewed by these satellites (though not necessarily with double coverage).

---

[3]Counselman III, C. C., *et al.*, "Astronomical Applications of Differential Interferometry," *Science*, Vol. 178, pp. 607 - 608, 10 November 1972.
[4]Counselman III, C. C., *et al.*, "Zonal and Meridional Circulation of the Lower Atmosphere of Venus Determined by Radio Interferometry," *Journal of Geophysical Research*, Vol. 85, No. A13, pp. 8026 - 8030, December 30, 1980.
[5]Draim, J. E., "Continuous Global N-Tuple Coverage with (2N+2) Satellites," *Journal of Guidance, Control, and Dynamics*, Vol. 14, No. 1, pp. 17 - 23, Jan. - Feb. 1991.

Sat. #	a (km)	e	*i* (deg)	ω (deg)	Ω(deg)	M (deg)
1	58,422	0.2335	27.45	-90	0	0
2	"	"	"	90	-60	60
3	"	"	"	-90	-120	120
4	"	"	"	90	-180	180
5	"	"	"	-90	-240	240
6	"	"	"	90	-300	300

Table 6.3 Proposed Mars 'Double Coverage' Constellation

7. Conclusions

Over the past two decades, relative-position uncertainties of sites on the Earth's surface have shrunk by orders of magnitude, revealing many new components of the signature of the Earth's surface dynamics. The technique of radio interferometry had enabled very long baselines to be measured to within a few parts per billion. The geodetic community presently conducts measurement campaigns using the signals of the GPS satellite constellation (established by the US Department of Defense). There appears to be no better satellite constellation than GPS, nor does there appear to be a likely successor in the near future.

At the start of the GeoBeacons study in 1988, it would have been prohibitively expensive to permanently maintain GPS receivers and retrieve measurements (by phone or by radio) from networks with large numbers of sites. If the role of the ground site became a more active one, that is, if we equipped ground sites with coded transmitters, could we monitor large networks more inexpensively?

This was the question addressed in this study. Two low-cost repeater satellite constellations were analyzed. In both cases, the satellites would be placed into coplanar orbits by a single launch of a low-cost launch vehicle. Stationkeeping would not be required. The spacecraft architecture was borrowed from an existing Microsat design. The resulting geometric positioning capabilities were compared to that of the full GPS constellation. A 'Multi-sat' configuration was found to yield PDOP values close to those obtained with GPS positioning. The 'Multi-sat' operating coverage area was not suitable for intercontinental baselines, but was large enough for large (500-1000 km dimension) networks. The GPS constellation clearly outperformed the GeoBeacon constellation in the four figures of merit. It is interesting to note, however, that by using observations from

consecutive passes, it is possible to obtain a three-dimensional distribution of $\Delta\hat{s}$ vectors with a one-plane satellite constellation.

A rough cost comparison (as opposed to a detailed cost breakdown) was performed between the two satellite systems in order to identify and estimate the expenditures which differed in the two systems. It was found that the total GeoBeacon project would become competitive with a GPS network at the 10,000 station level. If the satellite construction and launch costs could somehow be absorbed as part of a different project, as in the case of the GPS satellites, the GeoBeacon alternative becomes more cost effective at the 1,000 site level. Table 7.1 summarizes the comparison between the two systems.

Should this project be implemented? In the first GeoBeacon study[1], it was assumed that there would be a 'GPS-like' multi-plane, high altitude satellite constellation of repeaters available to relay transmitter signals to a central site. If this assumption were true, the hardware at each GeoBeacon site (a coded transmitter) would be virtually guaranteed to be less expensive than that for a GPS site (a receiver and means for retrieving data). Could this good fortune strike again, that is, could there be another satellite constellation which could accommodate the GeoBeacon concept? There are many plans at present, in both Europe and the United States, for low-earth orbiting constellations. None of these projects, however, have the 'two-satellite, two-frequency band' technical requirement of geodetic positioning. Therefore, it appears that our assumption of having a constellation of orbiting repeaters does not hold at present.

[1]Cangahuala, Ibid.

	GPS	GeoBeacons (Multi-sat)	Evaluation
(PDOP)	~ 5 at mid-latitudes; reaches 8 at polar latitudes	8-9 at mid-latitudes; 6-9 at polar latitudes	A single orbit plane constellation compares well to multi-plane GPS constellation
Observation Frequency	Continuous once full constellation is deployed	12-24h at mid-latitudes; drops to ~2h at polar latitudes	Multi-plane GPS has advantage in monitoring unforeseen activity (e.g. earthquake precursors)
Network Size	8000 km at equator; drops to 4000 km at polar latitudes	1500-2000 km at all latitudes	GPS can measure inter-continental baselines, but both are adequate for monitoring fault lines
Reliability	Geodetic positioning unaffected by SA and AS[2]; program likely to have lifespan of decades, but maintenance expense makes it vulnerable	Microsat spacecraft are already in operation	Since neither program requires significant advances in technology, no side has a clear advantage (pending successful implementation of a satellite constellation for data retrieval)
Cost	Receiver costs continue to drop; data retrieval costs comparable to that of the receiver	Site hardware will always be cheaper than that for GPS; satellite and launch costs have been minimized	Number of ground sites required for GeoBeacons to become cost-effective is at least one order of magnitude larger than any network in existence

Table 7.1 Overall Comparison of GPS and GeoBeacon Systems

The size of the network needed to achieve cost effectiveness is at least one order of magnitude larger than any network currently funded. Sponsoring agencies would not be able to gradually 'build up' to a 1000- to 10,000-site GeoBeacon network; they would have to fund it all at once to realize any cost savings. With GPS-based networks, sites can be

[2]SA: Selective Availability. AS: Anti-Spoofing.

gradually added to existing networks each year, as improved data retrieval techniques lower the cost per site. Many agencies have already invested in equipment for networks at the 10- to 100-site level. It is the author's opinion that the GeoBeacon 'breakeven' point would have to be as low as a few hundreds of sites, in order to overcome the inertia associated with switching from one measurement system to another. Therefore, due to the potential benefit of satellite-based data retrieval systems to GPS networks, the author concludes that GeoBeacons is unlikely to be sponsored at present.

The availability of the GPS constellation for geodesy was a windfall from a project with a different set of goals. At present, there are many organizations that are attempting to permanently maintain small GPS networks. My recommendation is that these groups (U.S. Geological Survey, university consortia, national geodetic laboratories in other countries) should coordinate their activities and investigate the use of satellite-based data retrieval. Just as signals from "satellites of opportunity" are now used to perform geodetic measurements, communication-satellite constellations such as ORBCOMM may soon relay phase measurements to geodetic laboratories.

Since GPS satellites do meet the requirements for use in a geodetic network, they are currently the preferred instrument for monitoring networks in the world today. However, the geodetic community has recognized the need to maintain other systems, such as satellite laser ranging (SLR) and very long baseline interferometry (VLBI)[3]. If the need arose to monitor another aspect of the Earth environment, it would enhance the chances of implementing a GeoBeacon network. As examples, its low-earth orbit could aid in gravity measurements, and its rapid passes over a particular site could aid in recreating instantaneous 'pictures' of the troposphere and ionosphere. Therefore, GeoBeacons may yet appear as part of another space-based application.

---

[3]International Global Network of Fiducial Stations: Scientific and Implementation Issues," Panel on a Global Network of Fiducial Sites, National Research Council, National Academy Press.

Perhaps the best opportunity to see GeoBeacons become reality is elsewhere in the solar system. Without the need for real-time positioning at remote sites, repeaters orbiting the body of interest would be the most sensible way to gather information across a planet (or moon) and return it to Earth for analysis.

Appendix A. Uplink and Downlink Power Budgets

The overall round trip link margin is the difference (in dB) between the total and required carrier-to-noise density ratios ($(C/N_0)_{tot}$ and $(C/N_0)_{req}$, respectively), minus L_i, the implementation loss.

$$\text{Margin}\big|_{dB} = \left(\frac{C}{N_0}\right)_{tot}\Big|_{dB\ Hz} - \left(\frac{C}{N_0}\right)_{req}\Big|_{dB\ Hz} - L_i\big|_{dB\ Hz} \tag{A.1}$$

$(C/N_0)_{req}$ is a product of the required signal-to-noise ratio (E_b/N_0) and the integration bandwidth, B_i. The total carrier-to-noise density ratio is a function of the uplink carrier-to-noise density ratio, as well as the ratio (F) of downlink receiver noise density (N_{0R}) to downlink signal noise density (N_{0S}).

$$\left(\frac{C}{N_0}\right)_{req}\Big|_{dB\ Hz} = \left(\frac{E_b}{N_0}\right)\Big|_{dB} + B_i\big|_{dB\ Hz} \tag{A.2}$$

$$\left(\frac{C}{N_0}\right)_{tot}\Big|_{dB\ Hz} = \left(\frac{C}{N_0}\right)_{up}\Big|_{dB\ Hz} + \left(\frac{1}{1+F}\right)_{req}\Big|_{dB} \tag{A.3}$$

$$F\big|_{dB} = N_{0R}\big|_{dB\ W/Hz} - N_{0S}\big|_{dB\ W/Hz} \tag{A.4}$$

At the central site, the leading noise source is assumed to be the receiver itself. The downlink receiver noise temperature (T_{rec}) is assumed to be ~100 K.

$$N_{0R}\big|_{dB\ W/Hz} = k\big|_{dB\ W/Hz/K} + T_{rec}\big|_{dB\ K} \tag{A.5}$$

The downlink bandwidth (R Hz wide) is assumed to be saturated with noise.

$$N_{0S}\big|_{dB\ W/Hz} = EIRP_{sat}\big|_{dB\ W} - L_{S_{down}}\big|_{dB} - L_a\big|_{dB} + G_{R_{dish}}\big|_{dB} - R\big|_{dB\ Hz} \tag{A.6}$$

The downlink vacuum path loss ($L_{S_{down}}$) is a function of ρ, the slant range, and λ, the signal wavelength. The slant range corresponds to a satellite at 1000 km altitude, as 'viewed' by a ground transmitter at an elevation angle of 15°.

$$L_{S_{down}}\Big|_{dB} = \left(\frac{4\pi\rho}{\lambda}\right)^2\Bigg|_{dB} \tag{A.7}$$

The receiving antenna gain at the central site ($G_{R_{dish}}$) includes a pointing error loss ($L_{P_{dish}}$) corresponding to a pointing error of 1.0 degrees.

$$G_{R_{dish}}\Big|_{dB} = G_{dish}\Big|_{dB} - L_{P_{dish}}\Big|_{dB} \tag{A.8}$$

The satellite EIRP is a function of P_{sat}, which we wish to determine, the satellite antenna transmitter gain ($G_{T_{sat}}$), and L_l, a sum of satellite line and hard limiter losses.

$$EIRP_{sat}\Big|_{dB\ W} = P_{sat}\Big|_{dB\ W} - L_l\Big|_{dB} + G_{T_{sat}}\Big|_{dB} \tag{A.9}$$

For the satellite, the pointing error for the gravity gradient case is 10 degrees, and non-existent for the magnetic stabilization case (since an omni-directional antenna is being used).

$$G_{T_{sat}}\Big|_{dB} = G_{sat}\Big|_{dB} - L_{P_{sat}}\Big|_{dB} \tag{A.10}$$

The uplink carrier-to-noise density ratio is a combination of the carrier-to-'radio noise' and carrier-to-interference density ratios ($(C/N_0)_m$ and (C/I), respectively), where B_i is the integration bandwidth. M_0 is the number of transmitters simultaneously operating, t_i is the coherent integration time (the reciprocal of the integration bandwidth), and R_c is the code chip rate. The difference between the two integration times is empirically based on the increase in ionospheric phase effect at lower frequencies.[1]

[1]Prof. Charles C. Counselman III, personal communication.

$$\left(\frac{C}{N_0}\right)_{up}\Big|_{dB\ Hz} = \left.\frac{1}{\left(\frac{1}{B_i}\left(\frac{C}{I}\right)^{-1} + \left(\frac{C}{N_0}\right)_{rn}^{-1}\right)}\right|_{dB\ Hz} \tag{A.11}$$

$$\left(\frac{C}{I}\right)\Big|_{dB} = \left(\frac{C}{I}\right)_1\Big|_{dB} - \sqrt{M_0}\Big|_{dB} \tag{A.12}$$

$$\left(\frac{C}{I}\right)_1\Big|_{dB} = \left(\frac{R_c\, t_i}{2}\right)\Big|_{dB} \tag{A.13}$$

The number of transmitters in operation is the product of the total number of transmitters in view M_i, and F_t, the duty cycle, which is assumed to be 100%. The design scenario for transmitter deployment is a 10,000 site network to be deployed over an area about the size of California. This network, with transmitter spacing on the order of 1 - 10 km, would fit well inside the GeoBeacon satellite footprint, and all stations could be observed simultaneously.

$$M_0|_{dB} = F_t|_{dB} + M_i|_{dB} \tag{A.14}$$

$(C/N_0)_{rn}$ is a function of ground transmitter power P, which we wish to minimize.

$$\left(\frac{C}{N_0}\right)_{rn}\Big|_{dB\ Hz} = EIRP_{gnd}|_{dB\ W} - L_{S_{up}}|_{dB} - L_a|_{dB} + G_{R_{sat}}|_{dB} - N_{0_N}|_{dB\ W/Hz} \tag{A.15}$$

$$EIRP_{gnd}|_{dB\ W} = P|_{dB\ W} - L_{l_{gnd}}|_{dB} + G_{T_{gnd}}|_{dB} \tag{A.16}$$

The vacuum path loss and satellite receiving antenna pointing losses are the same as those in (A.7) and (A.10), respectively.

$$L_{S_{up}}|_{dB} = \left.\left(\frac{4\pi\rho}{\lambda}\right)^2\right|_{dB} \tag{A.17}$$

$$G_{R_{sat}}|_{dB} = G_{sat}|_{dB} - L_{P_{sat}}|_{dB} \tag{A.18}$$

The satellite radio noise temperature (T_N), assumed to be higher than the satellite receiver noise temperature, was estimated in Chapter 2. The difference in the radio noise temperatures between the gravity gradient and magnetic stabilization systems arises from the incorporation of the galactic noise temperature into the omni-directional antenna noise temperature for the latter case.

$$N_{0N}|_{dB\ W/Hz} = k|_{dB\ W/Hz/K} + T_N|_{dB\ K} \tag{A.19}$$

A.1 Uplink Budget

Values explicitly selected for the baseline designs are entered in **boldface type**. Values for the magnetic stabilization case, when different from those of the gravity gradient case, will be included (in parentheses).

Item	*Symbol*	*Units*	*Uplink #1*	*Uplink #2*
Uplink Frequency	f	GHz	**0.401**	**2.036**
Wavelength	λ	cm	74.8	14.7
Peak Ground Transmitter Power	P	mw	**85.** **(40.)**	**30.** **(30.)**
"	P	dBw	-10.7 -14.0	-15.2 -15.2
GeoBeacon Transmitter Line Loss	L_{lgnd}	dB	**1.0**	**1.0**
Transmit Antenna Gain	G_{Tgnd}	dB	**4.4**	**4.4**
Equivalent Isotropic Radiated Power	$EIRP_{gnd}$	dBw	-7.3 (-10.6)	-11.8 (-11.8)
Propagation Path Length	ρ	km	**2410.**	**2410.**
Vacuum Path Loss	L_{Sup}	dB	152.1	166.3
Atmospheric Propagation Attenuation	L_a	dB	**0.5**	**0.5**
Receive Antenna Beamwidth	θ_S	deg	**113.** **(Omni-dir.)**	**113.** **(Omni-dir.)**
Receive Antenna Gain (Edge)	G_{sat}	dB	**4.4** **(0.0)**	**4.4** **(0.0)**

Receive Antenna Pointing Error	e_r	deg	**10.** **(0.0)**	**10.** **(0.0)**
Receive Antenna Pointing Loss	$L_{P_{sat}}$	dB	2.5 (0.0)	2.5 (0.0)
Net Receive Antenna Gain	$G_{R_{sat}}$	dB	1.9 (0.0)	1.9 (0.0)
Satellite Radio Noise Temperature	T_N	K	**5000.** **(1325.)**	**700.** **(375.)**
Satellite Receive G/T	$(G/T)_u$	dBK^{-1}	-35.1 (-31.2)	-26.6 (-25.7)
Receiver Noise Power Density	N_{0N}	dBw/Hz	-191.6 (-197.4)	-200.2 (-202.9)
Carrier-to-Receiver Noise Density Ratio	$(C/No)_m$	dB Hz	33.6 (34.2)	23.5 (24.3)
PN Code Chip Rate	R_c	MHz	**0.1**	**1.0**
Integration Time	t_i	s	**1.0**	**4.0**
Carrier-to-Int. Ratio (1 Int. Transmitter)	$(C/I)_1$	dB	47.0	63.0
Number of transmitters in area of interest	M_i	#	**10,000**	**10,000**
Size of area of interest (California)	A_i	km^2	**4.1e5**	**4.1e5**
Footprint Area (950 km alt.)	A_f	km^2	**1.2e7**	**1.2e7**
Area per GeoBeacon Transmitter	$A_t=A_f/M_i$	km^2	41.	41.
Maximum Average Transmitter Spacing	$D_{av}=\sqrt{A_t}$	km	6.4	6.4
Duty Cycle	F_t	-	**1.00**	**1.00**
Simultaneously Operating Transmitters	M_O	#	10,000	10,000
Total Carrier-to-Interference Ratio	(C/I)	dB	27.0	43.0
Uplink Carrier-to-Noise Density Ratio	$(C/No)_{up}$	dB Hz	26.1 (26.2)	23.3 (24.0)

Table A.1 Uplink Power Budgets

The crosstalk interference from other GeoBeacon transmitters is the limiting factor in the total uplink carrier-to-noise density ratio at the lower frequency allocation, and the carrier-to-receiver noise density ratio is the limiting factor at the higher frequency allocation.

A.2 Downlink Budgets

The downlink power budget follows the downlink signal from the satellite transponder to the dish antenna at the central site.

Item	*Symbol*	*Units*	*Downlink #1*	*Downlink #2*
Downlink Frequency	f	GHz	**1.596**	**2.2**
Satellite Transmitter Power	P_{sat}	mw	**270.** **(227.)**	**244.** **215.**
"	P_{sat}	dBw	-5.7 (-6.4)	-6.1 (-6.7)
Satellite Line Loss	L_{tl}	dB	**1.0**	**1.0**
Hard Limiter Loss	L_{hl}	dB	**1.5**	**1.5**
Satellite Losses	$L_l=L_{tl}L_{hl}$	dB	2.5	2.5
Transmit Antenna Beamwidth	θ_s	deg	**113.** **(Omni-dir.)**	**113.** **(Omni-dir.)**
Transmit Antenna Gain	G_{sat}	dB	**4.4** **(0.0)**	**4.4** **(0.0)**
Transmit Antenna Pointing Offset	e_t	deg	**10.0** **(0.0)**	**10.0** **(0.0)**
Transmit Antenna Pointing Loss	L_{Psat}	dB	2.5 (0.0)	2.5 (0.0)
Net Satellite Antenna Gain	G_{Tsat}	dB	1.9 (0.0)	1.9 (0.0)
Equivalent Isotropic Radiated Power	$EIRP_{sat}$	dBw	-6.3 (-8.9)	-6.7 (-9.2)
Propagation Path Length	ρ	km	**2410.**	**2410.**
Vacuum Path Loss	L_{Sdown}	dB	164.1	166.9
Propagation Loss	L_a	dB	**0.5**	**0.5**
Receive Antenna Diameter	D_r	m	**2.0**	**2.0**
Receive Antenna Gain	G_{dish}	dB	27.9	30.7
Receive Antenna Beamwidth	θ_r	deg	6.6	4.8
Receive Antenna Pointing Error	e_r	deg	**1.0**	**1.0**
Receive Antenna Pointing Loss	L_{Pdish}	dB	0.277	0.527

Net Receive Antenna Gain	G_{Rdish}	dB	27.6	30.2
System Noise Temperature	T_{rec}	K	**100.**	**100.**
Receive Antenna G/T	$(G/T)_d$	dBK^{-1}	7.6	10.2
Downlink Receiver Noise Density	N_{0R}	dBw/Hz	-208.6	-208.6
Transponder Bandwidth	R	MHz	**0.1**	**1.0**
'Received' Noise Density	N_{0S}	dBw/Hz	-193.3 (-196.0)	-204.0 (-206.5)
Noise Densities Ratio	F	-	0.03 (0.055)	0.35 (0.61)
Total Carrier-to-Noise Density Ratio	$(C/No)_{tot}$	dB Hz	26.0 (26.0)	22.0 (22.0)
Required Eb/No	(E_b/N_o)	dB	**24.**	**26.**
Integration Bandwidth	B_i	Hz	1.00	0.25
Required Carrier-to-Noise Density Ratio	$(C/N_o)_{req}$	dB Hz	24.0	20.0
Implementation Loss	L_i	dB	**2.**	**2.**
Margin	-	dB	**0.0 (0.0)**	**0.0 (0.0)**

Table A.2 Downlink Power Budgets

Values of F less than unity show that the noise contribution from the downlink is small compared to the uplink noise, especially at the lower frequency allocation. Therefore, the accuracy of this system is uplink-limited.

Appendix B. Analytic Expressions for Satellite Partial Derivatives

The partial derivatives of the satellite position vector **x** with respect to the satellite initial condition vector $(\mathbf{x} \ \dot{\mathbf{x}})_{t=t_0}$ can be expressed as the matrix version of the chain rule[1]:

$$\mathbf{M} \equiv \left[\frac{\delta \mathbf{x}}{\delta \mathbf{x}_0} \quad \frac{\delta \mathbf{x}}{\delta \dot{\mathbf{x}}_0} \right] = \begin{bmatrix} \frac{\delta x}{\delta x_0} & \frac{\delta x}{\delta y_0} & \frac{\delta x}{\delta z_0} & \frac{\delta x}{\delta \dot{x}_0} & \frac{\delta x}{\delta \dot{y}_0} & \frac{\delta x}{\delta \dot{z}_0} \\ \frac{\delta y}{\delta x_0} & \frac{\delta y}{\delta y_0} & \frac{\delta y}{\delta z_0} & \frac{\delta y}{\delta \dot{x}_0} & \frac{\delta y}{\delta \dot{y}_0} & \frac{\delta y}{\delta \dot{z}_0} \\ \frac{\delta z}{\delta x_0} & \frac{\delta z}{\delta y_0} & \frac{\delta z}{\delta z_0} & \frac{\delta z}{\delta \dot{x}_0} & \frac{\delta z}{\delta \dot{y}_0} & \frac{\delta z}{\delta \dot{z}_0} \end{bmatrix} = \tilde{\mathbf{X}} \, \tilde{\mathbf{Q}} = \left[\frac{\delta \mathbf{x}}{\delta \mathbf{q}} \right] \left[\frac{\delta \mathbf{q}}{\delta \mathbf{x}_0} \quad \frac{\delta \mathbf{q}}{\delta \dot{\mathbf{x}}_0} \right] \tag{B.1}$$

where $\mathbf{x}^T \equiv [x \ y \ z] \qquad \mathbf{x}_0^T \equiv [x \ y \ z]_{t=t0} \qquad \dot{\mathbf{x}}_0^T \equiv [\dot{x} \ \dot{y} \ \dot{z}]_{t=t0}$

Keplerian elements suffer a collapse of arguments of perigee, longitude of ascending node, and mean anomaly for circular equatorial (i=0°, e=0) orbits. Therefore, the set of orbital elements **q**, which is well suited for all values of orbit inclination and eccentricity[2], was selected as the intermediate variable set.

$$\mathbf{q}^T = [\ a \quad C \quad S \ U_{x0} \ U_{y0} \ U_{z0} \ S_{x0} \ S_{y0} \ S_{z0} \ ]$$

where $$C \equiv e \cos E_0 = 1 - \frac{r_0}{a} \qquad S \equiv e \sin E_0 = \frac{r_0 \dot{r}_0}{\sqrt{\mu a}} \tag{B.2 a,b}$$

and $$\vec{U}_0 = \left(\frac{\vec{r}}{|\vec{r}|} \right)_{t=t_0} \qquad \vec{S}_0 = \left(r \dot{\vec{r}} - \dot{r} \vec{r} \right)_{t=t_i} \tag{B.3 a,b}$$

The radius vector is a linear combination of the vectors $\mathbf{U}_0$ and $\mathbf{S}_0$:

$$\vec{r} = x_v \vec{U}_0 + \frac{y_v}{\sqrt{\mu p}} \vec{S}_0 \tag{B.4}$$

---

[1]Escobal, P. R., *Methods of Orbit Determination*, John Wiley & Sons, 1965.
[2]Baker, R. M. L., *Astrodynamics: Applications and Advanced Topics*, Academic Press, 1967.

where $x_\nu = r\cos(\nu - \nu_0) \qquad y_\nu = r\sin(\nu - \nu_0) \qquad p = a(1 - C^2 - S^2)$ (B.5 a,b,c)

The first factor of the matrix product, $\tilde{\mathbf{X}}$, contains the derivatives of satellite position with respect to the **q** frame:

$$\tilde{\mathbf{X}} \equiv \begin{bmatrix} \frac{\delta x}{\delta a} & \frac{\delta x}{\delta C} & \frac{\delta x}{\delta S} & \frac{\delta x}{\delta U_{x0}} & 0 & 0 & \frac{\delta x}{\delta S_{x0}} & 0 & 0 \\ \frac{\delta y}{\delta a} & \frac{\delta y}{\delta C} & \frac{\delta y}{\delta S} & 0 & \frac{\delta y}{\delta U_{y0}} & 0 & 0 & \frac{\delta y}{\delta S_{y0}} & 0 \\ \frac{\delta z}{\delta a} & \frac{\delta z}{\delta C} & \frac{\delta z}{\delta S} & 0 & 0 & \frac{\delta z}{\delta U_{z0}} & 0 & 0 & \frac{\delta z}{\delta S_{z0}} \end{bmatrix}$$

Differentiating equation (B.4) with respect to the orbit parameters a, C, and S, yields the first three columns of $\tilde{\mathbf{X}}$. By observing the lengthy coefficients of vectors $\mathbf{U}_0$ and $\mathbf{S}_0$, one can tell there is much algebraic manipulation involved.

$$\frac{\delta \mathbf{r}}{\delta a} = A_1 \mathbf{U}_0 + A_2 \mathbf{S}_0 \tag{B.6}$$

$$A_1 \equiv \frac{r}{a}\cos(\nu - \nu_0) + \frac{3}{2}a(M - M_0)\left\{\frac{1}{\sqrt{ap}}\left(\frac{p}{r_0} - C\right)\sin(\nu - \nu_0) + S\left(\frac{1}{p} - \frac{1}{r_0}\right)\left[1 - \cos(\nu - \nu_0)\right] - \frac{S}{r}\right\}$$

$$A_2 \equiv \frac{1}{\sqrt{\mu p}}\left\{\frac{r}{2a}\sin(\nu - \nu_0) - \frac{3}{2}\frac{\sqrt{ap}}{r_0}(M - M_0) + \frac{3}{2}\sqrt{\frac{a}{p}}(M - M_0)\left[1 - \cos(\nu - \nu_0)\right]\right\}$$

$$\frac{\delta \mathbf{r}}{\delta C} = C_1 \mathbf{U}_0 + C_2 \mathbf{S}_0 \tag{B.7}$$

$$C_1 \equiv -a + \frac{a^2 S}{\sqrt{ap}} \sin(\nu - \nu_0) + \left(\frac{r r_0 - a^2 S^2 + 2arC}{p} - \frac{ar}{r_0} \right) \left[1 - \cos(\nu - \nu_0) \right] + ar \left(\frac{C}{p} - \frac{1}{r_0} \right) \sin^2(\nu - \nu_0)$$

$$+ \frac{a^2 rS}{\sqrt{ap}} \left[\frac{2}{r_0} - \frac{1}{p}(1 + C) \right] \left[1 - \cos(\nu - \nu_0) \right] \sin(\nu - \nu_0) + \frac{a^2 S^2 r}{p} \left(\frac{1}{p} - \frac{1}{r_0} \right) \left[1 - \cos(\nu - \nu_0) \right]^2$$

$$C_2 \equiv \frac{ar}{\sqrt{\mu p}} \left\{ \frac{\sin(\nu - \nu_0)}{r_0} + \frac{1}{p} \sqrt{\frac{a}{p}} S \left[1 - \cos(\nu - \nu_0) \right]^2 - \frac{\sin(\nu - \nu_0)}{p} \left[1 - \cos(\nu - \nu_0) \right] \right\}$$

$$\frac{\delta \mathbf{r}}{\delta S} = S_1 \mathbf{U}_0 + S_2 \mathbf{S}_0 \tag{B.8}$$

$$S_1 \equiv \frac{ar}{\sqrt{ap}} \sin(\nu - \nu_0) \left\{ 1 + \left[1 - \cos(\nu - \nu_0) \right] \left(1 - \frac{r_0}{p} C \right) \right\} + S \frac{ar}{p} \left[1 - \cos(\nu - \nu_0) \right] \cos(\nu - \nu_0)$$

$$+ S \frac{ar_0}{p} \left[1 - \cos(\nu - \nu_0) \right] \left\{ \frac{r}{p} \left[1 - \cos(\nu - \nu_0) \right] - 1 \right\}$$

$$S_2 \equiv \frac{1}{\sqrt{\mu p}} \left\{ \frac{r r_0 \sqrt{ap}}{p^2} \left[1 - \cos(\nu - \nu_0) \right]^2 \right\}$$

The remaining entries of $\tilde{\mathbf{X}}$ are obtained from differentiating the vectors defined in (B.4):

$$\begin{bmatrix} \frac{\delta x}{\delta U_{x0}} & \frac{\delta x}{\delta U_{y0}} & \frac{\delta x}{\delta U_{z0}} \\ \frac{\delta y}{\delta U_{x0}} & \frac{\delta y}{\delta U_{y0}} & \frac{\delta y}{\delta U_{z0}} \\ \frac{\delta z}{\delta U_{x0}} & \frac{\delta z}{\delta U_{y0}} & \frac{\delta z}{\delta U_{z0}} \end{bmatrix} = \begin{bmatrix} x_\nu & 0 & 0 \\ 0 & x_\nu & 0 \\ 0 & 0 & x_\nu \end{bmatrix} \tag{B.9}$$

$$\begin{bmatrix} \frac{\delta x}{\delta S_{x0}} & \frac{\delta x}{\delta S_{y0}} & \frac{\delta x}{\delta S_{z0}} \\ \frac{\delta y}{\delta S_{x0}} & \frac{\delta y}{\delta S_{y0}} & \frac{\delta y}{\delta S_{z0}} \\ \frac{\delta z}{\delta S_{x0}} & \frac{\delta z}{\delta S_{y0}} & \frac{\delta z}{\delta S_{z0}} \end{bmatrix} = \begin{bmatrix} \frac{y_v}{\sqrt{\mu p}} & 0 & 0 \\ 0 & \frac{y_v}{\sqrt{\mu p}} & 0 \\ 0 & 0 & \frac{y_v}{\sqrt{\mu p}} \end{bmatrix} \tag{B.10}$$

The second matrix contains the derivatives of the **q** frame with respect to the initial conditions. This matrix only needs to be calculated once per satellite per observation span.

$$\tilde{\mathbf{Q}} \equiv \begin{bmatrix} \frac{\delta a}{\delta x_0} & \frac{\delta a}{\delta y_0} & \frac{\delta a}{\delta z_0} & \frac{\delta a}{\delta \dot{x}_0} & \frac{\delta a}{\delta \dot{y}_0} & \frac{\delta a}{\delta \dot{z}_0} \\ \frac{\delta C}{\delta x_0} & \frac{\delta C}{\delta y_0} & \frac{\delta C}{\delta z_0} & \frac{\delta C}{\delta \dot{x}_0} & \frac{\delta C}{\delta \dot{y}_0} & \frac{\delta C}{\delta \dot{z}_0} \\ \frac{\delta S}{\delta x_0} & \frac{\delta S}{\delta y_0} & \frac{\delta S}{\delta z_0} & \frac{\delta S}{\delta \dot{x}_0} & \frac{\delta S}{\delta \dot{y}_0} & \frac{\delta S}{\delta \dot{z}_0} \\ \frac{\delta U_{x0}}{\delta x_0} & \frac{\delta U_{x0}}{\delta y_0} & \frac{\delta U_{x0}}{\delta z_0} & 0 & 0 & 0 \\ \frac{\delta U_{y0}}{\delta x_0} & \frac{\delta U_{y0}}{\delta y_0} & \frac{\delta U_{y0}}{\delta z_0} & 0 & 0 & 0 \\ \frac{\delta U_{z0}}{\delta x_0} & \frac{\delta U_{z0}}{\delta y_0} & \frac{\delta U_{z0}}{\delta z_0} & 0 & 0 & 0 \\ \frac{\delta S_{x0}}{\delta x_0} & \frac{\delta S_{x0}}{\delta y_0} & \frac{\delta S_{x0}}{\delta z_0} & \frac{\delta S_{x0}}{\delta \dot{x}_0} & \frac{\delta S_{x0}}{\delta \dot{y}_0} & \frac{\delta S_{x0}}{\delta \dot{z}_0} \\ \frac{\delta S_{y0}}{\delta x_0} & \frac{\delta S_{y0}}{\delta y_0} & \frac{\delta S_{y0}}{\delta z_0} & \frac{\delta S_{y0}}{\delta \dot{x}_0} & \frac{\delta S_{y0}}{\delta \dot{y}_0} & \frac{\delta S_{y0}}{\delta \dot{z}_0} \\ \frac{\delta S_{z0}}{\delta x_0} & \frac{\delta S_{z0}}{\delta y_0} & \frac{\delta S_{z0}}{\delta z_0} & \frac{\delta S_{z0}}{\delta \dot{x}_0} & \frac{\delta S_{z0}}{\delta \dot{y}_0} & \frac{\delta S_{z0}}{\delta \dot{z}_0} \end{bmatrix}$$

Differentiating the vis-viva equation yields the derivatives of the semi-major axis with respect to satellite position and velocity:

$$\begin{bmatrix} \frac{\delta a}{\delta x_0} \\ \frac{\delta a}{\delta y_0} \\ \frac{\delta a}{\delta z_0} \end{bmatrix} = \begin{bmatrix} \frac{2a^2 x_0}{r_0^3} \\ \frac{2a^2 y_0}{r_0^3} \\ \frac{2a^2 z_0}{r_0^3} \end{bmatrix} \begin{bmatrix} \frac{\delta a}{\delta \dot{x}_0} \\ \frac{\delta a}{\delta \dot{y}_0} \\ \frac{\delta a}{\delta \dot{z}_0} \end{bmatrix} = \begin{bmatrix} \frac{2a^2 \dot{x}_0}{\mu} \\ \frac{2a^2 \dot{y}_0}{\mu} \\ \frac{2a^2 \dot{z}_0}{\mu} \end{bmatrix} \qquad \text{(B.11)}$$

Differentiating equations (B.2 a,b) yields

$$\begin{bmatrix} \frac{\delta C}{\delta x_0} \\ \frac{\delta C}{\delta y_0} \\ \frac{\delta C}{\delta z_0} \end{bmatrix} = \begin{bmatrix} \frac{V_0^2 x_0}{\mu r_0} \\ \frac{V_0^2 y_0}{\mu r_0} \\ \frac{V_0^2 z_0}{\mu r_0} \end{bmatrix} \begin{bmatrix} \frac{\delta C}{\delta \dot{x}_0} \\ \frac{\delta C}{\delta \dot{y}_0} \\ \frac{\delta C}{\delta \dot{z}_0} \end{bmatrix} = \begin{bmatrix} \frac{2r_0 \dot{x}_0}{\mu} \\ \frac{2r_0 \dot{y}_0}{\mu} \\ \frac{2r_0 \dot{z}_0}{\mu} \end{bmatrix} \qquad \text{(B.12)}$$

$$\begin{bmatrix} \frac{\delta S}{\delta x_0} \\ \frac{\delta S}{\delta y_0} \\ \frac{\delta S}{\delta z_0} \end{bmatrix} = \begin{bmatrix} \frac{\dot{x}_0}{\sqrt{\mu a}} - \frac{a S x_0}{r_0^3} \\ \frac{\dot{y}_0}{\sqrt{\mu a}} - \frac{a S y_0}{r_0^3} \\ \frac{\dot{z}_0}{\sqrt{\mu a}} - \frac{a S z_0}{r_0^3} \end{bmatrix} \begin{bmatrix} \frac{\delta S}{\delta \dot{x}_0} \\ \frac{\delta S}{\delta \dot{y}_0} \\ \frac{\delta S}{\delta \dot{z}_0} \end{bmatrix} = \begin{bmatrix} \frac{x_0}{\sqrt{\mu a}} - \frac{a S \dot{x}_0}{\mu} \\ \frac{y_0}{\sqrt{\mu a}} - \frac{a S \dot{y}_0}{\mu} \\ \frac{z_0}{\sqrt{\mu a}} - \frac{a S \dot{z}_0}{\mu} \end{bmatrix} \qquad \text{(B.13)}$$

Differentiating equations (B.3 a,b) yields

$$\begin{bmatrix} \frac{\delta U_{x0}}{\delta x_0} & \frac{\delta U_{x0}}{\delta y_0} & \frac{\delta U_{x0}}{\delta z_0} \\ \frac{\delta U_{y0}}{\delta x_0} & \frac{\delta U_{y0}}{\delta y_0} & \frac{\delta U_{y0}}{\delta z_0} \\ \frac{\delta U_{z0}}{\delta x_0} & \frac{\delta U_{z0}}{\delta y_0} & \frac{\delta U_{z0}}{\delta z_0} \end{bmatrix} = \begin{bmatrix} \left(\frac{1}{r_0} - \frac{x_0^2}{r_0^3}\right) & \left(-\frac{x_0 y_0}{r_0^3}\right) & \left(-\frac{x_0 z_0}{r_0^3}\right) \\ \left(-\frac{x_0 y_0}{r_0^3}\right) & \left(\frac{1}{r_0} - \frac{y_0^2}{r_0^3}\right) & \left(-\frac{y_0 z_0}{r_0^3}\right) \\ \left(-\frac{x_0 z_0}{r_0^3}\right) & \left(-\frac{y_0 z_0}{r_0^3}\right) & \left(\frac{1}{r_0} - \frac{z_0^2}{r_0^3}\right) \end{bmatrix} \tag{B.14}$$

$$\begin{bmatrix} \frac{\delta S_{x0}}{\delta x_0} & \frac{\delta S_{x0}}{\delta y_0} & \frac{\delta S_{x0}}{\delta z_0} \\ \frac{\delta S_{y0}}{\delta x_0} & \frac{\delta S_{y0}}{\delta y_0} & \frac{\delta S_{y0}}{\delta z_0} \\ \frac{\delta S_{z0}}{\delta x_0} & \frac{\delta S_{z0}}{\delta y_0} & \frac{\delta S_{z0}}{\delta z_0} \end{bmatrix}$$

$$= \begin{bmatrix} \dot{r}_0\left\{\frac{x_0^2}{r_0^2} - 1\right\} & \left(\frac{y_0\dot{x}_0 - x_0\dot{y}_0}{r_0} + \frac{x_0 y_0 \dot{r}_0}{r_0^2}\right) & \left(\frac{z_0\dot{x}_0 - x_0\dot{z}_0}{r_0} + \frac{x_0 z_0 \dot{r}_0}{r_0^2}\right) \\ \left(\frac{x_0\dot{y}_0 - y_0\dot{x}_0}{r_0} + \frac{x_0 y_0 \dot{r}_0}{r_0^2}\right) & \dot{r}_0\left\{\frac{y_0^2}{r_0^2} - 1\right\} & \left(\frac{z_0\dot{y}_0 - y_0\dot{z}_0}{r_0} + \frac{y_0 z_0 \dot{r}_0}{r_0^2}\right) \\ \left(\frac{x_0\dot{z}_0 - z_0\dot{x}_0}{r_0} + \frac{x_0 z_0 \dot{r}_0}{r_0^2}\right) & \left(\frac{y_0\dot{z}_0 - z_0\dot{y}_0}{r_0} + \frac{y_0 z_0 \dot{r}_0}{r_0^2}\right) & \dot{r}_0\left\{\frac{z_0^2}{r_0^2} - 1\right\} \end{bmatrix} \tag{B.15}$$

$$\begin{bmatrix} \frac{\delta S_{x0}}{\delta \dot{x}_0} & \frac{\delta S_{x0}}{\delta \dot{y}_0} & \frac{\delta S_{x0}}{\delta \dot{z}_0} \\ \frac{\delta S_{y0}}{\delta \dot{x}_0} & \frac{\delta S_{y0}}{\delta \dot{y}_0} & \frac{\delta S_{y0}}{\delta \dot{z}_0} \\ \frac{\delta S_{z0}}{\delta \dot{x}_0} & \frac{\delta S_{z0}}{\delta \dot{y}_0} & \frac{\delta S_{z0}}{\delta \dot{z}_0} \end{bmatrix} = \begin{bmatrix} \left(r_0 - \frac{x_0^2}{r_0}\right) & \left(-\frac{x_0 y_0}{r_0}\right) & \left(-\frac{x_0 z_0}{r_0}\right) \\ \left(-\frac{x_0 y_0}{r_0}\right) & \left(r_0 - \frac{y_0^2}{r_0}\right) & \left(-\frac{y_0 z_0}{r_0}\right) \\ \left(-\frac{x_0 z_0}{r_0}\right) & \left(-\frac{y_0 z_0}{r_0}\right) & \left(r_0 - \frac{z_0^2}{r_0}\right) \end{bmatrix} \qquad \text{(B.16)}$$

References

Abbot, R. I., Counselman III, C. C., Gourevitch, S. A., and Ladd, J. W., "GPS Orbit Determination: Bootstrapping to Resolve Carrier Phase Ambiguity," in *Proc. Fifth Intl. Geodetic Symposium on Satellite Positioning*, Vol. I, pp. 224-233, March, 1989.

Baker, R. M. L., *Astrodynamics: Applications and Advanced Topics*, Academic Press, 1967.

Baker, D. N., Chin, G., and Pfaff Jr., R. F., "NASA's Small Explorer Program," *Physics Today*, Vol. 44, No. 12, pp. 44-51, December 1991.

Bayer, T. J., Chatterjee, A. K., Klemetson, R. W., and Shaw Jr., L. T., "Expendable Launch Vehicles Summary for JPL Mission Planning," JPL D-6936, Rev. A, p. 2-21, February 1991.

Bock, Y., Gourevitch, S. A., Counselman III, C. C., King, R. W., and Abbot, R. I., "Interferometric Analysis of GPS Phase Observations," *Manuscripta Geodaetica*, Vol. 11, pp. 282 - 288, 1986

Brown, R. R., Green, P. E., Howland, B., Lerner, R. M., Manasse, R., and Pettengill, G., "Radio Observations of the Russian Earth Satellite," *Proc. IRE*, 45, 1552-1553, 1957.

Cangahuala, L. A., "Feasibility of Millimeter-Accuracy Geodetic Positioning and Vehicle Tracking with Repeater Satellites," AFGL Report GL-TR-89-0231, 27 July 1989.

Cangahuala, L. A., Clark, T. A., and Counselman, C. C., "GeoBeacon Satellite Orbit and Launch Possibilities," *Eos*, Vol. 71, p. 1277, 1990..

Cheng, U., Hurd, W. J., and Statman, J. L., "Spread-Spectrum Code Acquisition in the Presence of Doppler Shift and Data Modulation," *IEEE Transactions on Communications*, Vol. 38, No. 2, February 1990.

Code of Federal Regulations, Title 47, Chapter 1, Part 2, Subpart B, 1988.

Counselman III, C. C., Hinteregger, H. F., and Shapiro, I. I., "Astronomical Applications of Differential Interferometry," *Science*, Vol. 178, pp. 607-608, November 10, 1972.

Counselman III, C. C., Hinteregger, H. F., King, R. W., and Shapiro, I. I., "Precision Selenodesy via Differential Interferometry," *Science*, Vol. 181, pp. 772-774, August 11, 1973.

Counselman, C. C. and Shapiro, I. I., "Miniature Interferometer Terminals for Earth Surveying," *Bulletin Geodesique*, vol. 53, pp. 139-163, 1979.

Counselman III, C. C. and Gourevitch, S. A., "Miniature Interferometer Terminals for Earth Surveying: Ambiguity and Multipath with Global Positioning System," *IEEE Transactions on Geoscience and Remote Sensing*, Vol. GE-19, No. 4, October 1981.

Counselman III, C. C., Gourevitch, S. A., et al, "Zonal and Meridional Circulation of the Lower Atmosphere of Venus Determined by Radio Interferometry," *Journal of Geophysical Research*, Vol. 85, No. A13, pp. 8026 - 8030, December 30, 1980.

Counselman III, C. C., and Abbot, R. I., "An Improved Strategy for Determining Earth Satellite Orbits by Radio," Air Force Geophysics Laboratory Tech. Report No. AFGL-TR-88-0129, 24 pp., 27 May 1988.

Counselman III, C. C., "Ambiguity Bootstrapping to Determine GPS Orbits and Baselines," Report No. GL-TR-89-0278, Geophysics Laboratory, Air Force Systems Command, 11 pp., October 10, 1989.

Cudak, M. C., and Swenson, G. W., "Airborne Measurements of Incidental Radio Noise from Cities," *Radio Science*, Vol. 26, No. 3, pp. 773 - 781, May - June 1991.

Dorrer, M, Laborde, B., and Deschamps, P., "DORIS: System Assessment Results with DORIS on SPOT 2", IAF 90-336, 1990.

Draim, J. E., "Continuous Global N-Tuple Coverage with (2N+2) Satellites," *Journal of Guidance, Control, and Dynamics*, Vol. 14, No. 1, pp. 17 - 23, Jan. - Feb. 1991.

Escobal, P. R., *Methods of Orbit Determination*, John Wiley & Sons, 1965.

GLONASS Update, *The ION Newsletter*, The Institute of Navigation, Spring 1991.

Herman, J. R., "The Radio Noise Environment in Near Space: A Review," *Proc. IEEE International Symposium on Electromagnetic Compatibility*, June 20 - 22, 1978.

International Global Network of Fiducial Stations: Scientific and Implementation Issues," Panel on a Global Network of Fiducial Sites, National Research Council, National Academy Press.

Ippolito, L. J., *Radiowave Propagation in Satellite Communications*, Van Nostrand, Chapter 5, 1986.

King, J. A., McGwier, R., Price, H., and White, J., "The In-Orbit Performance of Four Microsat Spacecraft," presented at the Fourth USU Conference on Small Satellites, Logan, Utah, 1990.

King, R. W., Masters, E.G., Rizos, C., Stolz, A., and Collins, J., *Surveying With GPS*, Monograph 9, School of Surveying, The University of New South Wales, Kensington, N.S.W. Australia, 1985.

Loughmiller, D. and McGwier, B., "Microsat: The Next Generation of OSCAR Satellites," QST Magazine, June 1989.

Mueller, I. I. and Zerbini, S., eds., *The Interdisciplinary Role of Space Geodesy*, Lecture Notes in Earth Sciences, Springer-Verlag Publishers, 1989.

Pattan, Bruce, *WARC-92: Issues for U.S. International Spectrum Policy*, Federal Communications Commission, Office of Technology Assessment, November 1991.

Peterson, A. M., "Radio and Radar Tracking of the Russian Earth Satellite," *Proc. IRE*, 45, 1553-1555, 1957.

Richards, R. T., and Snively, L. O., "Geostar Positioning Analysis," *Proceedings of IEEE PLANS '86*, pp. 13-19, 1986.

Rosetti, C., "Annex: Satellite Land Navigation - Dreams and Reality," *Proceedings of Nav-85 Conference, Land Navigation and Location for Mobile Applications*, Royal Institute of Navigation, 1985.

Sarwate, D. V., and Pursley, M. B., "Correlation Properties of Pseudorandom and Related Sequences," *Proceedings of the IEEE*, Vol. 68, No. 5, May 1980.

Schaffrin, B., and Bock, Y., "A Unified Scheme for Processing Phase Observations," *Bulletin Géodésique*, Vol. 62, pp. 142 - 160, 1988.

Skomal, E. N., "Analysis of Spaceborne VHF Incidental Noise Over the Western Hemisphere," IEEE Transactions on Electromagnetic Compatibility, Vol. EMS-25, No. 3, pp. 321 - 328, August 1983.

Spilker Jr., J. J., "GPS Signal Structure and Performance Characteristics," *Global Positioning System, Navigation, Journal of the Institute of Navigation*, Vol. 25, No. 2, 1978.

Ward, W. W., Hurlbut, K. H., and Zamites, C. J., "The Results of the LES-5 and LES-6 RFI Experiments," *IEEE Transactions on Aerospace and Electrical Systems*, Vol. AES-11, No. 6, pp. 1059 - 1066, November 1975.

Wells, David, *Guide to GPS Positioning*, Canadian GPS Associates, Fredericton, N.B., Canada, 1986.

Wertz, J. R., and Larson, W. J., eds., *Space Mission Analysis and Design*, Chapter 11, 1991.

Wood, C. D., and Perry, G. E., "The Russian Satellite Navigation System," *Phil. Trans. R. Soc. Lond.* A Vol. 294, pp. 307-315, 1980.

Wu, S. C., Yunck, T. P., and Thornton, C. L., "Reduced Dynamics Technique for Precise Orbit Determination of Low Earth Satellites," *Journal of Guidance, Control, and Dynamics*, Vol. 14, No.1, pp;. 24-30, January-February 1991.